

AD-A263 898

12



NSWCDD/TR-92/164

**DETONATION WAVE CURVATURE, CORNER
TURNING, AND UNREACTED HUGONIOT OF
PBXN-111**

BY J. W. FORBES, E. R. LEMAR, G. T. SUTHERLAND, and R. N. BAKER

WEAPONS RESEARCH AND TECHNOLOGY DEPARTMENT

19 MARCH 1992

Approved for public release; distribution is unlimited.

DTIC
S **E** **D**
ELECTE
MAY 07 1993



NAVAL SURFACE WARFARE CENTER
DAHLGREN DIVISION • WHITE OAK DETACHMENT

Silver Spring, Maryland 20903-5640

93 5 06 008

93-09920



DETONATION WAVE CURVATURE, CORNER TURNING, AND UNREACTED HUGONIOT OF PBXN-111

**BY J. W. FORBES, E. R. LEMAR, G. T. SUTHERLAND and R. N. BAKER
WEAPONS SYSTEMS AND TECHNOLOGY DEPARTMENT**

19 MARCH 1992

Accession For	
NTIS CRA&I	<input checked="" type="checkbox"/>
DTIC TAB	<input type="checkbox"/>
Unannounced	<input type="checkbox"/>
Justification	
By	
Distribution/	
Availability Codes	
Dist	Avail and/or Special
A-1	

Approved for public release; distribution is unlimited.

DTIC QUALITY INSPECTED 5

**NAVAL SURFACE WARFARE CENTER
DAHLGREN DIVISION • WHITE OAK DETACHMENT
Silver Spring, Maryland 20903-5000**

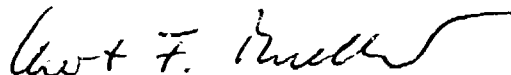
FOREWORD

This work was performed for and funded by the Office of Naval Technology, as part of the Explosives Project within the Explosives and Undersea Warheads Technology Block Program PE6C2314N. The results and conclusions in this report will be of interest to those seeking information on (1) modeling of detonation properties of nonideal explosives, (2) the shock wave sensitivity of explosives, (3) high-speed photographic techniques, and (4) design of explosive devices.

The authors wish to acknowledge many useful discussions on the contents of this paper with R. Bernecker, and S. Jacobs. D. Tasker made many useful comments on this paper.

Dr. R. Doherty and L. Roslund have given technical and moral support for this work. In addition, V. Ringbloom made the curved capillaries used to make the curved light sources for the corner turning experiments.

Approved by:



KURT F. MUELLER, Head
Explosives and Warheads Division

ABSTRACT

This study was undertaken to develop a data base on the detonation properties of PBXN-111 (formerly PBXW-115) and to improve our understanding of its divergent flow properties. This data base can be used to test curved wave front detonation theories and two-dimensional hydrodynamic flow detonation models which take into account the initiation and the growth of reactions and multiple energy release rates. A high speed streak camera was used to measure the wave front curvature and the corner turning ability of PBXN-111. The unreacted Hugoniot was measured using quartz and multiple in situ manganin stress gauges. These Hugoniot samples were dynamically loaded by the impact of projectiles from a light gas gun.

CONTENTS

	<u>Page</u>
INTRODUCTION	1
DETONATION WAVE ARRIVAL AT END OF CHARGE . . .	5
DETONATION WAVE CURVATURE RESULTS FOR UNCONFINED CHARGES	9
WOOD-KIRKWOOD REACTION ZONE LENGTH	15
CORNER TURNING	17
UNREACTED HUGONIOT	28
DISCUSSION AND SUMMARY OF RESULTS	33
REFERENCES	38

Appendixes

A	BREAKOUT POSITION VERSUS TIME DATA	A-1
B	ERROR ANALYSIS	B-1

ILLUSTRATIONS

<u>Figure</u>		<u>Page</u>
1	ANGLE THAT THE CURVED DETONATION WAVE FRONT MAKES WITH THE EDGE OF THE CHARGE	3
2	DETONATION WAVE BREAKOUT EXPERIMENTAL ARRANGEMENT	6
3	DETONATION WAVE BREAKOUT FOR BRASS ENCASED CHARGES	8
4	DETONATION WAVE BREAKOUT FOR A 48.12 mm DIAMETER CYLINDRICAL PBXN-111 CHARGE; (A) STREAK CAMERA FILM RECORD, (B) BREAKOUT DISTANCE VERSUS TIME	11
5	WAVE CURVATURE AS A FUNCTION OF DIAMETER .	13
6	DETONATION WAVE CORNER TURNING EXPERIMENTAL ARRANGEMENTS; (A) ISOMETRIC VIEW OF UNCONFINED BOWL WITH AN UNCONFINED CYLINDRICAL BOOSTER, (B) SIDE VIEW OF UNCONFINED BOWL WITH AN UNCONFINED CYLINDRICAL BOOSTER, (C) SIDE VIEW OF UNCONFINED BOWL WITH BRASS CONFINED CYLINDRICAL BOOSTER, (D) SIDE VIEW OF BOWL WITH TOP CONFINED BY STEEL PLATE AND A COMP B CYLINDRICAL BOOSTER	18
7	EXPECTED STREAK CAMERA FILM RECORD FOR IDEAL CORNER TURNING	20
8	STREAK CAMERA FILM RECORDS OF THE CORNER TURNING EXPERIMENTS, (A) UNCONFINED CYLINDRICAL PBXN-111 BOOSTER, (B) BRASS CONFINED PBXN-111 CYLINDRICAL BOOSTER, (C) UNCONFINED COMP B BOOSTER, (D) UNCONFINED COMP B BOOSTER, (E) UNCONFINED COMP B CYLINDRICAL BOOSTER WITH TOP OF BOWL CONFINED BY A 12.7 mm THICK STEEL PLATE	21
9	DETONATION WAVE BREAKOUT POSITIONS VERSUS TIME OF ARRIVAL PROFILES FOR CYLINDRICAL BOOSTERS SIMILAR TO THOSE USED IN CORNER TURNING EXPERIMENTS	25
10	EXPERIMENTAL ARRANGEMENTS FOR HUGONIOT MEASUREMENTS	29
11	HUGONIOT OF PBXN-111	30

ILLUSTRATIONS (Continued)

<u>Figure</u>		<u>Page</u>
A-1	DETONATION WAVE PROFILE FOR A 40.90 mm DIAMETER CYLINDRICAL PBXN-111 CHARGE . .	A-2
A-2	DETONATION WAVE PROFILE FOR A 41.05 mm DIAMETER CYLINDRICAL PBXN-111 CHARGE . .	A-3
A-3	DETONATION WAVE PROFILE FOR A 48.02 mm DIAMETER CYLINDRICAL PBXN-111 CHARGE . .	A-4
A-4	DETONATION WAVE PROFILE FOR A 48.12 mm DIAMETER CYLINDRICAL PBXN-111 CHARGE . .	A-5
A-5	DETONATION WAVE PROFILE FOR A 68.25 mm DIAMETER CYLINDRICAL PBXN-111 CHARGE . .	A-6
B-1	ENVELOPE OF PARALLEL LINES THAT MAKE UP STREAK CAMERA FILM TRACE	B-6
B-2	ANGLE THAT THE CURVED DETONATION WAVE FRONT MAKES WITH THE EDGE OF THE CHARGE	B-9
B-3	DETONATION WAVE CORNER TURNING EXPERIMENTAL ARRANGEMENT	B-15

TABLES

<u>Table</u>		<u>Page</u>
1	PBXN-111 CURVATURES, CJ ZONE LENGTHS, AND ANGLES AT CHARGE EDGE	14
2	TIMES OF ARRIVAL FOR PBXN-111 CORNER TURNING EXPERIMENTS	26
3	UNREACTED HUGONIOT OF PBXN-111	31
A-1	TIME VS. BREAKOUT POSITION DATA, SHOT E701, READING A FOR 40.90 mm DIA. UNCONFINED PBXN-111	A-7
A-2	TIME VS. BREAKOUT POSITION DATA, SHOT E701, READING B FOR 40.90 mm DIA. UNCONFINED PBXN-111	A-8
A-3	TIME VS. BREAKOUT POSITION DATA, SHOT E701, READING C FOR 40.90 mm DIA. UNCONFINED PBXN-111	A-9
A-4	TIME VS. BREAKOUT POSITION DATA, SHOT E681, READING 3 FOR 41.05 mm DIA. UNCONFINED PBXN-111	A-10
A-5	TIME VS. BREAKOUT POSITION DATA, SHOT E681, READING 4 FOR 41.05 mm DIA. UNCONFINED PBXN-111	A-11
A-6	TIME VS. BREAKOUT POSITION DATA, SHOT E681, READING 5 FOR 41.05 mm DIA. UNCONFINED PBXN-111	A-12
A-7	TIME VS. BREAKOUT POSITION DATA, SHOT E681, READING 6 FOR 41.05 mm DIA. UNCONFINED PBXN-111	A-13
A-8	TIME VS. BREAKOUT POSITION DATA, SHOT E681, READING B FOR 41.05 mm DIA. UNCONFINED PBXN-111	A-14
A-9	TIME VS. BREAKOUT POSITION DATA, SHOT E681, READING C FOR 41.05 mm DIA. UNCONFINED PBXN-111	A-15
A-10	TIME VS. BREAKOUT POSITION DATA, SHOT E646, READING B FOR 48.02 mm DIA. UNCONFINED PBXN-111	A-16
A-11	TIME VS. BREAKOUT POSITION DATA, SHOT E646, READING C FOR 48.02 mm DIA. UNCONFINED PBXN-111	A-17

TABLES (Continued)

<u>Table</u>		<u>Page</u>
A-12	TIME VS. BREAKOUT POSITION DATA, SHOT E646, READING 2 FOR 48.02 mm DIA. UNCONFINED PBXN-111	A-18
A-13	TIME VS. BREAKOUT POSITION DATA, SHOT E700, READING A FOR 48.12 mm DIA. UNCONFINED PBXN-111	A-19
A-14	TIME VS. BREAKOUT POSITION DATA, SHOT E700, READING B FOR 48.12 mm DIA. UNCONFINED PBXN-111	A-20
A-15	TIME VS. BREAKOUT POSITION DATA, SHOT E700, READING C FOR 48.12 mm DIA. UNCONFINED PBXN-111	A-21
A-16	TIME VS. BREAKOUT POSITION DATA, SHOT E645, READING B FOR 68.25 mm DIA. UNCONFINED PBXN-111	A-22
A-17	TIME VS. BREAKOUT POSITION DATA, SHOT E645, READING 2 FOR 68.25 mm DIA. UNCONFINED PBXN-111	A-23
A-18	TIME VS. BREAKOUT POSITION DATA, SHOT E645, READING 3 FOR 68.25 mm DIA. UNCONFINED PBXN-111	A-24
A-19	TIME VS. BREAKOUT POSITION DATA, SHOT E647, READING B FOR 48.45 mm DIA. PBXN-111 CONFINED BY A 17.1 mm THICK BRASS CYLINDER WALL	A-25
A-20	TIME VS. BREAKOUT POSITION DATA, SHOT E647, READING C FOR 48.45 mm DIA. PBXN-111 CONFINED BY A 17.1 mm THICK BRASS CYLINDER WALL	A-26
A-21	TIME VS. BREAKOUT POSITION DATA, SHOT E648, READING B FOR 67.92 mm DIA. PBXN-111 CONFINED BY 7.3 mm THICK BRASS	A-27
A-22	TIME VS. BREAKOUT POSITION DATA, SHOT E648, READING C FOR 67.92 mm DIA. PBXN-111 CONFINED BY 7.3 mm THICK BRASS	A-28
A-23	TIME VS. BREAKOUT POSITION DATA, SHOT E689, READING B FOR 50.86 mm DIA. UNCONFINED CAST COMP B	A-29
A-24	TIME VS. BREAKOUT POSITION DATA, SHOT E689, READING 2 FOR 50.86 mm DIA. UNCONFINED CAST COMP B	A-30

TABLES (Continued)

<u>Table</u>		<u>Page</u>
A-25	TIME VS. BREAKOUT POSITION DATA, SHOT E693, READING A FOR 50.87 mm DIA. CAST COMP B WITH 12.68 mm THICK STEEL COLLAR AT END	A-31
A-26	TIME VS. BREAKOUT POSITION DATA, SHOT E693, READING 2 FOR 50.87 mm DIA. CAST COMP B WITH 12.68 mm THICK STEEL COLLAR AT END	A-32
B-1	ERROR IN ANGLE Γ ON FILM	B-10
B-2	ERROR IN DETONATION WAVE ANGLE α AT EDGE OF CHARGE	B-12
B-3	ERROR IN DIFFERENCE OF TIME Δt BETWEEN TWO POINTS ON THE FILM	B-16
B-4	ERROR IN ANGLE θ OF CORNER TURNING EXPERIMENTS	B-18

INTRODUCTION

OVERVIEW

This study was undertaken to develop a data base on the detonation properties of PBXN-111 in order to improve the understanding of its initiation and divergent flow properties. The detonation wave corner turning, wave curvature, and unreacted Hugoniot data, along with the previously published data on detonation velocities and failure diameters, make up a complete data base on detonation properties of this nonideal explosive. This detonics data base can be used to calibrate two-dimensional hydrodynamic flow detonation models which take into account ignition and growth of reactions and multiple energy release rates.

METHODS

A high speed streak camera was used to measure wave front curvature and corner turning ability of detonation waves in PBXN-111. In addition, the unreacted Hugoniot was measured using quartz and multiple in situ manganin stress gauges. These Hugoniot samples were dynamically loaded by projectiles from a light gas gun.

PBXN-111 EXPLOSIVE

PBXN-111 (formerly PBXW-115) is a cast cured explosive with cyclotrimethylene trinitramine (RDX), ammonium perchlorate (AP),

aluminum (Al) and hydroxy terminated poly butadiene binder (HTPB). PBXN-111 composition is similar to some propellants^{1,2} except that PBXN-111 contains RDX instead of cyclotetramethylene tetranitrimine (HMX). The initial density of the PBXN-111 used in this work was 1.79 g/cm³. The median particle size of the RDX was calculated³ to be 60 μm . The nominal sizes for AP and Al particles were 200 and 5 μm , respectively. PBXN-111 cylinders have failure diameters of a few centimeters and very curved wave fronts.⁴

DETONATION WAVE CURVATURE AND REACTION ZONE LENGTHS

Detonation waves in nonideal composite explosives have curved wave fronts (see Figure 1). This curvature results from the reacting explosive having a finite size, a varying energy release rate, and hydrodynamic flow. Wave curvature data are used to test curved front detonation theories. Detonation velocity and wave front curvature data of PBXN-111 were used to calculate reaction zone lengths from the Wood-Kirkwood theory.⁵ The calculated reaction zone lengths are a few millimeters. These zone lengths are consistent with previously published calculations on ammonium perchlorate⁶ and two plastic-bonded 2,4,6-trinitro-1,3,5-benzene-triamine (TATB) explosives.^{7,8} Recent improvements in the time resolution of reaction zone length measurements⁸ have provided data accurate enough to distinguish between various analytical curved wave front theories. D. Price⁹ has pointed out that zone length is calculated well by the Wood-Kirkwood curved front theory.

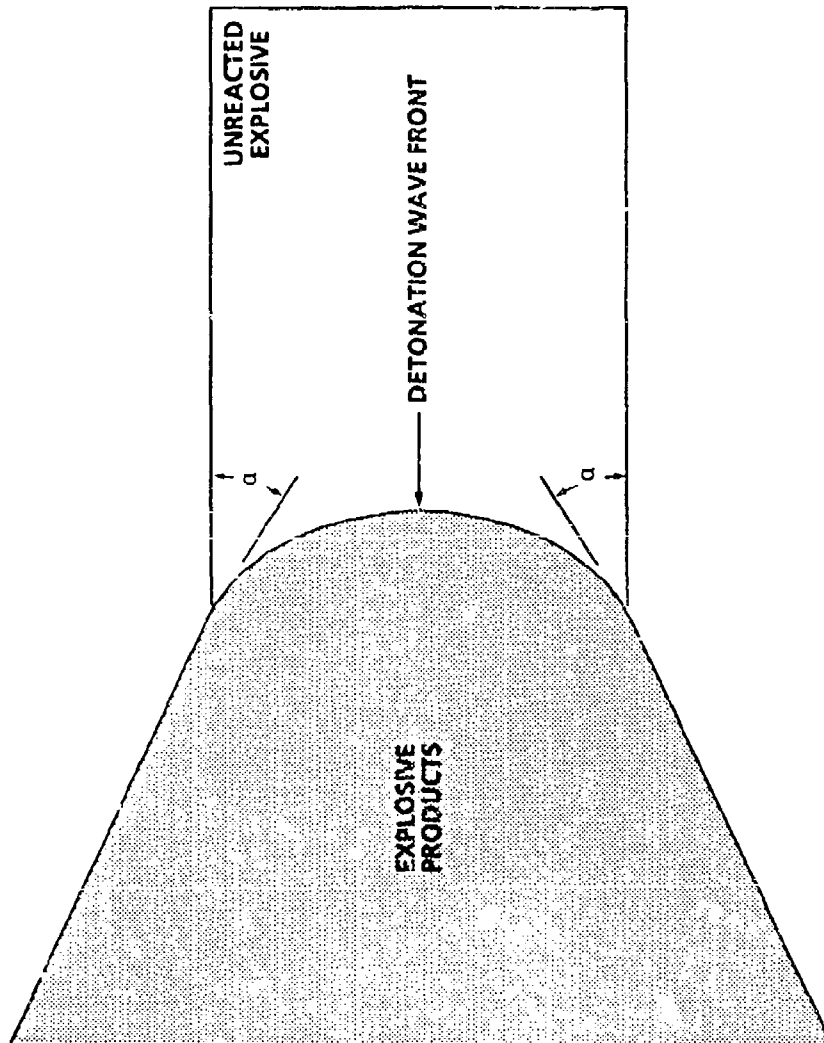


FIGURE 1. ANGLE THAT THE CURVED DETONATION WAVE FRONT MAKES WITH THE EDGE OF THE CHARGE

CORNER TURNING

The ability of a detonation wave to turn a corner is a complicated function of wave shape, stress, and initiation of the explosive not normal (i.e., lateral) to the shock front. Corner turning experiments on TATB compositions using flash X-ray techniques have shown that substantial amounts of material at corners go unreacted.^{10,11} Experiments using streak photography have also shown substantial unreacted TATB¹² at corners. In common with other explosives,^{13,14,15} the detonation wave in PBXN-111 does not follow a simple spherical expansion process from the corner. The understanding of how a detonation wave turns a corner is of great practical importance to insure proper performance of many explosive devices. At present, the propagation of detonation waves turning through angles must be measured experimentally for every geometry of interest to insure proper performance. However, fewer confirmation-type experiments on PBXN-111 will be required in the future because modeling accuracy will improve due to the data published here.

UNREACTED HUGONIOT

The determination of stress states induced in explosives by shock compression, when reaction does not occur, requires an unreacted Hugoniot. The unreacted Hugoniot is also used to determine if reactions occur in shocked explosives. Exothermic reactions have occurred when stresses greater than predicted by the unreacted Hugoniot are observed. One-dimensional strain light gas gun experiments were used in this study to determine the unreacted Hugoniot of PBXN-111.

DETONATION WAVE ARRIVAL AT END OF CHARGE

A streak camera was used to record the detonation wave arrival at the ends of confined and unconfined cylindrical PBXN-111 charges. The experimental setup used to obtain these breakout data is shown in Figure 2. Aluminized Mylar or Teflon tape was glued to the end of the charge as a light reflector. Two of the experiments had lines drawn on the Teflon tape at accurately known distances from the charge edges. These lines appeared on the streak record and confirmed, within experimental error, that the records terminated right at the charges edge. The camera and exploding wire light source were positioned such that the alignment and/or reflectivity was destroyed when the shock arrived at the reflecting material. This greatly reduced the amount of light reaching the film.

Streak camera breakout records (i.e., time versus position across the charge diameter) were obtained on five different 305 mm long unconfined charges with diameters of 41, 48, and 68 mm. These streak camera film records show that the detonation waves arrived at the center about 1 μ s before arriving at the edges. These results clearly show that the detonation waves had curved wave fronts. As would be expected, the larger diameter charges had less wave front curvature than the smaller diameter charges. Appendix A gives the breakout position versus time data for these experiments.

Wave arrival experiments were also conducted on the bare ends of 305 mm long brass confined charges with diameters of 68 and 48 mm. The 48 mm diameter cylindrical charge had a 17 mm

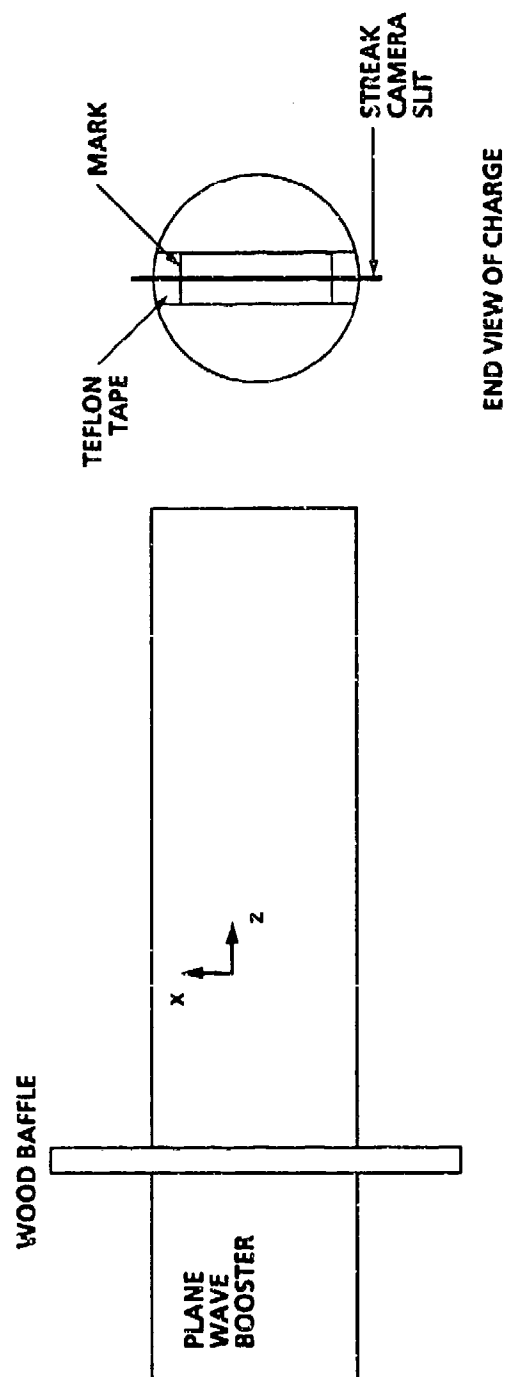


FIGURE 2. DETONATION WAVE BREAKOUT EXPERIMENTAL ARRANGEMENT

thick brass case while the 68 mm diameter charge had a 7 mm thick brass case. In both experiments the time of arrival of the detonation wave was earlier than for an unconfined charge of the same diameter. The wave arrival results for the brass confined charges are given in Figure 3 and Appendix A.

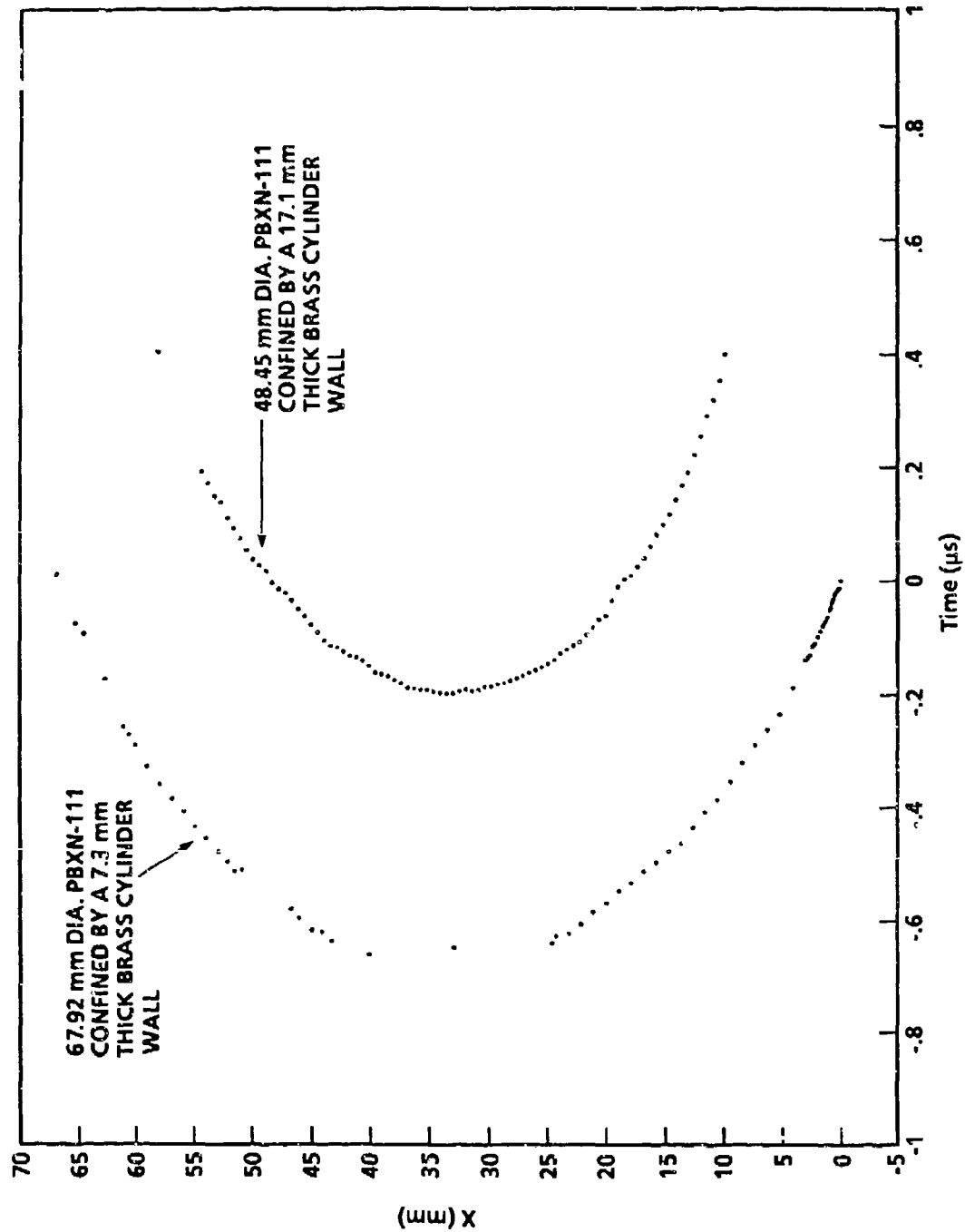


FIGURE 3. DETONATION WAVE BREAKOUT FOR BRASS ENCASED CHARGES

DETONATION WAVE CURVATURE RESULTS FOR UNCONFINED CHARGES

Wave arrival distance-time data and detonation velocities are required to determine the wave front shape inside an explosive charge. The detonation velocity in the PBXN-111 charges was assumed to be steady. This assumption appears justifiable since the measured velocities were constant within experimental error over the last 30-40 mm of propagation distance. Wave front curvature measurements⁶ on porous RDX and Tetryl explosives, have shown that the length to diameter ratios of these materials need to be greater than five before constant curvature can be attained. It is possible that the wave curvature in the PBXN-111 experiments would be slightly different than measured in this study if the detonation waves propagated for longer distances.

In the following discussion, the Z axis (wave propagation axis) is taken to be along the axis of the cylindrical charge and the X axis is taken to be along a charge diameter (see Figure 2). For any X value, the Z position of the wave front at the instant the wave breaks out at the center is obtained from

$$Z = D * (T_0 - T_x) \tag{1}$$

where T_x is the breakout time at the position X, T_0 is the time the wave breaks out at the center, and D is the steady detonation velocity.

The values of D used in Equation (1) were obtained from the following equation.

$$D = 6.195 \text{ mm}/\mu\text{sec} \left(1 - \frac{6.87}{d}\right) \quad (2)$$

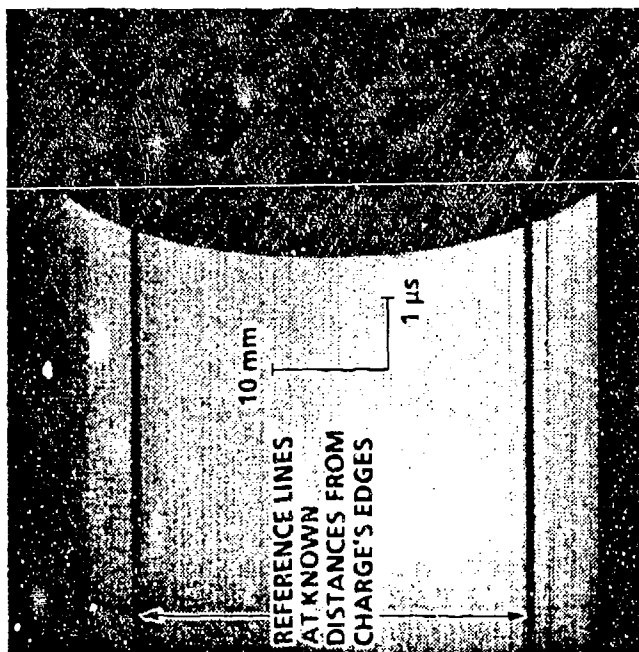
where d is the charge diameter in mm. This expression was obtained by least squares fitting all the measured detonation velocities.⁴

Wave front shape data for each experiment were least squares fitted to circles of the form

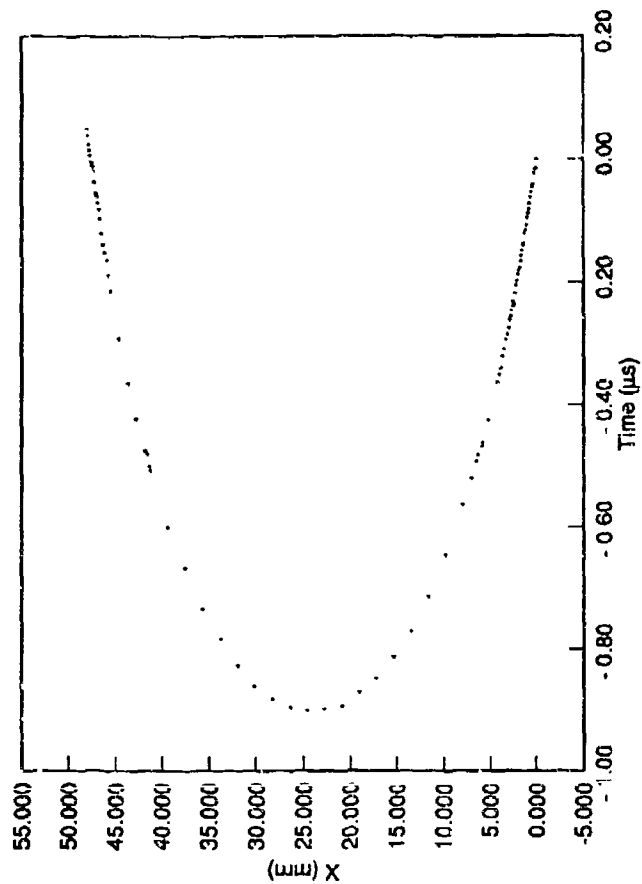
$$(X - a)^2 + (Z - b)^2 = R^2 \quad (3)$$

where R is the radius of curvature and the point $(X=a, Z=b)$ is the center of the circle. It should be noted that the value of " a " will be zero if the position of the Z axis is chosen exactly at the center of the wave front. The inclusion of " a " in the fit means that the position of the Z axis is determined by the fit, i.e., the wave was not always centered on the axis. The magnitude of " a " ranged from 0 to 2 mm.

The wave fronts were not spherical over the entire diameter of the cylindrical PBXN-111 charges. This was particularly true near the edges of the cylinders. As a result, the best fit for the radius depended on how much of the data across the diameter of the charge was used. In this work the data were fit over the center 50 percent of the charge diameter. Figure 4 shows a



(A) STREAK CAMERA FILM RECORD



(B) BREAKOUT DISTANCE VERSUS TIME

FIGURE 4. DETONATION WAVE BREAKOUT FOR A 48.12 mm DIAMETER CYLINDRICAL PBXN-111 CHARGE

typical fit of curvature data for a 48.12 mm diameter charge. The raw data from all the record readings of wave curvature are given in Appendix A.

The spherical radii of curvature for the unconfined breakout experiments, are given in Table 1. The spherical radii of the 41.05, 48.02, and 68.25 mm diameter charges are improved values over those previously published.⁴ The results show that wave curvature increases with charge diameter (see Figure 5). This is consistent with the findings of Campbell, et al.⁷ Table 1 also gives the angles that the detonation waves make with the edges of the charges (see Figure 2). The wave front appeared linear (i.e., not curved) over the last 3 mm at the charge edges. The estimates of error are made in Appendix B.

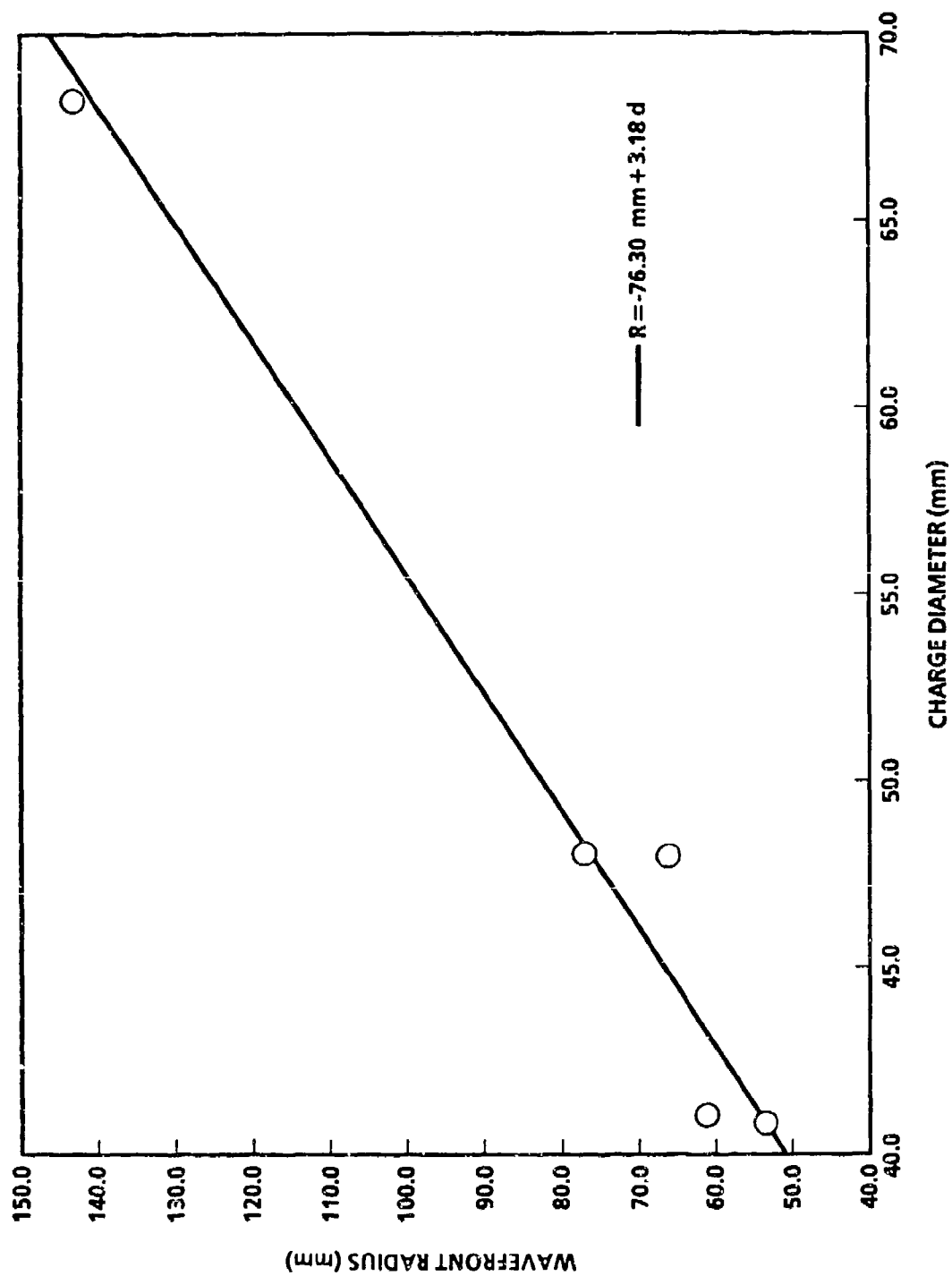


FIGURE 5. WAVE CURVATURE AS A FUNCTION OF DIAMETER

TABLE 1. PBXN-111 WAVE CURVATURES, CJ ZONE LENGTHS,
AND ANGLES AT CHARGE EDGE

CHARGE DIAMETER (mm)	SPHERICAL RADIUS* (mm)	CJ ZONE LENGTH** (mm)	ANGLE AND DISTANCE FITTED AT EDGE OF CHARGE			
			RIGHT		LEFT	
			α	S	α	S
			(Deg)	(mm)	(Deg)	(mm)
40.90 ⁺	53.7 \pm 0.4	2.6	61.4 \pm 1.1	3.2	61.1 \pm 1.3	3.1
41.05 ⁺	61.2 \pm 0.6	2.9	63.9 \pm 0.9	3.4	63.9 \pm 1.0	3.5
48.02	(66.5 \pm 1.1)	(2.7)	63.8 \pm 1.1	3.6	62.2 \pm 1.4	2.5
48.12 ⁺	77.2 \pm 0.5	3.1	61.9 \pm 1.2	2.9	63.3 \pm 1.1	3.1
68.25	143.1 \pm 1.0	4.1	62.1 \pm 1.3	3.0	63.0 \pm 1.9	2.9

+ THESE EXPERIMENTS USED TEFLON TAPE AS A REFLECTOR WHILE OTHERS USED ALUMINIZED MYLAR.

* FITTED OVER THE CENTER 50%. PARENTHESIS INDICATES POOR CENTER OF RECORD.

**CALCULATED USING WOOD-KIRKWOOD THEORY WITH C = 3.5

WOOD-KIRKWOOD REACTION ZONE LENGTH

Calculations of the detonation zone length in PBXN-111 were performed for the five unconfined charges of different diameters for which wave curvatures were measured. These calculations were based on the Wood-Kirkwood curved detonation front theory.⁵ The expression defining zone length from this theory is

$$\frac{D^{\circ} - D}{D^{\circ}} = \frac{C * L_{CJ}}{R} \quad (4)$$

where D is the measured detonation velocity, D° is the infinite diameter detonation velocity, L_{CJ} is the reaction zone length at the center of the charge, C is a constant dependent on the equation of state of the material and R is the spherical radius of curvature of the wave front. A recent review⁹ of selected measurements and calculations of detonation zone lengths indicates that the Wood-Kirkwood theory predicts the correct order of magnitude. Even so, this theory does not adequately explain all of the nonideal hydrodynamic behavior. However, it does provide a recognizable starting point for discussing some implications of the present data.

Wood and Kirkwood⁵ used the properties of a liquid explosive to calculate a value of 3.5 for C . This value for C was used for calculating L_{CJ} for PBXN-111. Table 1 gives charge diameters, radii of curvature of the detonation waves and calculated detonation zone lengths. Table 1 shows that the detonation zone

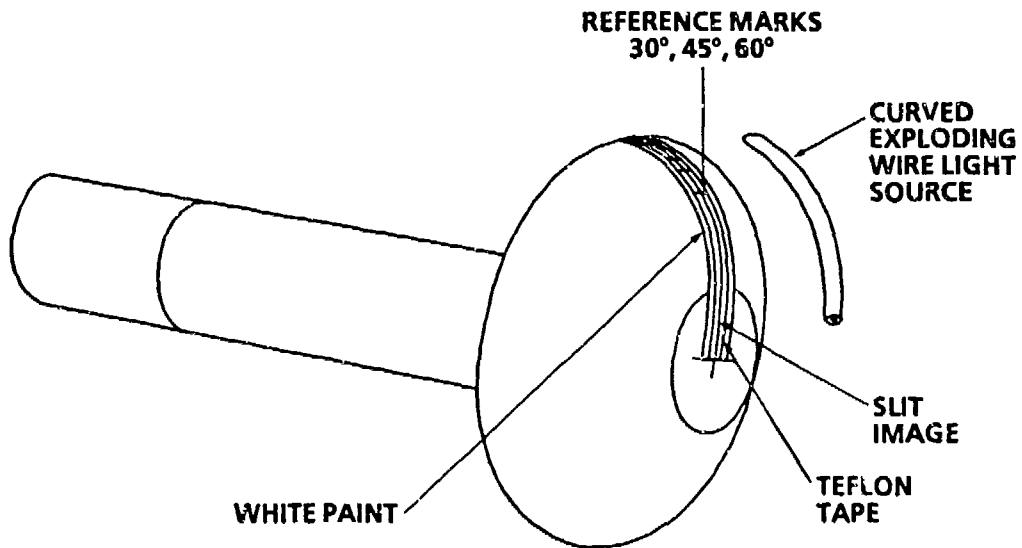
lengths are related to the diameter of the charges. The large scatter in this limited data set is to be expected because of experimental uncertainty in determining R. The detonation zone length for a charge at its failure diameter is 2.3 mm. This zone length was calculated using Equations (2), (4), and a wave front radius of 45 mm. This wave front radius was obtained by extropolating the wave front radius versus charge diameter data in Figure 5 to the 38 mm failure diameter.⁴

CORNER TURNING

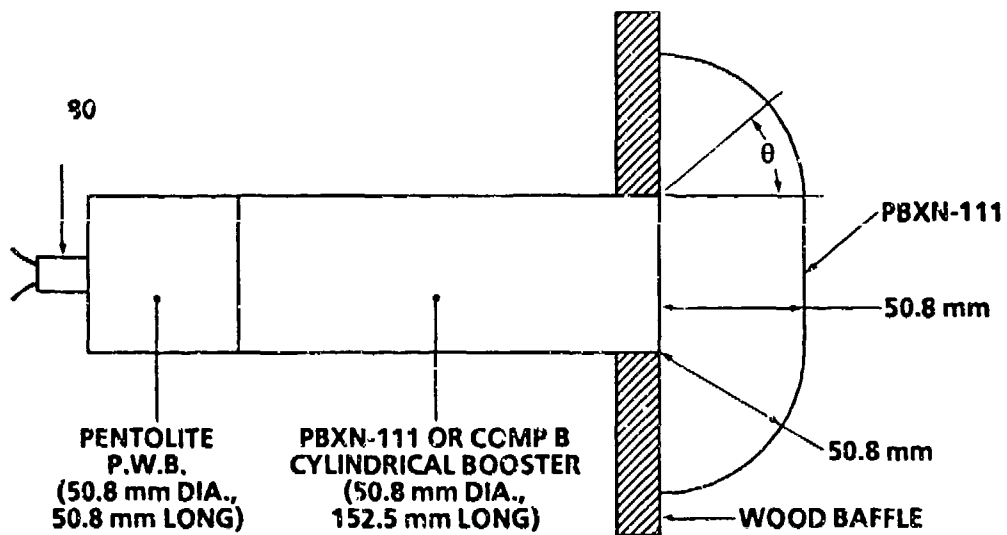
Five corner turning experiments have been performed on PBXN-111. Figure 6(A)-6(D) are schematics of experimental setups. The acceptor charges were the shape of solid bowls. The curved surface of the PBXN-111 bowl was machined with a spherical radius of 50.8 mm measured from a centered circle of 50.8 mm on the flat part of the PBXN-111 bowl where the booster charge will be in contact with the bowl. The bowl-shaped charge was boosted by a 50.8 mm diameter, 152.5 mm long cylinder of PBXN-111 or cast Comp B.

The arrival of the detonation (or shock wave) was observed on the curved surface and bottom of the bowl by a streak camera recording light reflected from an attached Teflon tape. Thin dark lines were placed on the Teflon tape perpendicular to the camera slit to place accurate markers on the film for specific angles, θ . The amount of light being reflected changed significantly when the shock wave entered the Teflon tape. The detonation wave in the PBXN-111 bowl would breakout simultaneously along the curved surface and the flat bottom if a flat-front shock wave initiated the PBXN-111 bowl charge without any delay and the detonation wave expanded spherically from the corner. The resulting streak camera film record would be a vertical line as depicted by the dashed line in Figure 7. A curved line on the film record would be expected for a detonation wave that turns the corner after some time delay (nonideal corner turning) or if it does not expand spherically from the corner.

Figure 8(A) is the streak record for the corner turning experiment using an unconfined PBXN-111 cylindrical booster

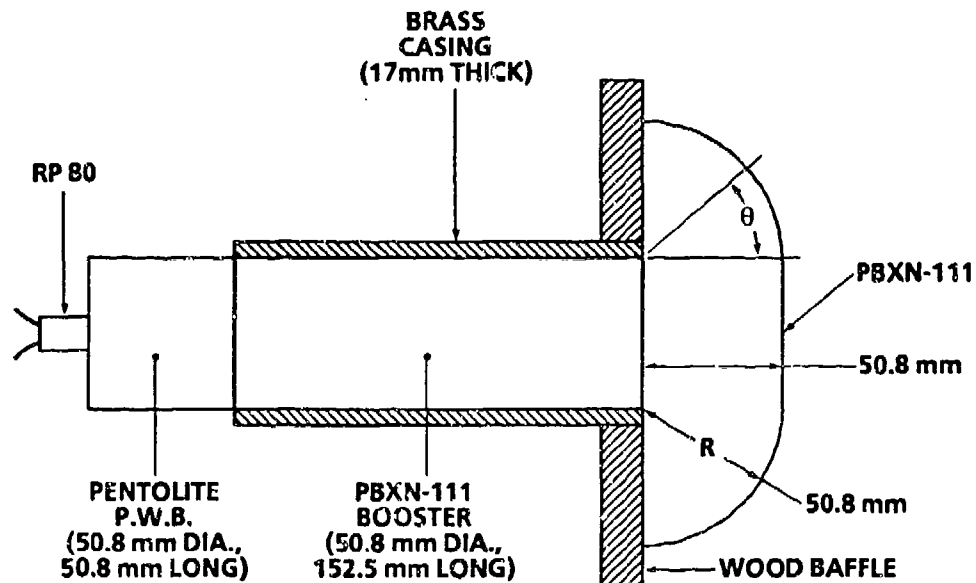


(A) ISOMETRIC VIEW OF UNCONFINED BOWL WITH AN UNCONFINED CYLINDRICAL BOOSTER

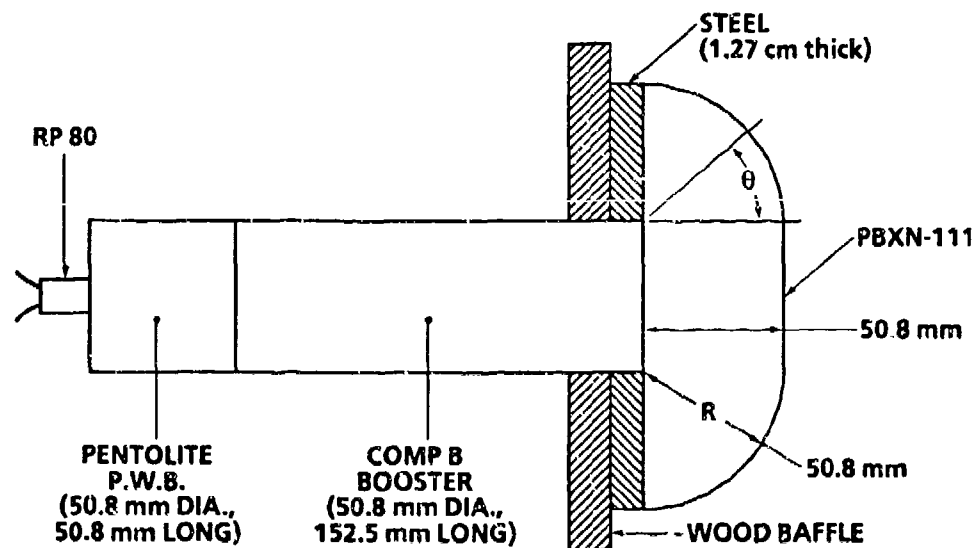


(B) SIDE VIEW OF UNCONFINED BOWL WITH AN UNCONFINED CYLINDRICAL BOOSTER

FIGURE 6. DETONATION WAVE CORNER TURNING EXPERIMENTAL ARRANGEMENTS



(C) SIDE VIEW OF UNCONFINED BOWL WITH BRASS CONFINED CYLINDRICAL BOOSTER



(D) SIDE VIEW OF BOWL WITH TOP CONFINED BY STEEL PLATE AND A COMP B CYLINDRICAL BOOSTER

FIGURE 6. (CONTINUED)

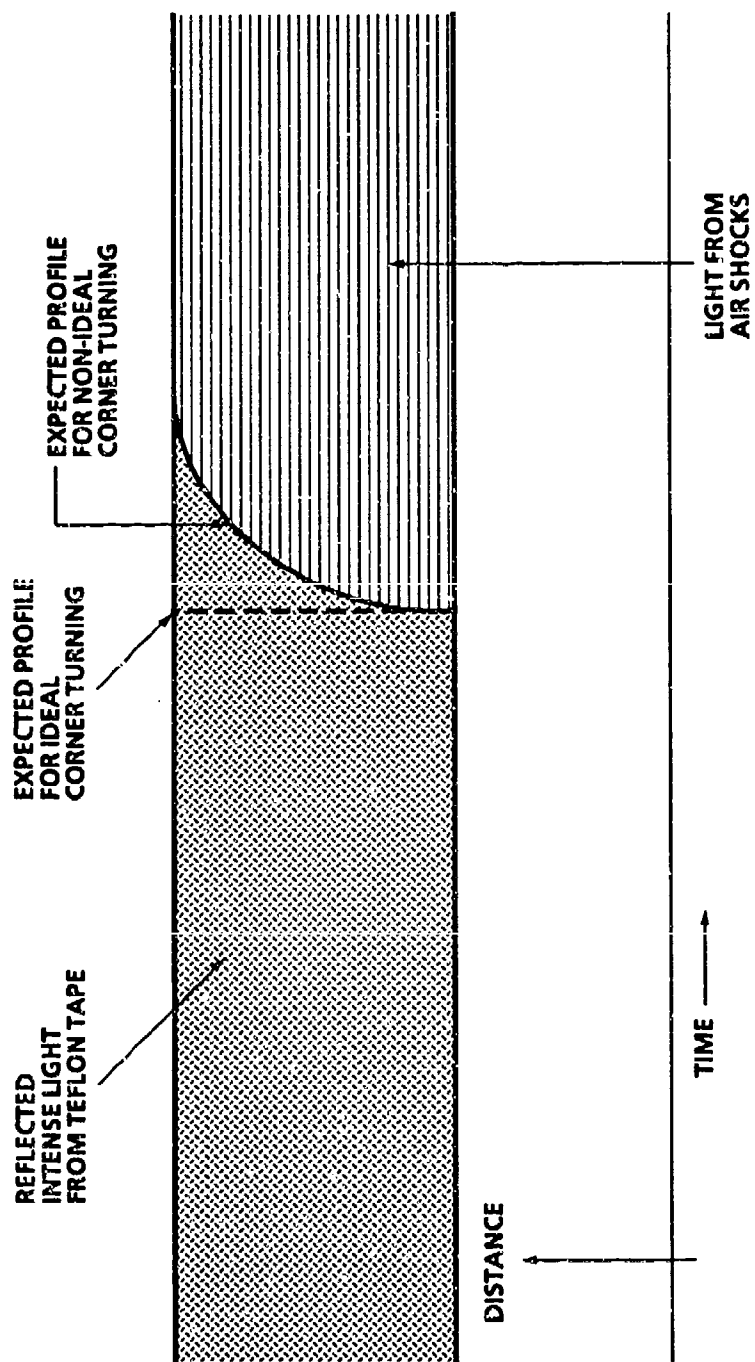


FIGURE 7. EXPECTED STREAK CAMERA FILM RECORD FOR IDEAL CORNER TURNING

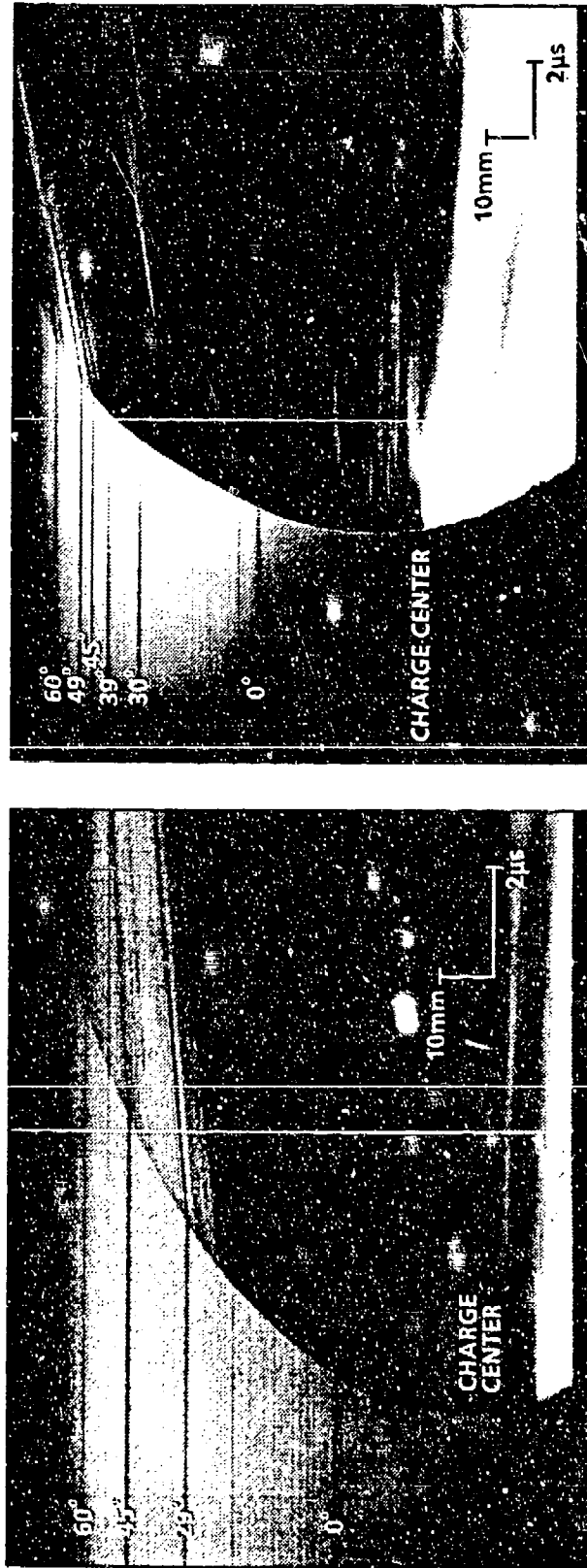
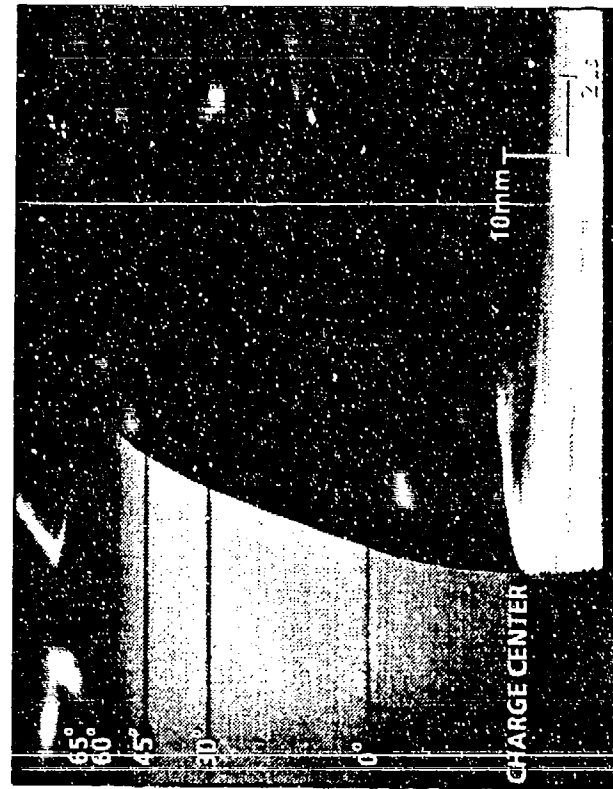


FIGURE 8. STREAK CAMERA FILM RECORDS OF THE CORNER TURNING EXPERIMENTS

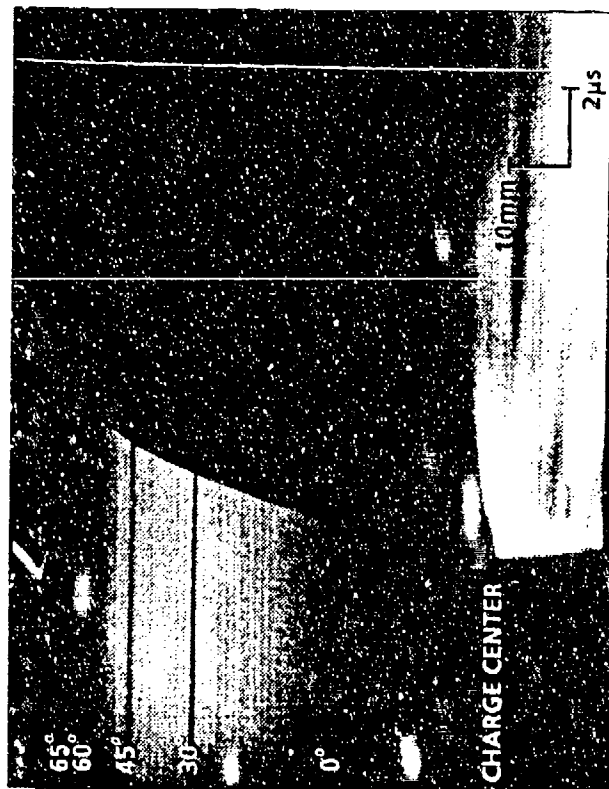
(Figure 6(B)). The detonation wave arrived at the flat bottom a few microseconds before it arrived at the curved surface. The slit of the streak camera covered more of the charge than was covered with Teflon tape. This allowed recording of the wave arrival beyond the bottom center of the charge, where the tape ended, because a luminous air shock was created at the surface when the wave arrived. This air shock provided adequate light for the camera.

Figure 8(B) is the streak record of the experiment using the brass confined PBXN-111 booster (Figure 6(C)). Figure 8(C) is the record for the unconfined Comp B booster. Figure 8(D) is the record for the experiment with a steel plate on top of the bowl charge (Figure 6(D)).

Table 2 gives the times of wave arrival as a function of angle θ for all experiments. Note that the angle θ is measured from a reference line which is along the booster's surface and parallel to its cylindrical axis (see Figure 6). The wave arrived at the same locations on the curved surface of the bowl a few microseconds sooner for the confined PBXN-111 booster arrangement than for the unconfined PBXN-111 booster arrangement. Most of the differences in arrival times can be attributed to the flatter wave front (i.e., a larger radius of curvature) in the confined booster. The experiments using a Comp B booster turned the corner better than the experiments with a PBXN-111 booster. Again, this may be explained by the flatter wave front in the Comp B booster. The best corner turning occurred with a cylindrical Comp B booster and the bowl top confined by a 12.7 mm thick steel plate, as shown in Figure 6(D). Time of arrival profiles for detonation waves at the ends of various cylindrical boosters like those depicted in Figures 6(A)-6(D) are given in Figure 9. The cast Comp B cylindrical booster charges had



(D) UNCONFINED COMP B BOOSTER



(C) UNCONFINED COMP B BOOSTER

FIGURE 8. (CONTINUED)



(E) UNCONFINED COMP B CYLINDRICAL BOOSTER WITH
TOP OF BOWL CONFINED BY A 12.7mm THICK
STEEL PLATE

FIGURE 8. (CONTINUED)

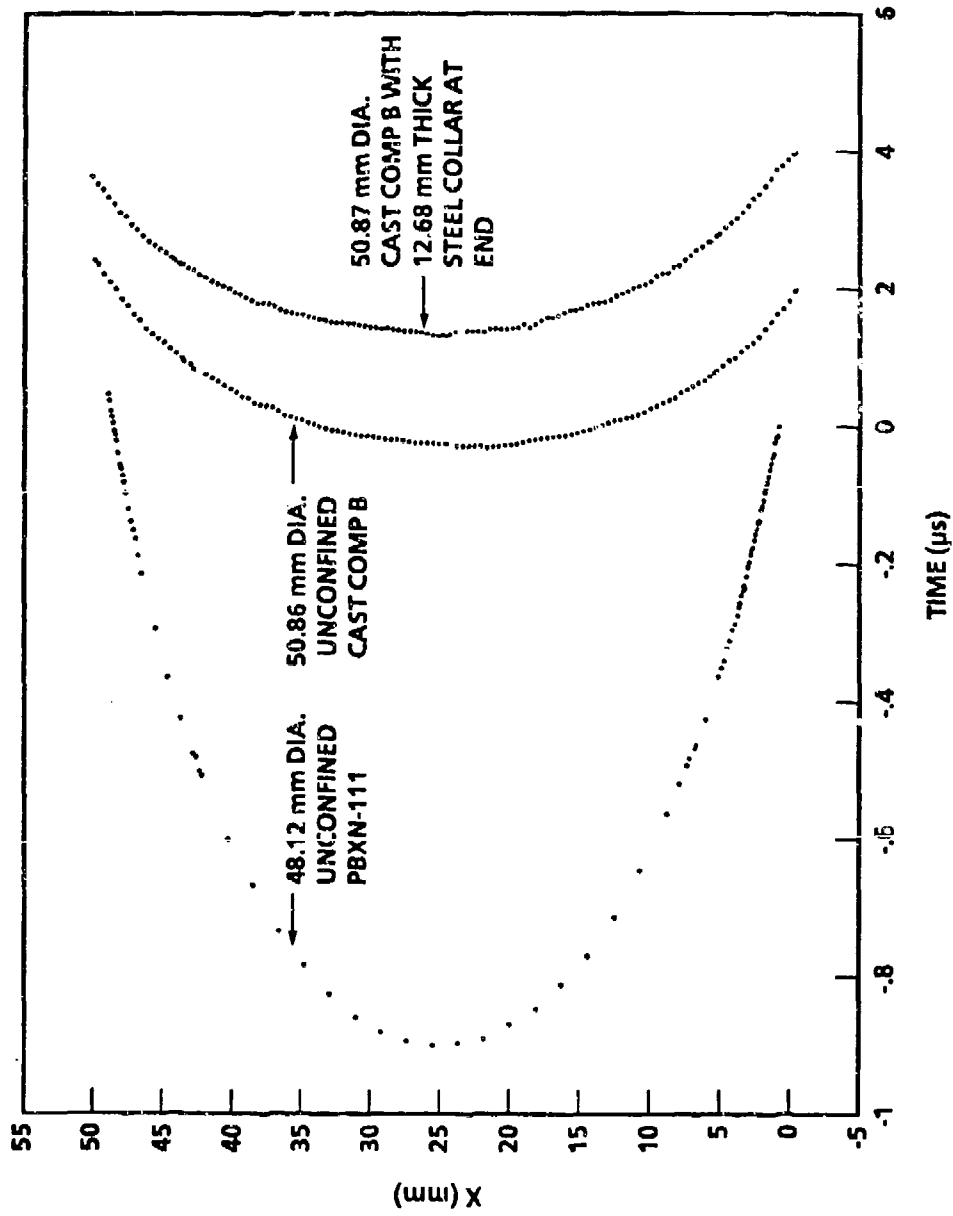


FIGURE 9. DETONATION WAVE BREAKOUT POSITIONS VERSUS TIME OF ARRIVAL PROFILES FOR CYLINDRICAL BOOSTERS SIMILAR TO THOSE USED IN CORNER TURNING EXPERIMENTS

TABLE 2. TIMES OF ARRIVAL FOR CORNER TURNING EXPERIMENTS*

	ANGLE θ (deg)							
	0	29	30	39	45	49	60	65
TIME ARRIVAL** (MICROSEC)								
A. Unconfined Bowl with an Unconfined PBXN-111 Cylindrical Booster	0.7	3.5			5.5		7.4	
B. Unconfined Bowl with a Brass Confined Cylindrical PBXN-111 Booster	0.6		2.4	3.1	3.6	4.0	5.0	
C. Unconfined Bowl with an Unconfined Cylindrical Comb B Booster	0.8		2.0		2.8		3.8	4.3
	0.6		2.2		3.1		4.2	4.7
D. Top of Bowl Confined by 1.27 cm Thick Steel Plate with Cylindrical Unconfined Comb B Booster	0.7		1.9		2.3		2.7	2.8

* Zero time is when wave arrives at center of bowl

**The error in time of arrival is $\pm 0.019 \mu\text{s}$ for one average deviation others are from in situ multiple manganin gauges.

NSWCDD/TR-92/164

initial densities of $1.67 \pm 0.005 \text{ g/cm}^3$ and a constant detonation velocity of $7.86 \pm 0.06 \text{ mm}/\mu\text{s}$.

UNREACTED HUGONIOT

Flat discs of PBXN-111 were shocked by the impact of 6061-T6 projectiles from a light gas gun. The induced stress was measured using either quartz stress gauges on the back surface of samples or in situ manganin stress gauges. Figure 10A and 10B give schematics of the experimental arrangements. Table 3 and Figure 11 give the results from these experiments. The unreacted Hugoniot for stresses up to 42 kbar can be expressed as

$$U_s = 2.117 \pm 0.034 \text{ mm}/\mu\text{s} + (2.758 \pm 0.081) u_p \quad (15)$$

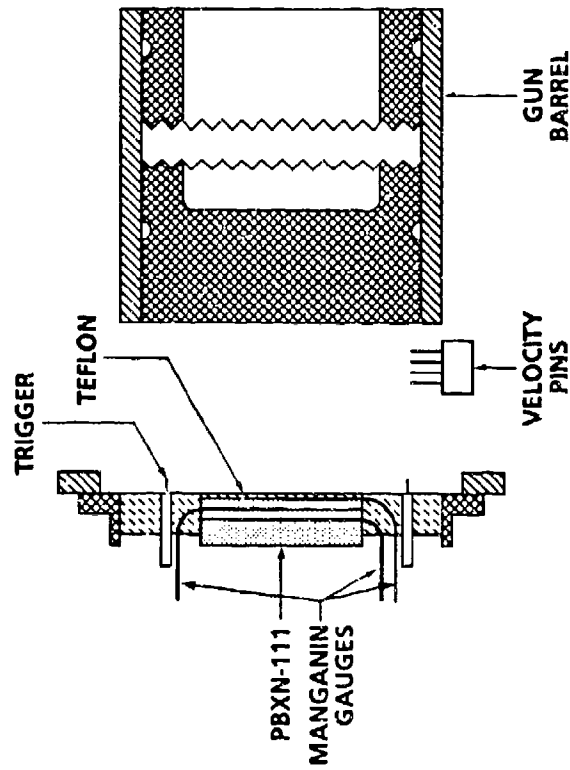
for an initial density of 1.79 g/cm³.

In all experiments, shock transit times, stress profiles and projectile velocities were measured. For the Teflon encapsulated manganin gauge experiments, the transit times through the Teflon layers were taken into account. Impedance matching was used to obtain particle velocities from the shock and projectile velocity data; the Hugoniots of Teflon¹⁶ and 6061-T6 aluminum¹⁷ were used. The in situ manganin gauges showed only a very slight increase in stress as a function of time for these experiments, which indicates that these were unreacted Hugoniot data.

The experiments at 39 and 42 kbar had an early step in the stress and then a second step increase followed by a rise in stress as a function of time. These records show that some low

PROJECTILE

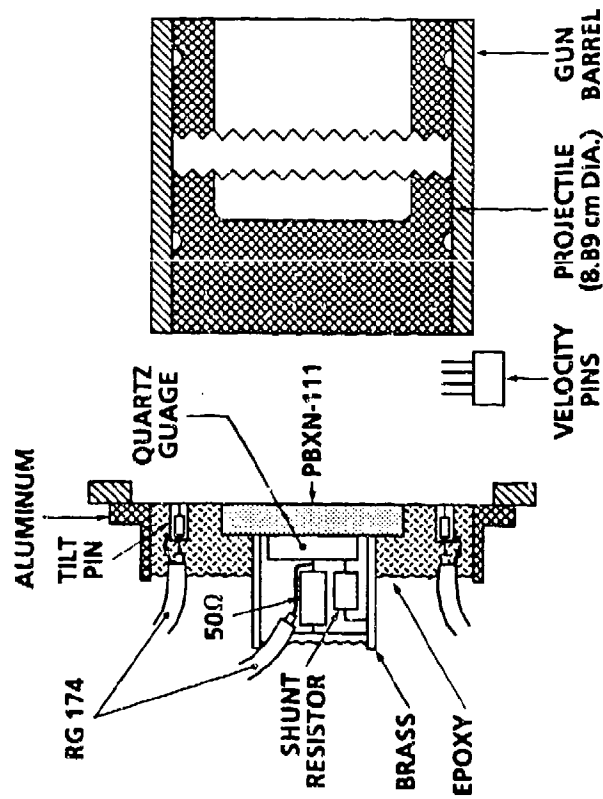
TARGET



B. MANGANIN GAUGE EXPERIMENTS

PROJECTILE

TARGET



A. QUARTZ GAUGE EXPERIMENTS

FIGURE 10. EXPERIMENTAL ARRANGEMENTS FOR HUGONIOT MEASUREMENTS

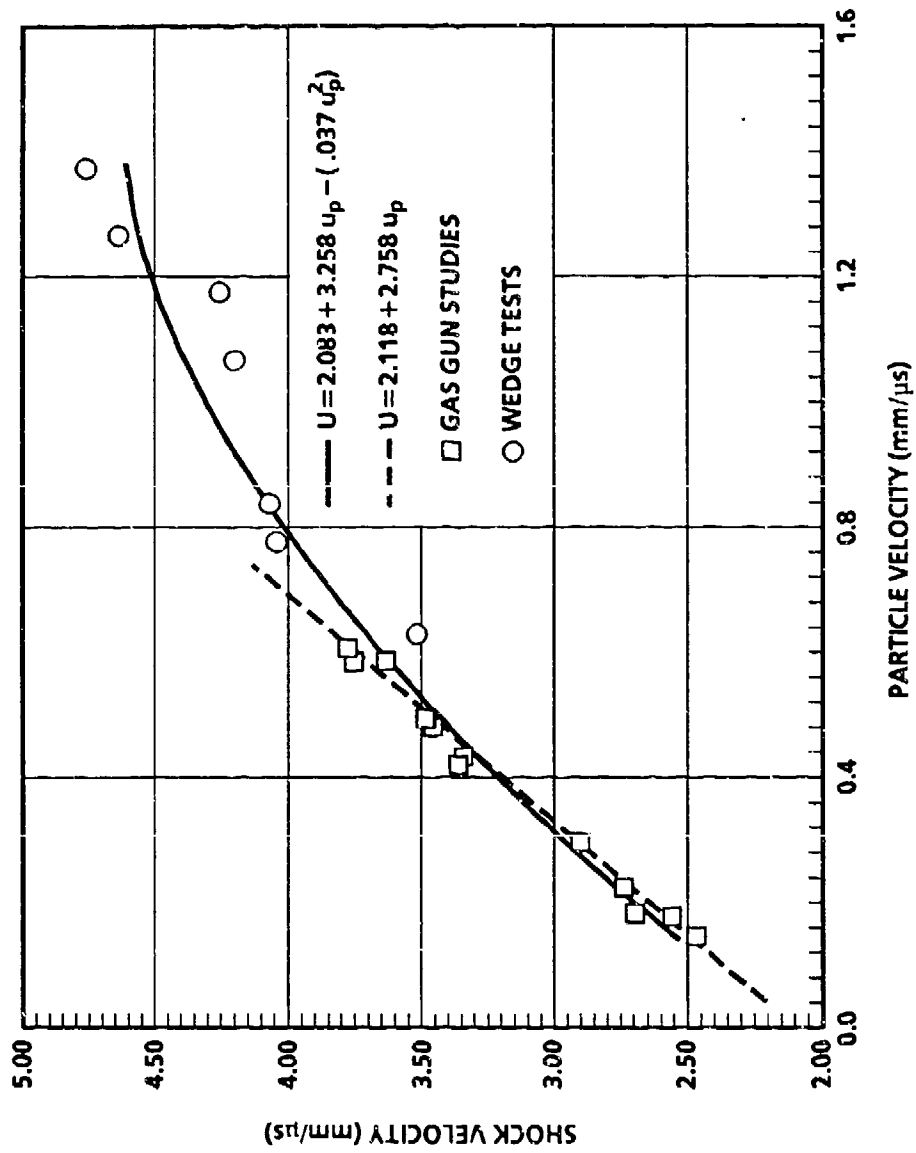


FIGURE 11. HUGONIOT OF PBXN-111

TABLE 3. UNREACTED HUGONIOT OF PBXN-111

SHOCK VELOCITY (mm/ μ s)	PARTICLE VELOCITY (mm/ μ s)	CALCULATED PEAK STRESS (kbar)	6061-T6 PROJECTILE VELOCITY (mm/ μ s)
3.788	0.615	42.0	0.8852
3.763	0.592	39.7	0.8512
3.653	0.591	39.6	0.8512
3.505	0.497	31.0	0.6985
3.479	0.488	30.2	0.6985
3.355	0.432	25.6	0.5990
3.371	0.420	24.6	0.5990
2.900	0.296	15.5	0.3936
2.741*	0.226	11.1	0.2947
2.702	0.186	8.8	0.2409
2.558	0.179	8.4	0.2409
2.469*	0.149	6.7	0.1886

*Quartz gauges were used on these experiments while all others are from in situ multiple manganin gauges.

level reaction was likely occurring. The shock velocity data from the first step in stress were used to obtain the unreacted Hugoniot for these two experiments reported in Table 3.

Figure 11 shows the data measured in this work along with wedge test results.¹⁸ Based on our manganin gauge results, the wedge test data above 30 kbar will be influenced by reaction.

MODIFIED GAS TEST RESULTS

Low level reactions in PBXN-111 for the stresses between 24 and 48 kbar have been found in the modified gap test (MGT).¹⁹ A free-surface velocity was measured in each MGT experiment for each input peak stress. At 24 kbar, an increase in free-surface velocity occurred relative to the inert velocity. The free-surface velocity increased slightly for increased input stresses from 24 to 48 kbar. These MGT results are consistent with and support the gas gun results for the 39 and 42 kbar input stresses discussed earlier.

DISCUSSION AND SUMMARY OF RESULTS

OVERVIEW

This study was undertaken to develop a data base on the detonation properties of PBXN-111 (formerly PBXW-115) and to improve our understanding of its divergent flow properties. This data base can be used to test curved wave front detonation theories and two-dimensional hydrodynamic flow detonation models which take into account the initiation and the growth of reactions and multiple energy release rates. A high speed streak camera was used to measure wave front curvature and the corner turning ability of PBXN-111. The unreacted Hugoniot was measured using quartz and multiple in situ manganin stress gauges. These Hugoniot samples were dynamically loaded by the impact of a projectile from a light gas gun.

CORNER TURNING

PBXN-111 corner turning experiments were performed on bowl-shaped charges with smaller diameter cylindrical booster charges centered on the flat top of the bowl. The symmetrical geometry and charge sizes were the same for all experiments. Experiments were performed on unconfined PBXN-111 charges that were initiated by cylindrical PBXN-111 boosters. These showed that a detonation wave in PBXN-111, that turns through angles from 0 to 65 degrees, arrived 3.5 to 7.4 μ s later at the curved surface, 5.1 cm away,

than the wave that did not turn but traveled a direct path of an equivalent distance of 5.1 cm. A stronger Comp B booster, with less wave front curvature, gave times of arrival differences of 2 to 4.7 μ s. The largest effect was found when the flat top of the PBXN-111 bowl had a steel plate against it (see Figure 6(D)). The differences in time of arrival for the wave front turning through 0 to 65 degrees, and the arrival time for the wave front with the direct (i. e., non-turning) path, were between 1.9 to 2.8 μ s.

DETONATION WAVE CURVATURE AND REACTION ZONE LENGTHS

The detonation waves' spherical curvatures for PBXN-111, over the center 50 percent of the charges, ranged from 54 to 143 mm for charge diameters of 41 to 68 mm. The curvature did not remain spherical near the edges of the charges. Note also that the wave fronts appear linear over about the last 3 mm at the charges' edges. The angle between the detonation wave front and the edge of the charge was about 62 degrees over this last 3 mm for all the charges. Detonation velocity and wave front curvature data of PBXN-111 were used to calculate reaction zone lengths of 2-4 mm using the Wood-Kirkwood theory.⁵ The calculated detonation zone length of the 38 mm failure diameter is 2.3 mm. These zone lengths are consistent with previously published calculations on ammonium perchlorate⁶ and two plastic-bonded TATB explosives.^{7,8}

ACCURACY OF VARIOUS MODELS

D. Price⁹ has pointed out that zone length is calculated well by the Wood-Kirkwood curved front theory. The reason for

these accurate predictions is not obvious since this theory treats the flow and its divergence only along the center line of the charge. More recent curved front theories^{20,21,22} treat the flow away from the center line which is a more correct approach. The accuracies of these recent theories are unknown at present because of insufficient data to test them. The application of this PBXN-111 detonation properties data base to these new theories is the subject of future work.

The accuracy of modeling detonation properties will improve if further theoretical and experimental research are done; this research will determine the constitutive relation (i.e., time dependent equation of state) of reacted and/or reacting products of composite explosives. The energy release rates of constituents in heterogeneous explosives are a function of particle size.²³ The particle size dependence of reaction rates needs to be part of any theoretical treatment of the constitutive relation. In addition, energy release and/or chemical reactions are likely to occur beyond the sonic CJ plane (the point in the flow where the sum of the particle velocity and the sound velocity equals the detonation velocity), and well into the product expansion wave in aluminized explosives. A number of studies on heterogeneous explosives strongly support the idea that energy is released beyond the sonic CJ plane.^{24,25,26} Moreover, conductivity studies^{27,28} of PBXN-111 show that conduction occurs long past the sonic CJ plane, which is consistent with late-time energy release and/or chemistry. The time-dependent equation resulting from the theoretical work will need to be calibrated by experimental data of explosive products expansion. A products expansion experiment can be suggested; stress gauges would be placed close to underwater explosive charges, and the stress and flow characteristics would be recorded for the necessary long times after the detonation.

Two-dimensional codes using phenomenological initiation models give reasonable predictions of detonation properties^{29,30,31} as expected. The detonation velocity as a function of charge diameter is required to determine the reaction rate model parameters for initiation in the CPEX code^{22,30,31} calculations. Reactive stress profiles of PBXN-111 at input stresses above 35 kbar are needed to determine the parameters for phenomenological ignition and growth models, such as the Lee-Tarver model.³² Reactive profiles of PBXN-111 for one-dimensional strain experiments, as described in the Hugoniot section, are currently being done by the authors. Therefore, reasonably accurate phenomenological modeling of PBXN-111 will be available soon.

PARTICLE SIZE, SHAPE, AND QUALITY EFFECTS

Phenomenological initiation models are not detailed enough to predict the large differences in detonation properties that result from the different initial physical states of the ingredients. Shock sensitivity has been shown to be a function of crystal size,^{33,34} shape,³⁵ and quality.³⁶ Akimova³⁷ has also observed that the addition of small particle size aluminum to cast TNT compositions decreases the failure diameter. Anderson^{38,39} has found that the failure diameter of PBXN-111 varies significantly with different particle sizes of RDX. The failure diameter of unconfined Australian³⁰ PBXN-111 is twice (80 mm versus 38 mm) that of PBXN-111 made in the United States.⁴ This is a dramatic result! The particle sizes of the ingredients for U. S. and Australian charges are about the same. This large difference in failure diameters is likely due to the types and densities of defects in the RDX, which strongly affect the initiation properties of the explosive. RDX used in Australian

PBXN-111 samples is HMX-free while US-made RDX typically has about 10 percent HMX. The presence of HMX is known⁴⁰ to be associated with a large number of defects in RDX.

The development of initiation models that take the physical state (i.e., size, shape, quality) of initial ingredients into account is suggested for future work. This will provide a predictive capability for hydrodynamic modeling of the detonation process.

SUMMARY

The major findings of this work are as follows: (1) PBXN-111 has large detonation wave front curvature with spherical radii ranging from 54 to 143 mm for charge diameters from 41 to 68 mm; (2) these curvature data imply that the sonic reaction zone length ranges from 2.6 to 4.1 mm according to Wood-Kirkwood curved-front theory; (3) the detonation wave fronts intersect the edges of the charges at angles of about 62 degrees; (4) detonation waves turning corners are delayed by a few microseconds and do not follow a simple spherical expansion process at the corners; (5) the unreacted Hugoniot was measured for stresses up to 40 kbar, however, evidence from the multiple stress gauge records indicates that significant low level reactions exists at 30 kbar; and (6) experimental and theoretical work on initiation models, that account for the initial physical state of explosive ingredients and the time-dependence of the explosive product expansion, are required before predictive modeling of detonation properties can be achieved.

REFERENCES

1. Dick, J. J., "Detonation Initiation Behavior of Some HMX/AP/Al Propellants," Comb. and Flame, Vol. 37, 1980., pp. 95-99.
2. Price, D. and Clairmont, Jr., A. R., "Explosive Behavior of Simplified Propellant Model," Comb. and Flame, Vol. 29, 1977, pp. 87-93.
3. Forbes, J. W., and Watt, J. W., Minimum Priming Charge Initiation Thresholds of Cast H-6, NAVSWC TR 90-168, 10 Aug 1990.
4. Forbes, J. W., Lemar, E. R., and R. N. Baker, "Detonation Wave Propagation in PBXW-115," Proc. Ninth Symposium (International) on Detonation, Portland, OR, Aug 1989, pp. 806-815.
5. Wood, W. W. and Kirkwood, J. G., "Diameter Effect in Condensed Explosives. The Relation Between Velocity and Radius of Curvature of the Detonation Wave," J. Chem. Phys., Vol 22, Nov 1954, pp. 1920-1924.
6. Erkman, J. O. and Price, D., Comparison of Curvature of Detonation Front in AP with that Found in Some Conventional Explosives, NOLTR 69-235, May 1970.
7. Campbell, A. W. and Engelke, R., "The Diameter Effect in High-Density Heterogeneous Explosives," Proc. Sixth Symposium (International) on Detonation, Coronado, CA, 24-27 Aug 1976, pp. 642-652.
8. Sheffield, S. A.; Bloomquist, D. D.; and Tarver, C. M., "Subnanosecond Measurements of Detonation Fronts in Solid High Explosives," J. Chem. Phys., Vol. 80, 1984, pp. 3831-3844.
9. Price, D., Review of Information on Composite Explosives: I. General Background, Final Progress Report, ATR 88-0046, Nov 1988.

10. Dick, R., "Pulsed High Energy Radiography Machine Emitting X-rays (PHERMEX): Applications to Study High Pressure Flow and Detonation Waves," Proc. First European Conf. on Cineradio-graphy on Photons and Particles, Paris, France, 1981, Pub. by SPIE, Vol. 312, 1983, pp. 66-81.
11. Mader, C., LASL PHERMEX Data, Vol. III, University of California Press, Berkeley, 1980.
12. Cox, M. and Campbell, A. W., "Corner-Turning in TATB," Proc. Seventh Symposium (International) on Detonation, Annapolis, MD, 16-19 Jun 1981, pp. 624-633.
13. Boggs, E. M.; Messerly, G. H.; and Strecker, H. A., "Initiation Studies on Solid Explosives," OSRD 5617, 14 Dec 1945.
14. Jackson, R. K., Green, L. G., Barlett, R. H., Hofer, W. W., Krammer, P. E., Lee, R. S., Nidick, Jr., E. J., Shaw, L. L., and Weingart, R. C., "Initiation and Detonation Characteristics of TATB," Proc. Sixth Symposium (International) on Detonation, Coronado, CA, 24-27 Aug 1976, pp. 755-765.
15. Held, M., Corner-Turning Distance and Retonation Radius," Prop. Expl., Pyrotech, 14, 1989, pp.153-161
16. Champion, A. R., "Shock Compression of Teflon from 2.5 to 25 Kbar - Evidence for a Shock-Induced Transition," J. Appl. Phys., 42, 1971, pp. 5546-5550.
17. Lundergan, C. D. Hermann, W., "Equation of State of 6061-T6 Aluminum at Low Pressures," J. Appl. Phys., 34, 1963, pp. 2046-2052.
18. Los Alamos National Laboratory Letter Report on Wedge Test of PBXW-115, J. C. Dallman, 17 Feb 1987.
19. Lemar, E. R., Liddiard, T. P. , Forbes, J. W., Sutherland, G. T., and Wilson, W. H., The Analysis of Modified Gap Test Data for Several Insensitive Explosives, NSWCTR 91-501, 1992.
20. Stewart, D. S., Bdzil, J. B., "Examples of Detonation Shock Dynamics For Detonation Wave Spread Application," Proc. Ninth Symposium (International) on Detonation, Portland, OR, Aug 1989, pp 773-783.

21. Lambourn, B. D., Swift, D. C., "Application of Whitham's Shock Dynamics Theory to the Propagation of Divergent Detonation Waves," Proc. Ninth Symposium (International) on Detonation, Portland, OR, Aug 1989, pp 784-797.
22. Kirby, I.J. and Leiper, G. A., "A Small Divergent Detonation Theory for Intermolecular Explosives," Proc. Eighth Symposium (International) on Detonation, Albuquerque, NM, July 1985, pp. 176-186.
23. Finger, M, Hornig, H. C., Lee, E. L., Kury, J. W., "Metal Acceleration by Composite Explosives," Proc. Fifth Symposium (International) on Detonation, Pasadena, CA 1970, pp 137-151.
24. Price, D., Review of Information on Composite Explosives: I. General Background, ATR-TR-88-0046, Nov 1988, Advanced Technology and Research Corp., MD.
25. Fluckiger, R., "Characterization and Performance Tests of Hexals," Proc. Int. Symp. Pyro. and Expls., Beijing, 1987, pp.270-275.
26. Gimenez, P, Bedoch, J. P., Saint-Martin, C., Baudin, G., and Longueville, Y., "F.P.I. Velocimetry Techniques Applied to Various Problems in Detonics," Proc. Ninth Symposium (International) on Detonation, Portland, OR, Aug 1989, pp. 1371-1377.
27. Tasker, D. G., Lee, R. J., "The Measurement of Electrical Conductivity in Detonating Condensed Explosives," Proc. Ninth Symposium (International) on Detonation, Portland, OR, Aug 1989, pp 396-406.
28. Tasker, D. G, Lee, R. J., Gustavson, P. K., The Measurement of Electrical Conductivity in Detonating Condensed Explosives, NSWCDD/TR-92/218, May 1992.
29. Tarver, C. M., "The Structure of Detonation Waves in Solid Explosives," Shock Waves in Condensed Matter-1991, Schmidt, Dick, Forbes, Tasker, eds., Elsevier Science Publications B.
30. Jones, D. A., Kennedy, D. L., Application of the CPEX non-ideal Explosive Model to PBXW-115, MRL-TR-91-40, 1990.V., 1992.
31. Kennedy, D. L., and Jones, D. A., "Modelling Shock Initiation and Detonation in the Non-Ideal Explosive PBXN-111," Proc. Tenth Symposium (International) on Detonation, Boston, MA, Aug. 1993.

32. Lee, E. L., Tarver, C. M., "Phenomenological Model of Shock Initiation in Heterogeneous Explosives," Phys. Fluids, 23(12), 1980, pp. 2362-2372.
33. Moulard, H., "Particular Aspect of the Explosive Particle Size Effect on Shock Sensitivity of Cast PBX Formulations," Proc. Ninth Symposium (International) on Detonation, Portland, OR, Aug 1989, pp 18-24.
34. Simpson, R. I., Helm, F. H., Crawford, P. C., and Kury, J. W., "Particle Size Effects in the Initiation of Explosives Containing Reactive and Non-Reactive Continuous Phases," Proc. Ninth Symposium (International) on Detonation, Portland, OR, Aug 1989, pp 25-38.
35. van der Steen, A. C., Verbeek, H. J. , and Meulenbrugge, J. J., " Influence of RDX Crystal Shape on the Shock Sensitivity of PBXs," Proc. Ninth Symposium (International) on Detonation, Portland, OR, Aug 1989, pp 83-88.
36. van der Steen, A., Duvalois, W, Hordjk, A., "Crystal Quality and Less Sensitive Explosives," Proc. Insens. Munitions Tech. Symp., 16-18 June 1992, Williamsburg, VA, pp. 203-210.
37. Akimova, L. N. and Stesik, L. N., "Detonation Capacity of Perchlorate Explosives," Combustion, Explosion and Shock Waves, Vol 12, 1976, p. 247.
38. Anderson, E. W., Detonation and Sensitivity Studies of RDX/Aluminum/Ammonium Perchlorate/HTPB Binder Explosives, NSWCDD/TR-92/364 (to be published in 1993).
39. Anderson, E. W., PBXN-111 Detonation and Sensitivity Studies, NSWCDD/TR-92/362 (to be published in 1993).
40. Gallagher, P. M., Krukonis, V. J., VandeKieft, L. J., "Gas Anti-Solvent Recrystallization: Application to the Separation and Subsequent Processing of RDX and HMX," Proc. Second International Symposium, Boston, MA, 1991, pp 45-47.

APPENDIX A

BREAKOUT POSITION VERSUS TIME DATA

The following tables contain the original breakout data generated in this study (Tables A-1 through A-26). The (t,X) data are the original data as read from the photographic records after converting to distance and time using the camera speed and optical magnification. The zero time and zero position are arbitrary. All other points are relative to this arbitrarily selected point. The (t,X) data can be converted to (Z,X) data for charges for which a steady detonation velocity is known. The photographic records were not always read with the same orientation. A standard orientation of the films in the reader was selected (see Figures A-1 to A-5). The top of the film in the reader with this standard film orientation is indicated in the tables by putting the word top at the beginning of the data. The few records that were read in an inverted orientation, as compared to the standard orientation, start the data tables with the word bottom. Knowing the orientation of the film in the reader was important only for the averaging of the multiple readings of a record for the angle the detonation wave makes with the edge of the charge. The least squares fit of the wave curvature data to a circle as described in the text was not affected by the films orientation in the reader. The cast Comp B cylindrical charges of Tables A-23 to A-26 had initial densities of $1.67 \pm 0.005 \text{ g/cm}^3$ and constant detonation velocities of $7.86 \pm 0.06 \text{ mm}/\mu\text{s}$.

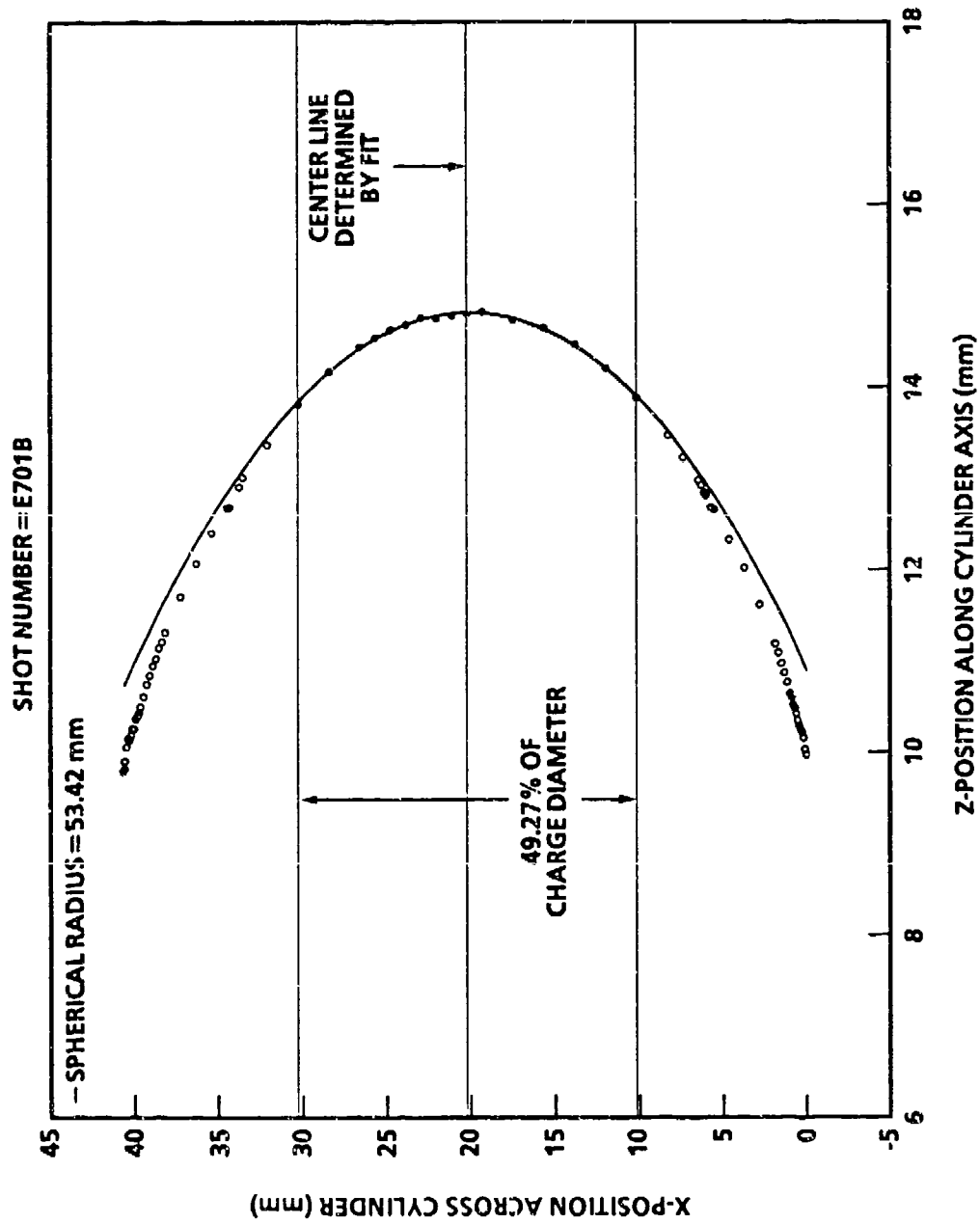


FIGURE A-1. DETONATION WAVE PROFILE FOR A 40.90 mm DIAMETER CYLINDRICAL PBXN-111 CHARGE

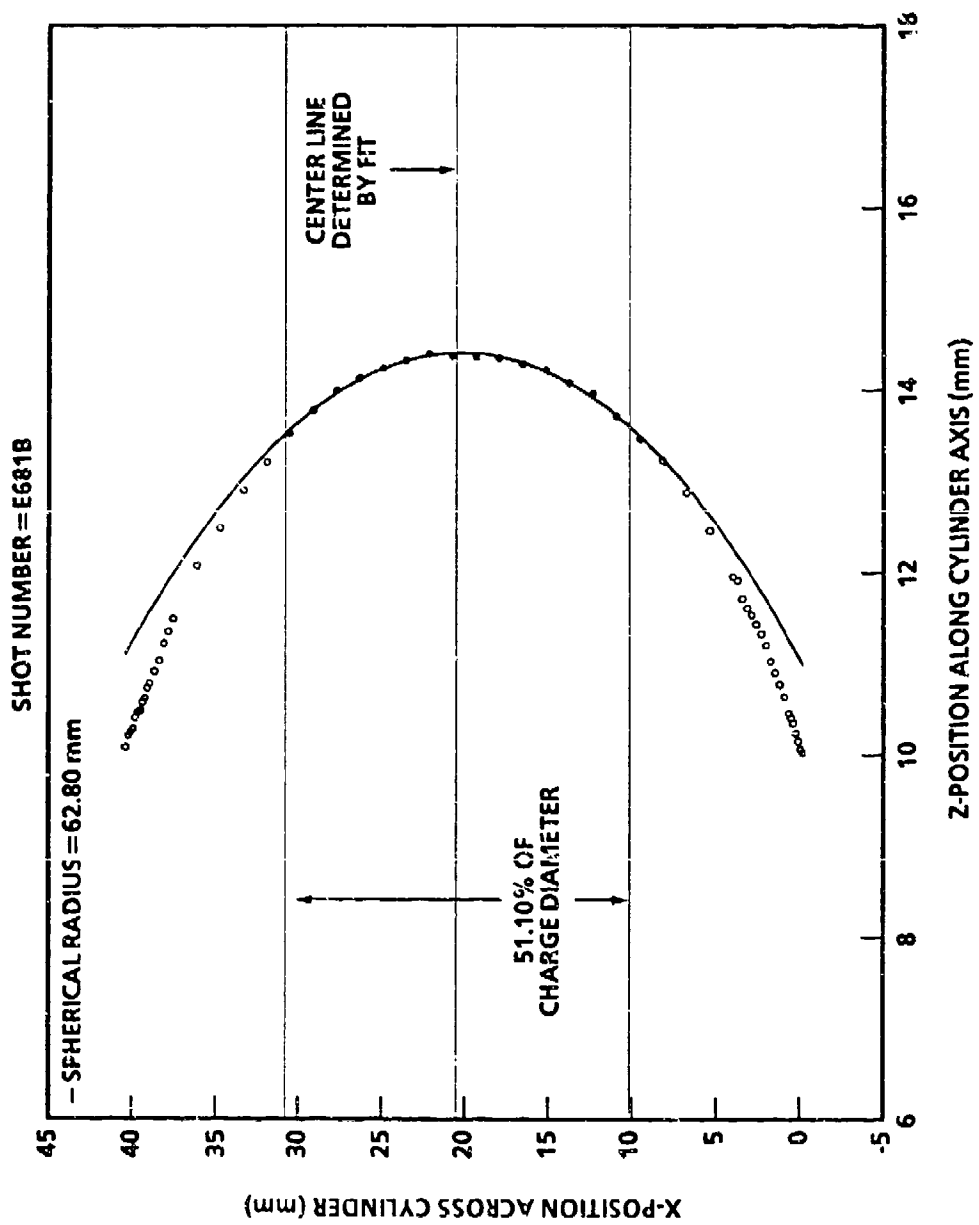


FIGURE A-2. DETONATION WAVE PROFILE FOR A 41.05 mm DIAMETER CYLINDRICAL PBXN-111 CHARGE

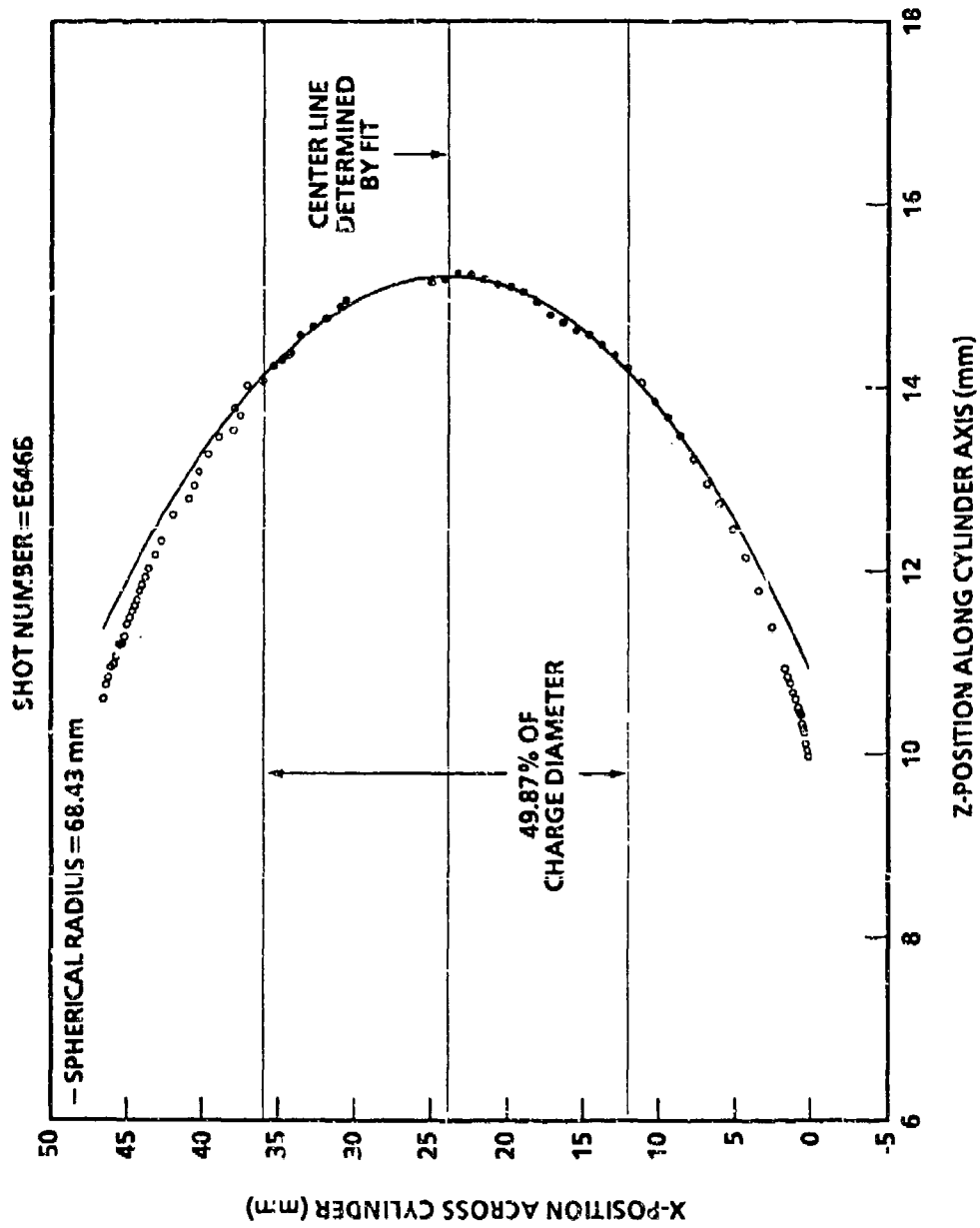


FIGURE A-3. DETONATION WAVE PROFILE FOR A 48.02 mm DIAMETER CYLINDRICAL PBXN-111 CHARGE

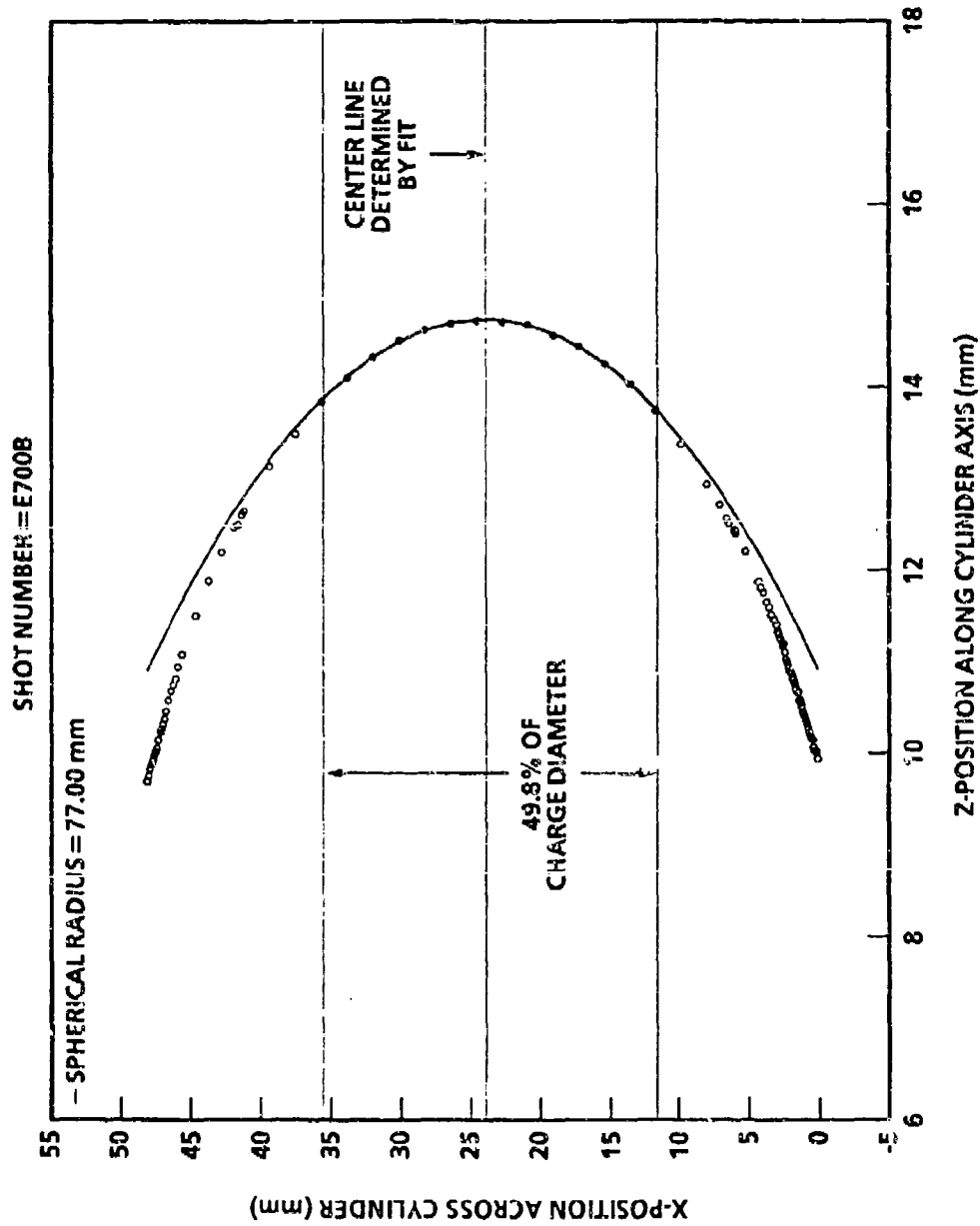


FIGURE A-4. DETONATION WAVE PROFILE FOR A 48.12 mm DIAMETER CYLINDRICAL PBXN-111 CHARGE

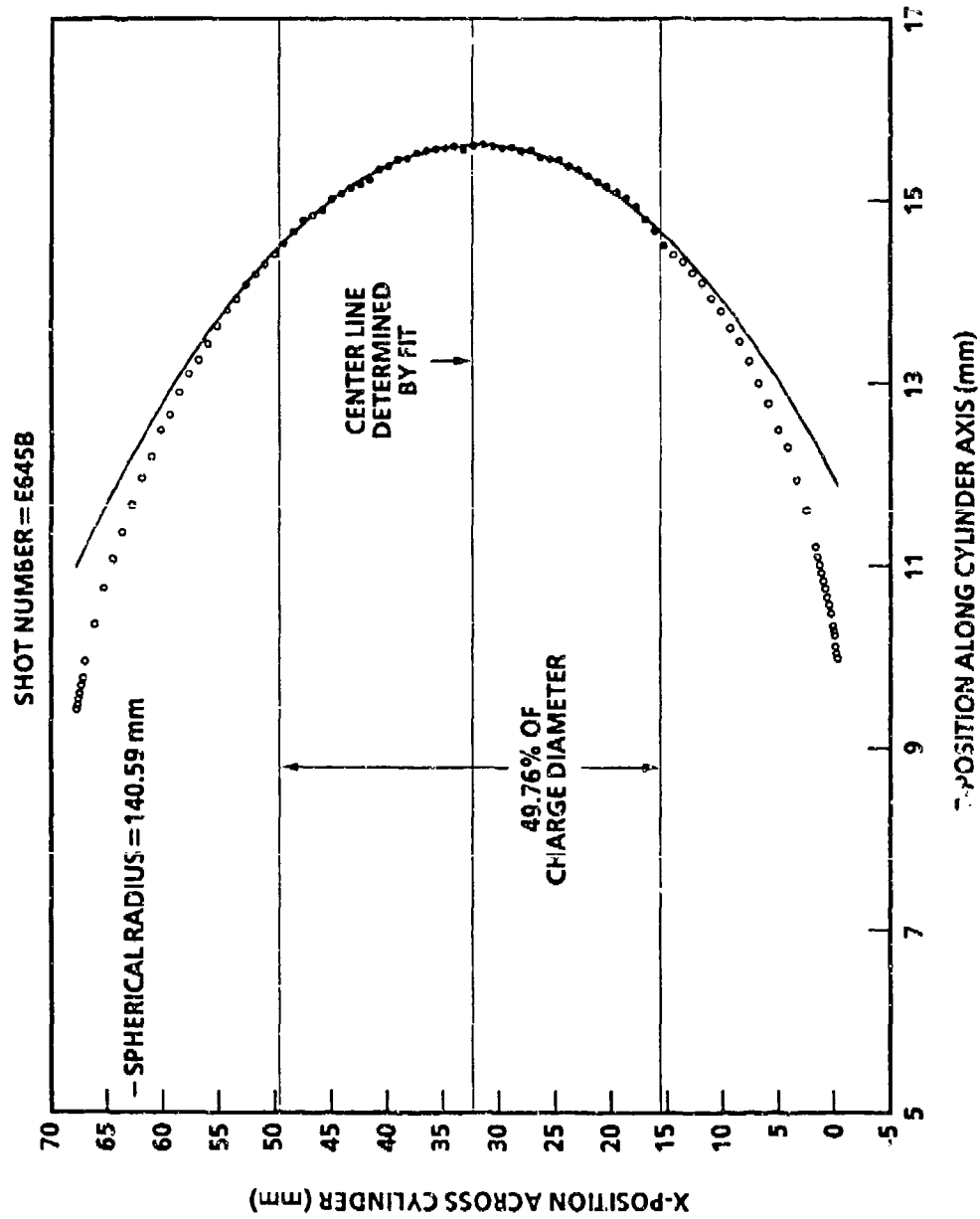


FIGURE A-5. DETONATION WAVE PROFILE FOR A 68.25 mm DIAMETER CYLINDRICAL PBXN-111 CHARGE

TABLE A-1. TIME VS. BREAKOUT POSITION DATA, SHOT E701, READING A FOR
40.90 mm DIA. UNCONFINED PBXN-111

Time (μ s)	X (mm)	Time (μ s)	X (mm)	Time (μ s)	X (mm)
	Top	-0.303733	3.004639	-0.820939	29.032660
-0.000000	0.000000	-0.339551	3.461271	-0.755035	30.859190
-0.011462	0.082194	-0.421215	4.374535	-0.673370	32.685720
-0.018625	0.173520	-0.481388	5.287800	-0.563052	34.512250
-0.022923	0.264846	-0.596005	7.114327	-0.441273	36.338780
-0.035818	0.356173	-0.694861	8.940855	-0.289406	38.165310
-0.041548	0.447500	-0.769362	10.767380	-0.196280	39.078570
-0.053010	0.538826	-0.830968	12.593910	-0.147568	39.535198
-0.058741	0.630152	-0.879680	14.420440	-0.094558	39.991840
-0.075933	0.721479	-0.912632	16.246970	-0.070202	40.174490
-0.093126	0.904132	-0.932690	18.073490	-0.061606	40.265820
-0.114616	1.086784	-0.939853	19.900020	-0.057308	40.357140
-0.130376	1.178111	-0.942719	21.726550	-0.045847	40.448470
-0.179088	1.634743	-0.928392	23.553080	-0.031519	40.539799
-0.224934	2.091375	-0.905468	25.379610		Bottom
-0.266483	2.548007	-0.866785	27.206140		

TABLE A-2. TIME VS. BREAKOUT POSITION DATA, SHOT E701, READING B FOR
40.90 mm DIA. UNCONFINED PBXN-111

Time (μ s)	X (mm)	Time (μ s)	X (mm)	Time (μ s)	X (mm)
Top		-0.581979	6.503561	-0.334818	37.280980
-0.000000	0.000000	-0.629400	7.419559	-0.257220	38.196970
-0.011496	0.091602	-0.675384	8.335553	-0.237103	38.380170
-0.035925	0.183203	-0.754418	10.167540	-0.224170	38.563360
-0.047421	0.274800	-0.817645	11.999530	-0.201178	38.746570
-0.053168	0.366402	-0.869377	13.831520	-0.186808	38.929770
-0.061790	0.457999	-0.903864	15.663510	-0.166690	39.112970
-0.071849	0.549601	-0.921108	17.495501	-0.148009	39.296160
-0.086219	0.641198	-0.938352	19.327480	-0.122144	39.479360
-0.097715	0.732799	-0.934041	20.243480	-0.100589	39.662560
-0.103463	0.824396	-0.929730	21.159470	-0.086219	39.754160
-0.120707	0.915998	-0.923982	22.075470	-0.080471	39.845760
-0.126455	1.007595	-0.925419	22.991460	-0.074723	39.937360
-0.150884	1.190794	-0.911049	23.907460	-0.053168	40.028960
-0.171001	1.373993	-0.900991	24.823450	-0.054605	40.120560
-0.191119	1.557191	-0.882310	25.739450	-0.040235	40.212160
-0.214111	1.740390	-0.863629	26.655440	-0.030177	40.303750
-0.232792	1.923589	-0.810460	28.487430	-0.033051	40.395360
-0.316137	2.839587	-0.741485	30.319420	-0.015807	40.486950
-0.393734	3.755580	-0.656703	32.151410	0.014370	40.578560
-0.454088	4.671574	-0.587727	33.617001	0.035925	40.670150
-0.518752	5.587567	-0.567610	33.827680	0.035925	40.660990
-0.523063	5.752447	-0.524500	34.377270	0.031614	40.596880
-0.548929	6.045566	-0.523063	34.532990	Bottom	
-0.554677	6.137163	-0.469894	35.448990		
-0.570484	6.320362	-0.403793	36.364980		

TABLE A-3. TIME VS. BREAKOUT POSITION DATA, SHOT E701, READING C FOR
40.80 mm DIA. UNCONFINED PBXN-111

Time (μ s)	X (mm)	Time (μ s)	X (mm)	Time (μ s)	X (mm)
Bottom		-0.684210	9.006919	-0.562029	33.746170
-0.000000	0.000000	-0.714396	9.923188	-0.500221	34.662430
-0.000000	0.027488	-0.754644	10.839460	-0.447036	35.578710
-0.011499	0.210742	-0.787704	11.755730	-0.386665	36.494970
-0.034498	0.393995	-0.819327	12.671990	-0.366541	36.678230
-0.061809	0.577249	-0.846638	13.588260	-0.350730	36.861490
-0.073308	0.760503	-0.863887	14.504530	-0.334918	37.044740
-0.091994	0.943756	-0.878261	15.420800	-0.324856	37.227990
-0.117868	1.127010	-0.891198	16.337070	-0.310482	37.411240
-0.135117	1.310263	-0.908447	17.253330	-0.298982	37.594501
-0.156678	1.493518	-0.902697	18.169610	-0.280296	37.777750
-0.181114	1.676772	-0.914196	19.085870	-0.258735	37.960999
-0.204113	1.860025	-0.912759	20.002140	-0.245798	38.144260
-0.217050	2.043279	-0.907010	20.918410	-0.224237	38.327510
-0.231424	2.226532	-0.908447	21.834680	-0.211300	38.510770
-0.247235	2.409786	-0.902697	22.750950	-0.194051	38.694020
-0.261609	2.593040	-0.899822	23.667210	-0.173927	38.877270
-0.288920	2.776294	-0.886886	24.583480	-0.158115	39.060530
-0.300420	2.959548	-0.869637	25.499750	-0.136354	39.243780
-0.309044	3.142801	-0.843763	26.416020	-0.113556	39.427030
-0.324856	3.326055	-0.822202	27.332290	-0.097744	39.610290
-0.340668	3.509308	-0.804953	28.248560	-0.076183	39.793550
-0.416851	4.425577	-0.767580	29.164820	-0.053184	39.976799
-0.472910	5.341845	-0.733082	30.081090	-0.030186	40.160050
-0.533281	6.258114	-0.692835	30.997370	-0.013499	40.343300
-0.586460	7.174383	-0.661212	31.913630	0.005750	40.526550
-0.633212	8.090651	-0.609464	32.829899		Top

TABLE A-4. TIME VS. BREAKOUT POSITION DATA, SHOT E681, READING 3 FOR
41.05 mm DIA. UNCONFINED PBXN-111

Time (μ s)	X (mm)	Time (μ s)	X (mm)	Time (μ s)	X (mm)
	Top	0.067184	13.490100	0.103133	28.283110
0.843921	0.000000	0.044200	14.628020	0.133188	29.421040
0.744324	0.972925	0.032413	15.765940	0.176210	30.558960
0.634119	2.110849	0.015323	16.903870	0.213927	31.696890
0.540416	3.248772	0.005893	18.041790	0.257537	32.834810
0.448480	4.386698	0.004125	19.179720	0.311756	33.972740
0.383654	5.524622	-0.000000	20.317640	0.378350	35.110660
0.309988	6.662548	0.004125	21.455570	0.447302	36.248580
0.264609	7.800472	0.022394	22.593490	0.537469	37.386510
0.212748	8.938395	0.017090	23.731420	0.619976	38.524430
0.161476	10.076320	0.034181	24.869340	0.718983	39.662360
0.124938	11.214240	0.060112	26.007270	0.812686	40.800290
0.088399	12.352170	0.076023	27.145190		Bottom

TABLE A-5. TIME VS. BREAKOUT POSITION DATA, SHOT E681, READING 4 FOR
41.05 mm DIA. UNCONFINED PBXN-111

Time (μ s)	X (mm)	Time (μ s)	X (mm)	Time (μ s)	X (mm)
	Top	0.077996	12.974770	0.101994	28.034770
0.855552	0.000000	0.051597	14.133230	0.136192	29.193230
0.836353	0.231691	0.039598	15.291690	0.169791	30.351690
0.715160	1.390152	0.017399	16.450150	0.211188	31.510150
0.605356	2.548613	0.010799	17.608620	0.259186	32.668620
0.510571	3.707075	0.004200	18.767080	0.314383	33.827080
0.427776	4.865536	0.002400	19.925540	0.374979	34.985540
0.359980	6.024000	-0.000000	21.084000	0.439776	36.144001
0.298783	7.182461	0.003600	22.242460	0.521971	37.302460
0.251986	8.340921	0.011999	23.400920	0.622765	38.460920
0.196789	9.499384	0.034798	24.559390	0.690562	39.619380
0.148792	10.657840	0.046797	25.717850	0.861552	40.725720
0.111594	11.816310	0.077396	26.876310		Bottom

TABLE A-6. TIME VS. BREAKOUT POSITION DATA, SHOT E681, READING 5 FOR
41.05 mm DIA. UNCONFINED PBXM-111

Time (μ s)	X (mm)	Time (μ s)	X (mm)	Time (μ s)	X (mm)
Bottom		-0.724161	12.067090	-0.331666	36.956340
-0.000000	0.000000	-0.758921	13.465350	-0.305596	37.235990
0.004345	0.041948	-0.777749	14.863640	-0.279526	37.515650
-0.008690	0.321603	-0.793681	16.261910	-0.263595	37.795300
-0.042001	0.601257	-0.824095	17.650180	-0.233180	38.074950
-0.065175	0.880913	-0.828441	19.058450	-0.221593	38.354610
-0.102831	1.160567	-0.818302	20.456720	-0.173799	38.634260
-0.133246	1.440221	-0.825544	21.855000	-0.144832	38.913910
-0.163660	1.719875	-0.809612	23.253270	-0.128901	39.193570
-0.176695	1.999529	-0.802371	24.651540	-0.102831	39.473230
-0.204213	2.279184	-0.779197	26.049810	-0.097037	39.613050
-0.221593	2.558839	-0.761818	27.448080	-0.082554	39.752880
-0.253456	2.838494	-0.727058	28.846360	-0.057933	39.892710
-0.279526	3.118148	-0.663331	30.244630	-0.043450	40.032530
-0.298354	3.397802	-0.614089	31.642900	-0.031863	40.172360
-0.320079	3.677456	-0.544569	33.041170	-0.014483	40.312180
-0.399737	5.075729	-0.490981	34.439450	-0.002896	40.452020
-0.482291	6.474000	-0.414220	35.837720	0.010138	40.591840
-0.564846	7.872274	-0.391047	36.117370	Top	
-0.612640	9.270544	-0.366426	36.397020		
-0.676366	10.668820	-0.347597	36.676680		

TABLE A-7. TIME VS. BREAKOUT POSITION DATA, SHOT E681, READING 6 FOR
41.05 mm DIA. UNCONFINED PBXN-111

Time (μ s)	X (mm)	Time (μ s)	X (mm)	Time (μ s)	X (mm)
	Top				
-0.000000	0.000000	-0.307231	3.481386	-0.340406	37.459710
-0.011539	0.139255	-0.328867	3.759896	-0.323097	37.738220
-0.011539	0.139255	-0.344734	4.038410	-0.304346	38.016730
-0.021636	0.278511	-0.357715	4.316921	-0.265402	38.295240
-0.036060	0.417769	-0.388006	4.595432	-0.245208	38.573750
-0.054811	0.696280	-0.406757	4.873942	-0.216360	38.852270
-0.092314	0.974790	-0.630329	9.051603	-0.196166	39.130780
-0.106738	1.253301	-0.809186	16.014380	-0.158664	39.409290
-0.132701	1.531812	-0.840919	22.977150	-0.138470	39.687801
-0.158664	1.810322	-0.701006	29.939920	-0.108180	39.966310
-0.174530	2.088833	-0.548112	34.117590	-0.082217	40.244820
-0.204821	2.367343	-0.468780	35.510140	-0.064908	40.384080
-0.230784	2.645854	-0.426950	36.206410	-0.054811	40.523340
-0.253862	2.924365	-0.376466	36.902690	-0.044714	40.662590
-0.294249	3.202875	-0.359158	37.181198		Bottom

TABLE A-8. TIME VS. BREAKOUT POSITION DATA, SHOT E681, READING B FOR
41.05 mm DIA. UNCONFINED PBXN-111

Time (μ s)	X (mm)	Time (μ s)	X (mm)	Time (μ s)	X (mm)
Top		-0.472241	5.580142	-0.556260	33.550810
-0.000000	0.000000	-0.551914	6.978681	-0.476587	34.949340
-0.007243	0.139850	-0.518549	8.377213	-0.396915	36.347870
-0.024626	0.279706	-0.664904	9.775745	-0.283924	37.746399
-0.042009	0.419353	-0.714156	11.174280	-0.256401	38.026110
-0.063738	0.559413	-0.761960	12.572810	-0.231775	38.305820
-0.075327	0.699263	-0.783689	13.971340	-0.195560	38.585520
-0.085467	0.839119	-0.812661	15.369880	-0.172383	38.865230
-0.120233	1.104841	-0.824249	16.768410	-0.146308	39.144930
-0.144859	1.384547	-0.837287	18.166940	-0.136168	39.284790
-0.169486	1.664254	-0.838735	19.565470	-0.114439	39.424640
-0.194111	1.943960	-0.841632	20.964010	-0.105747	39.564499
-0.228878	2.223666	-0.845978	22.362540	-0.088364	39.704350
-0.253504	2.503373	-0.832941	23.761070	-0.085467	39.844200
-0.273784	2.783079	-0.815558	25.159599	-0.073878	39.984050
-0.292616	3.062785	-0.795277	26.558140	-0.050701	40.123910
-0.307102	3.342492	-0.767754	27.956670	-0.043458	40.263760
-0.327382	3.622198	-0.725745	29.355210	-0.036215	40.403620
-0.366494	3.901904	-0.677941	30.753740	-0.011589	40.585420
-0.375186	4.181611	-0.615652	32.152270	Bottom	

TABLE A-9. TIME VS. BREAKOUT POSITION DATA, SHOT E681, READING C FOR
41.05 mm DIA. UNCONFINED PBXN-111

Time (μ s)	X (mm)	Time (μ s)	X (mm)	Time (μ s)	X (mm)
	Top	-0.805005	14.499110	-0.640541	31.212780
-0.000000	0.000000	-0.816546	15.891910	-0.592934	32.605590
-0.064920	0.571049	-0.825202	17.284720	-0.536670	33.998390
-0.183218	1.963860	-0.828087	18.677530	-0.468865	35.391201
-0.308730	3.356665	-0.835300	20.070330	-0.372206	36.784000
-0.416929	4.749470	-0.833858	21.463140	-0.278434	38.176810
-0.500603	6.142274	-0.829530	22.855950	-0.151479	39.569620
-0.569851	7.535082	-0.822317	24.248750	-0.004328	40.962420
-0.636213	8.927885	-0.797791	25.641560	0.038952	41.032060
-0.682378	10.320690	-0.763168	27.034360		Bottom
-0.732871	11.713500	-0.744413	28.427170		
-0.770381	13.106300	-0.688149	29.819970		

TABLE A-10. TIME VS. BREAKOUT POSITION DATA, SHOT E646, READING B FOR
48.02 mm DIA. UNCONFINED PBXN-111

Time (μs)	X (mm)	Time (μs)	X (mm)	Time (μs)	X (mm)
	Top	-0.848374	13.652780	-0.659210	38.783550
-0.000000	0.000000	-0.869870	14.515780	-0.624816	39.491210
-0.014331	0.086303	-0.878468	15.378790	-0.588989	40.121201
-0.027228	0.172601	-0.894232	16.241800	-0.560328	40.449150
-0.050157	0.258904	-0.909995	17.104799	-0.533100	40.802980
-0.060189	0.345203	-0.934358	17.967810	-0.500139	41.864480
-0.068787	0.431505	-0.955853	18.830820	-0.447116	42.563520
-0.087417	0.517804	-0.965885	19.693830	-0.418455	42.969130
-0.093149	0.604106	-0.971617	20.556830	-0.391226	43.409260
-0.103181	0.707668	-0.981649	21.419840	-0.372597	43.625020
-0.120377	0.880269	-0.991680	22.282850	-0.356833	43.858030
-0.134708	1.052871	-0.994546	23.145850	-0.343935	44.030630
-0.153338	1.225472	-0.981649	24.008860	-0.325306	44.203230
-0.166235	1.398073	-0.975916	24.871870	-0.313841	44.375830
-0.183432	1.570674	-0.940090	30.524570	-0.302376	44.548430
-0.269416	2.433681	-0.927192	30.912920	-0.289479	44.721030
-0.343935	3.296687	-0.902830	31.775930	-0.276581	44.893640
-0.412722	4.159698	-0.887067	32.638930	-0.250786	45.066240
-0.470045	5.022704	-0.869870	33.501940	-0.236456	45.238840
-0.523069	5.885710	-0.832610	34.106050	-0.233589	45.411440
-0.563194	6.748717	-0.828311	34.321800	-0.207794	45.584040
-0.614784	7.611723	-0.818279	34.710150	-0.192031	45.756640
-0.662075	8.474733	-0.806815	35.227950	-0.186298	45.929240
-0.700768	9.337740	-0.775288	35.875210	-0.164802	46.101850
-0.732296	10.200750	-0.766689	36.953970	-0.150472	46.248560
-0.770988	11.063750	-0.720831	37.816980	-0.121811	46.412530
-0.801083	11.926760	-0.705067	37.445880		
-0.828311	12.789770	-0.674973	37.920530		Bottom

TABLE A-11. TIME VS. BREAKOUT POSITION DATA, SHOT E646, READING C FOR
48.02 mm DIA. UNCONFINED PBXN-111

Time (μ s)	X (mm)	Time (μ s)	X (mm)	Time (μ s)	X (mm)
	Top	-0.858812	22.636290	-0.609526	35.872610
-0.000000	0.000000	-0.858812	22.931390	-0.585030	36.306580
-0.036906	0.286425	-0.847284	23.131020	-0.574943	36.740560
-0.115277	1.154381	-0.863135	23.512920	-0.554770	37.174540
-0.180120	2.022337	-0.854489	23.650470	-0.533155	37.608520
-0.422201	5.494160	-0.858812	23.825380	-0.502895	38.476470
-0.508659	7.230070	-0.855930	24.025010	-0.399146	40.212390
-0.546124	8.479927	-0.857371	23.990299	-0.259373	42.382280
-0.561974	8.748995	-0.789646	28.859530	-0.190207	43.250230
-0.642668	10.701890	-0.815583	29.033120	-0.126804	43.944590
-0.697425	11.569850	-0.746417	31.376600	-0.056197	44.552170
-0.703189	11.795520	-0.714716	32.296630	0.027378	45.420120
-0.716157	12.272890	-0.714716	32.713250	0.066284	45.854099
-0.724803	12.741590	-0.701747	33.043070	0.097985	45.940899
-0.732008	13.045370	-0.703189	33.320820	0.139773	46.114490
-0.746417	13.314440	-0.681574	33.702720	0.162828	46.183920
-0.752181	13.739740	-0.668605	34.136700		Bottom
-0.762268	14.312590	-0.657078	34.570680		
-0.756504	14.859400	-0.645550	35.004660		

TABLE A-12. TIME VS. BREAKOUT POSITION DATA, SHOT E646, READING 2 FOR
48.02 mm DIA. UNCONFINED PBXN-111

Time (μ s)	X (mm)	Time (μ s)	X (mm)	Time (μ s)	X (mm)
	Top	0.096275	15.047940	0.176744	33.766950
0.830553	0.000000	-0.000000	23.169320	0.211230	34.632770
0.760143	0.865818	0.008622	23.377120	0.244280	35.498590
0.612138	2.597454	0.017243	24.165010	0.308943	37.230220
0.494308	4.329096	0.002874	26.173710	0.412403	38.961860
0.390848	6.060732	0.028739	27.706210	0.497183	40.693501
0.323312	8.502344	0.034487	28.572030	0.596331	42.425140
0.185366	11.576000	0.056041	29.437850	0.740025	44.156780
0.172433	12.121470	0.086216	30.303670	0.925391	45.888410
0.136510	12.987290	0.090528	31.169490	1.005860	46.295350
0.113518	13.853110	0.117830	32.035310		Bottom
0.100586	14.718930	0.148005	32.901130		

TABLE A-13. TIME VS. BREAKOUT POSITION DATA, SHOT E700, READING A FOR
48.12 mm DIA. UNCONFINED PBXN-111

Time (μs)	X (mm)	Time (μs)	X (mm)	Time (μs)	X (mm)
	Top				
-0.000000	0.000000	-0.550321	7.442755	-0.695445	37.028840
-0.012932	0.138688	-0.636533	9.291884	-0.627912	38.877970
-0.020116	0.231142	-0.699755	11.141010	-0.541700	40.727110
-0.033048	0.323601	-0.758667	12.990150	-0.442556	42.576240
-0.033048	0.323601	-0.800336	14.839280	-0.310364	44.425370
-0.050290	0.508514	-0.842005	16.688410	-0.241394	45.349930
-0.064659	0.693427	-0.872180	18.537540	-0.158056	46.274502
-0.084775	0.878340	-0.886548	20.386670	-0.057475	47.199060
-0.096270	0.970794	-0.900917	22.235800	-0.041669	47.383980
-0.132192	1.433078	-0.903791	24.084930	-0.018679	47.568890
-0.169551	1.895358	-0.895170	25.934060	-0.001437	47.753799
-0.215530	2.357643	-0.887985	27.783190	0.012932	47.938720
-0.264384	2.819927	-0.867869	29.632320	0.031611	48.123630
-0.327606	3.744492	-0.842005	31.481450		Bottom
-0.393702	4.669057	-0.810394	33.330580		
-0.439682	5.593621	-0.755793	35.179720		

TABLE A-14. TIME VS. BREAKOUT POSITION DATA, SHOT E700, READING B FOR
48.12 mm DIA. UNCONFINED PBXN-111

Time (μ s)	X (mm)	Time (μ s)	X (mm)	Time (μ s)	X (mm)
	Top	-0.255467	2.768666	-0.733390	35.623540
-0.000000	0.000000	-0.261207	2.860957	-0.665936	37.469320
-0.014352	0.092287	-0.274124	2.953244	-0.599916	39.315090
-0.015787	0.184578	-0.285606	3.137821	-0.508063	41.160870
-0.022963	0.276864	-0.294217	3.322399	-0.500887	41.299301
-0.040186	0.369155	-0.310005	3.506977	-0.480794	41.576170
-0.044491	0.461442	-0.321486	3.691554	-0.475053	41.806890
-0.053103	0.553733	-0.340144	3.876137	-0.423386	42.729780
-0.061714	0.646020	-0.350190	4.060714	-0.364542	43.652670
-0.071760	0.738311	-0.363107	4.245292	-0.292782	44.575560
-0.080372	0.830598	-0.424821	5.168181	-0.213846	45.498450
-0.087548	0.922889	-0.462137	5.841890	-0.188012	45.775320
-0.094724	1.015175	-0.467877	5.897264	-0.163613	45.959900
-0.106205	1.107466	-0.482229	6.321793	-0.150697	46.144480
-0.114816	1.199753	-0.492276	6.469453	-0.137780	46.329050
-0.120557	1.292044	-0.519545	7.013958	-0.119122	46.513630
-0.136345	1.384331	-0.562601	7.936847	-0.096159	46.698210
-0.139215	1.476622	-0.644408	9.782628	-0.080372	46.790501
-0.147826	1.568913	-0.713298	11.628410	-0.070325	46.882790
-0.156438	1.661200	-0.769271	13.474190	-0.060279	46.975070
-0.165049	1.753491	-0.810892	15.319960	-0.054538	47.067370
-0.175095	1.845777	-0.846772	17.165740	-0.037315	47.251940
-0.179401	1.938068	-0.869735	19.011520	-0.020093	47.344230
-0.186577	2.030355	-0.891263	20.857300	-0.011482	47.436520
-0.196623	2.122646	-0.897004	22.703080	-0.005741	47.528810
-0.203799	2.214933	-0.899874	24.548860	0.005741	47.621101
-0.218151	2.307224	-0.894134	26.394640	0.014352	47.713390
-0.235374	2.399511	-0.881217	28.240420	0.022963	47.805680
-0.231068	2.491802	-0.859689	30.086201	0.037315	47.897960
-0.238244	2.510258	-0.825244	31.931970	0.047362	47.990260
-0.245420	2.676379	-0.782188	33.777750		Bottom

TABLE A-15. TIME VS. BREAKOUT POSITION DATA, SHOT E700, READING C FOR
48.12 mm DIA. UNCONFINED PBXN-111

Time (μs)	X (mm)	Time (μs)	X (mm)	Time (μs)	X (mm)
Bottom		-0.871608	17.531140	-0.448835	42.854940
-0.000000	0.000000	-0.890430	18.462170	-0.440147	43.041150
0.005791	0.027931	-0.907804	19.393190	-0.434356	43.227350
-0.021718	0.214135	-0.915043	20.324210	-0.415534	43.413550
-0.043436	0.400340	-0.913596	21.255230	-0.408295	43.599760
-0.066601	0.586544	-0.928074	22.186250	-0.392368	43.785970
-0.083975	0.772748	-0.935313	23.117280	-0.379338	43.972170
-0.095558	0.958953	-0.935313	24.048300	-0.367755	44.158370
-0.114380	1.145157	-0.935313	24.979320	-0.348933	44.344580
-0.136098	1.331361	-0.933866	25.910340	-0.335902	44.530780
-0.144785	1.517566	-0.923731	26.841370	-0.319976	44.716980
-0.163607	1.703770	-0.920835	27.772390	-0.302601	44.903190
-0.179534	1.889975	-0.907804	28.703410	-0.291019	45.089390
-0.199804	2.076179	-0.896221	29.634430	-0.275092	45.275600
-0.218626	2.262383	-0.884638	30.565450	-0.257718	45.461800
-0.236000	2.448588	-0.867264	31.496470	-0.243239	45.648010
-0.253374	2.634793	-0.849890	32.427502	-0.227313	45.834210
-0.319976	3.565815	-0.832516	33.358520	-0.208491	46.020420
-0.388025	4.496836	-0.807902	34.289540	-0.192564	46.206620
-0.445059	5.427858	-0.781841	35.220560	-0.170847	46.392820
-0.506749	6.358880	-0.747093	36.151580	-0.157816	46.579030
-0.553080	7.289902	-0.725375	37.082600	-0.131755	46.765230
-0.597963	8.220925	-0.690626	38.013630	-0.117276	46.951440
-0.647191	9.151945	-0.651534	38.944650	-0.095559	47.137640
-0.677596	10.082970	-0.615338	39.875670	-0.075288	47.323850
-0.713792	11.013990	-0.570454	40.806690	-0.053571	47.510050
-0.748540	11.945010	-0.521227	41.737720	-0.036196	47.696260
-0.781841	12.876040	-0.502405	41.923920	-0.021718	47.882460
-0.797767	13.807600	-0.498062	42.110130	-0.007239	48.068660
-0.825276	14.738000	-0.483563	42.296330	Top	
-0.845546	15.669100	-0.479239	42.482540		
-0.857129	16.600120	-0.463313	42.668740		

TABLE A-16. TIME VS. BREAKOUT POSITION DATA, SHOT E645, READING B FOR
68.25 mm DIA. UNCONFINED PBXN-111

Time (μs)	X (mm)	Time (μs)	X (mm)	Time (μs)	X (mm)
Top		-0.887457	18.109830	-0.871712	46.976890
-0.000000	0.000000	-0.904634	18.958870	-0.860261	47.825930
-0.010020	0.110374	-0.916085	19.807899	-0.838790	48.674960
-0.022902	0.195279	-0.927536	20.656930	-0.815888	49.523990
-0.044373	0.280180	-0.936124	21.505960	-0.794417	50.373020
-0.054393	0.365085	-0.947575	22.354990	-0.775810	51.222050
-0.062981	0.449986	-0.959027	23.204020	-0.755770	52.071080
-0.087315	0.619792	-0.966183	24.053050	-0.735731	52.920120
-0.104491	0.789598	-0.979066	24.902090	-0.707103	53.769140
-0.118805	0.959404	-0.980497	25.751120	-0.685633	54.618170
-0.137413	1.129211	-0.983360	26.600150	-0.654142	55.467201
-0.151726	1.299017	-0.997674	27.449180	-0.618357	56.316240
-0.167472	1.468823	-0.996243	28.298210	-0.586867	57.165270
-0.183217	1.638633	-1.003399	29.147240	-0.559671	58.014301
-0.198962	1.808439	-1.001968	29.996270	-0.523886	58.863330
-0.219002	1.978245	-1.004631	30.845301	-0.479513	59.712360
-0.290571	2.827275	-1.009125	31.694340	-0.449454	60.561390
-0.330333	3.676306	-1.006262	32.543370	-0.396493	61.410430
-0.415101	4.525336	-0.999105	33.392399	-0.354983	62.259460
-0.448023	5.374367	-1.004831	34.241430	-0.302022	63.108480
-0.500984	6.223400	-1.001968	35.090460	-0.247629	63.957520
-0.539632	7.072431	-1.000537	35.939490	-0.194668	64.806550
-0.584004	7.921462	-0.997674	36.788520	-0.135931	65.655580
-0.622651	8.770491	-0.991949	37.637550	-0.065844	66.504610
-0.648417	9.619522	-0.981929	38.486580	0.005725	67.353640
-0.682770	10.468560	-0.979066	39.335610	0.038647	67.523450
-0.707103	11.317590	-0.966183	40.184640	0.052961	67.693250
-0.737162	12.166620	-0.960458	41.033670	0.070138	67.863060
-0.758633	13.015650	-0.940419	41.882710	0.078726	67.947960
-0.778672	13.864680	-0.931830	42.731740	0.091608	68.032870
-0.792986	14.713710	-0.924674	43.580770	0.100197	68.117770
-0.811594	15.562740	-0.913222	44.429798	Bottom	
-0.840222	16.411770	-0.903203	45.278830		
-0.863124	17.260799	-0.883163	46.127860		

TABLE A-17. TIME VS. BREAKOUT POSITION DATA, SHOT E645, READING 2 FOR
68.25 mm DIA. UNCONFINED PBXN-111

Time (μ s)	X (mm)	Time (μ s)	X (mm)	Time (μ s)	X (mm)
	Top	0.044474	27.594360	0.041605	42.915100
1.103245	0.000000	0.053082	28.445510	0.050213	44.617410
1.077422	0.357483	0.037301	30.147820	0.124815	48.873170
0.916741	2.059788	0.021520	31.850120	0.196547	53.128930
0.789057	3.762093	0.014347	32.701270	0.314189	57.384701
0.639854	6.315552	-0.000000	35.254730	0.500693	61.640460
0.443307	10.571310	0.007173	36.105880	0.743148	65.895220
0.291234	14.827090	0.012912	37.808190	1.001386	68.449680
0.182201	19.082840	0.014347	39.510490		Bottom
0.086080	23.338600	0.022955	40.361650		
0.077472	25.892060	0.008608	41.212799		

TABLE A-18. TIME VS. BREAKOUT POSITION DATA, SHOT E645, READING 3 FOR
68.25 mm DIA. UNCONFINED PBXN-111

Time (μ s)	X (mm)	Time (μ s)	X (mm)	Time (μ s)	X (mm)
Bottom		-0.792308	15.628340	-0.695791	53.225230
-0.000000	0.000000	-0.822560	16.482820	-0.666979	54.079700
-0.004322	0.076901	-0.839846	17.337290	-0.638168	54.934180
-0.018727	0.247800	-0.862896	18.191760	-0.612238	55.788660
-0.041776	0.418691	-0.888826	19.046240	-0.574784	56.643130
-0.059063	0.589590	-0.897469	19.900710	-0.551735	57.497610
-0.077790	0.760480	-0.904672	20.755190	-0.518602	58.352080
-0.086434	0.931379	-0.898910	21.609670	-0.472504	59.206550
-0.106602	1.102270	-0.924839	22.464140	-0.427847	60.061030
-0.123888	1.273169	-0.933483	23.318620	-0.391832	60.915510
-0.139735	1.444059	-0.943567	24.173090	-0.345734	61.769970
-0.152699	1.614958	-0.943567	25.027560	-0.327007	62.197220
-0.168546	1.785849	-0.950770	25.882040	-0.299636	62.624450
-0.195916	1.956748	-0.966616	26.736510	-0.283790	62.795350
-0.206000	2.127639	-0.973819	27.590990	-0.278028	62.966250
-0.226168	2.298537	-0.972378	28.445460	-0.267944	63.137130
-0.237692	2.469428	-0.972378	29.299940	-0.254979	63.308030
-0.249217	2.640327	-0.975259	30.154410	-0.237692	63.478930
-0.263623	2.811218	-0.968057	31.008890	-0.231530	63.649820
-0.270825	2.982116	-0.979581	31.863360	-0.230490	63.820720
-0.286672	3.153007	-0.970938	32.717830	-0.221846	63.991600
-0.295315	3.323906	-0.981021	33.572310	-0.210322	64.162498
-0.309721	3.494797	-0.968057	34.426790	-0.201679	64.333410
-0.321245	3.665696	-0.965175	35.281260	-0.185832	64.504303
-0.332769	3.836594	-0.963735	36.135740	-0.174308	64.675180
-0.341413	4.007485	-0.963735	36.990210	-0.169986	64.846090
-0.363021	4.178384	-0.953651	37.844680	-0.155581	65.016980
-0.373105	4.349275	-0.946448	38.699160	-0.142615	65.187880
-0.371665	4.520174	-0.937805	39.553630	-0.129651	65.358760
-0.400476	4.947404	-0.929161	40.408110	-0.118126	65.529660
-0.429287	5.374644	-0.924839	41.262580	-0.109482	65.700560
-0.449455	5.801882	-0.926280	42.117060	-0.087874	65.871460
-0.476826	6.229121	-0.908994	42.971540	-0.074909	66.042350
-0.494112	6.656360	-0.888826	43.826010	-0.063385	66.213250
-0.512839	7.083591	-0.887385	44.680480	-0.051860	66.384140
-0.556056	7.938069	-0.860015	45.534950	-0.038895	66.555040
-0.581986	8.792548	-0.855693	46.389430	-0.021009	66.725920
-0.615119	9.647016	-0.835525	47.243910	-0.014406	66.913910
-0.645371	10.501500	-0.819579	48.098380	0.005762	67.067720
-0.681385	11.355970	-0.799511	48.952860	0.015846	67.238620
-0.707315	12.210440	-0.777903	49.807330	0.027371	67.409500
-0.731805	13.064920	-0.754854	50.661810	0.048979	67.580399
-0.760616	13.919390	-0.739007	51.516280		
-0.786546	14.773870	-0.718840	52.370750		

Top

TABLE A-19. TIME VS. BREAKOUT POSITION DATA, SHOT E647, READING B FOR
48.45 mm DIA. PBXN-111 CONFINED BY 17.1 mm THICK BRASS

Time (μ s)	X (mm)	Time (μ s)	X (mm)	Time (μ s)	X (mm)
	Top	-0.490963	16.214780	-0.459380	37.002960
-0.000000	0.000000	-0.508189	17.308890	-0.439282	38.097080
-0.020096	0.109409	-0.525416	18.403010	-0.406264	39.191190
-0.050244	0.218823	-0.542643	19.497120	-0.384730	40.285310
-0.034453	0.328232	-0.545513	20.591240	-0.337357	41.379420
-0.180881	4.081045	-0.552691	21.685360	-0.307210	42.473540
-0.199543	4.825046	-0.565612	22.779470	-0.261272	43.567650
-0.208157	4.978222	-0.567048	23.873580	-0.213898	44.661760
-0.223947	5.459634	-0.562740	24.967699	-0.190930	45.208820
-0.233996	5.787865	-0.555562	26.061810	-0.167960	45.755880
-0.245481	6.367746	-0.556998	27.155930	-0.157911	45.974701
-0.288548	7.461359	-0.561305	28.250040	-0.137814	46.193530
-0.327308	8.555979	-0.554127	29.344160	-0.123458	46.412350
-0.344535	9.650092	-0.542643	30.438270	-0.113409	46.631170
-0.368940	10.744210	-0.532594	31.532390	-0.066036	46.849998
-0.397651	11.838320	-0.516802	32.626499	-0.087569	47.068820
-0.429233	12.932440	-0.508189	33.720620	-0.070342	47.287650
-0.462251	14.026550	-0.486656	34.814730	-0.060293	47.506470
-0.482349	15.120670	-0.472300	35.908850		Bottom

TABLE A-20. TIME VS. BREAKOUT POSITION DATA, SHOT E647, READING C FOR
48.45 mm DIA. PBXN-111 CONFINED BY 17.1 mm THICK BRASS

Time (μs)	X (mm)	Time (μs)	X (mm)	Time (μs)	X (mm)
Top		-0.545986	15.172920	-0.541686	30.932750
0.000000	0.000000	-0.553151	15.716360	-0.535954	31.476200
-0.045857	0.499967	-0.558863	16.259800	-0.533088	32.019640
-0.081683	1.043410	-0.563182	16.803250	-0.525923	32.563080
-0.110343	1.586852	-0.568914	17.346690	-0.518758	33.106520
-0.146169	2.130295	-0.573213	17.890130	-0.515892	33.649970
-0.179129	2.673738	-0.577512	18.433580	-0.505861	34.193410
-0.210656	3.217181	-0.581811	18.977020	-0.492963	34.736850
-0.232151	3.760623	-0.583244	19.520460	-0.478633	35.280290
-0.257946	4.304066	-0.587543	20.063900	-0.464303	35.823740
-0.283741	4.847508	-0.588977	20.607340	-0.451405	36.367180
-0.300937	5.390951	-0.594709	21.150790	-0.435642	36.910620
-0.319566	5.934394	-0.596142	21.694230	-0.422745	37.454060
-0.341062	6.477836	-0.593276	22.237670	-0.415579	37.997510
-0.361124	7.021279	-0.596142	22.781120	-0.404115	38.540950
-0.375455	7.564721	-0.600441	23.324560	-0.384053	39.084390
-0.391218	8.108164	-0.600441	23.868000	-0.374022	39.627840
-0.398383	8.651606	-0.599008	24.411440	-0.363990	40.171280
-0.411280	9.195049	-0.597575	24.954880	-0.346794	40.714720
-0.435642	9.738491	-0.594709	25.498330	-0.326732	41.258160
-0.462870	10.281930	-0.593276	26.041770	-0.309535	41.801610
-0.470035	10.825380	-0.591843	26.585210	-0.290906	42.345050
-0.482932	11.368820	-0.590410	27.128660	-0.262245	42.888490
-0.495829	11.912260	-0.581811	27.672100	-0.252214	43.431940
-0.508727	12.455710	-0.576079	28.215540	-0.230718	43.975380
-0.514459	12.999150	-0.568914	28.758980	-0.209223	44.518820
-0.521624	13.542590	-0.564615	29.302430	0.002866	48.279440
-0.528789	14.086030	-0.563182	29.845870	Bottom	
-0.540253	14.629480	-0.551718	30.389310		

TABLE A-21. TIME VS. BREAKOUT POSITION DATA, SHOT E648, READING B FOR
67.92 mm DIA. PBXN-111 CONFINED BY 7.3 mm THICK BRASS

Time (μ s)	X (mm)	Time (μ s)	X (mm)	Time (μ s)	X (mm)
Top		-0.262849	6.250362	-0.619059	44.924480
-0.000000	0.000000	-0.290139	7.306165	-0.597514	46.033070
-0.012927	0.105583	-0.321738	8.361967	-0.581714	46.698220
-0.014363	0.211161	-0.354774	9.417776	-0.512771	50.889770
-0.018672	0.316744	-0.386373	10.473580	-0.515643	51.491570
-0.021545	0.422321	-0.409355	11.529380	-0.498407	52.114498
-0.024418	0.527904	-0.435209	12.585190	-0.479735	52.864120
-0.033036	0.633482	-0.463935	13.640990	-0.456754	53.962160
-0.038781	0.739065	-0.478299	14.696800	-0.435209	54.912390
-0.047399	0.844643	-0.496971	15.752600	-0.409355	55.873160
-0.051708	0.971340	-0.514207	16.808410	-0.386373	56.928970
-0.064635	1.182501	-0.534316	17.864210	-0.360520	57.984770
-0.071817	1.393661	-0.548679	18.920010	-0.328920	59.040580
-0.078998	1.604822	-0.570224	19.975820	-0.291575	60.096380
-0.089053	1.815983	-0.586024	21.031620	-0.272903	60.624280
-0.099107	2.027143	-0.607569	22.087430	-0.258540	61.152180
-0.110598	2.238304	-0.624804	23.143230	-0.173796	62.746450
-0.116343	2.449465	-0.629113	24.199040	-0.093362	64.541310
-0.132143	2.660625	-0.642041	24.547450	-0.076126	65.217030
-0.136452	2.871786	-0.650659	32.919980	0.010054	66.832410
-0.140761	3.082947	-0.663586	40.088890	Bottom	
-0.188160	4.138755	-0.639168	43.298530		
-0.235559	5.194558	-0.621932	44.122060		

TABLE A-22. TIME VS. BREAKOUT POSITION DATA, SHOT E648, READING C FOR
67.92 mm DIA. PBXN-111 CONFINED BY 7.3 mm THICK BRASS

Time (μs)	X (mm)	Time (μs)	X (mm)	Time (μs)	X (mm)
	Top	-0.621415	17.894730	-0.594458	51.187250
0.000000	0.000000	-0.635602	18.414930	-0.588783	51.707450
-0.032631	0.208078	-0.644115	18.935120	-0.578852	52.227640
-0.045400	0.728274	-0.651209	19.455320	-0.577433	52.747840
-0.083707	1.248470	-0.658303	19.975510	-0.563246	53.268030
-0.131944	1.768665	-0.669653	20.495710	-0.557571	53.788230
-0.174507	2.288861	-0.681002	21.015900	-0.541964	54.308420
-0.191532	2.809056	-0.692353	21.536100	-0.534871	54.828620
-0.205719	3.329252	-0.699446	22.056290	-0.516427	55.348810
-0.222745	3.849448	-0.700865	22.576490	-0.505077	55.869010
-0.251120	4.369643	-0.713634	23.096690	-0.492308	56.389198
-0.286589	4.889839	-0.715053	23.616880	-0.473864	56.909401
-0.306451	5.410034	-0.720728	24.137080	-0.465352	57.429590
-0.322057	5.930230	-0.744847	24.657270	-0.446908	57.949790
-0.349014	6.450426	-0.749103	25.177470	-0.429883	58.469990
-0.374551	6.970621	-0.750521	25.697660	-0.415695	58.990180
-0.387320	7.490817	-0.756197	26.223610	-0.394414	59.510370
-0.407183	8.011012	-0.750521	28.298640	-0.384483	60.030580
-0.421370	8.531208	-0.774640	30.296190	-0.368876	60.550770
-0.434139	9.051404	-0.759034	31.190930	-0.360364	61.070960
-0.455420	9.571599	-0.774640	32.158490	-0.341920	61.591160
-0.466770	10.091800	-0.740590	34.384930	-0.323476	62.111360
-0.475283	10.611990	-0.742009	42.687250	-0.299357	62.631550
-0.489470	11.132190	-0.734915	43.280280	-0.290845	63.151750
-0.499402	11.652380	-0.720728	42.884930	-0.270982	63.671940
-0.512171	12.172580	-0.695190	45.423480	-0.242607	64.192140
-0.527777	12.692770	-0.692353	45.954080	-0.224163	64.712330
-0.537708	13.212970	-0.675327	46.505490	-0.194370	65.232530
-0.543383	13.733160	-0.663977	47.025690	-0.168832	65.752730
-0.544802	14.253360	-0.655465	47.545880	-0.146132	66.272920
-0.568921	14.773560	-0.648371	48.066070	-0.123432	66.793110
-0.578852	15.293750	-0.642696	48.586270	-0.100732	67.313310
-0.580271	15.813950	-0.632765	49.106470	-0.082288	67.833510
-0.598715	16.334140	-0.624252	49.626660	-0.021281	67.833510
-0.607227	16.854340	-0.608646	50.146860		Bottom
-0.608646	17.374530	-0.598715	50.667060		

TABLE A-23. TIME VS. BREAKOUT POSITION DATA, SHOT E689, READING B FOR 50.86 mm DIA. UNCONFINED CAST COMP B*

Time (μ s)	X (mm)	Time (μ s)	X (mm)	Time (μ s)	X (mm)
	Top	-0.158769	8.315300	-0.138627	43.980410
-0.000000	0.000000	-0.201424	12.592720	-0.125594	44.382490
-0.018958	0.615948	-0.229860	16.870130	-0.073460	46.812060
-0.004739	0.188206	-0.244078	21.147560	-0.040285	49.523020
-0.011848	0.444851	-0.247633	25.356530	-0.030806	49.378510
-0.023697	1.043690	-0.246448	25.655950	-0.008294	49.806250
-0.037915	1.471432	-0.236969	29.702390	-0.000000	50.234001
-0.093603	4.037882	-0.219196	33.979810	0.001185	50.430760
-0.135072	6.313469	-0.195499	38.257230		Bottom
-0.143366	6.878088	-0.151660	42.534650		

* Charge was at a slight angle to the camera axis which allowed the measurement of detonation velocity along side as well as breakout.

TABLE A-24. TIME VS. BREAKOUT POSITION DATA, SHOT E689, READING 2 FOR
50.86 mm DIA. UNCONFINED CAST COMP B*

Time (μs)	X (mm)	Time (μs)	X (mm)	Time (μs)	X (mm)
	Top	-0.212286	16.556801	-0.199168	34.179560
0.000000	0.000000	-0.213479	16.986620	-0.195590	34.609380
-0.002385	0.223508	-0.214672	17.416450	-0.193205	35.039200
-0.016697	0.653332	-0.215864	17.846270	-0.189627	35.469030
-0.028623	1.083155	-0.217057	18.276090	-0.188434	35.898850
-0.036971	1.512978	-0.218250	18.705910	-0.184856	36.328680
-0.047705	1.942802	-0.219442	19.135740	-0.182471	36.758499
-0.057246	2.372625	-0.221827	19.565560	-0.176508	37.188320
-0.069172	2.802449	-0.224213	19.995380	-0.171737	37.618150
-0.077520	3.232272	-0.225405	20.425210	-0.169352	38.047970
-0.083483	3.662095	-0.226598	20.855030	-0.166967	38.477790
-0.090639	4.091919	-0.227791	21.284860	-0.164582	38.907620
-0.098988	4.521742	-0.227791	21.714680	-0.158618	39.337440
-0.102565	4.951566	-0.228983	22.144501	-0.156233	39.767260
-0.110914	5.381389	-0.227791	22.574330	-0.149078	40.197090
-0.118069	5.811212	-0.227791	23.004150	-0.144307	40.626910
-0.121647	6.008931	-0.227791	23.433970	-0.139537	41.056730
-0.126418	6.318404	-0.226598	23.863800	-0.133574	41.486550
-0.132381	6.670860	-0.226598	24.293620	-0.128803	41.916380
-0.135959	7.100683	-0.224213	25.041510	-0.122840	42.346210
-0.140729	7.530506	-0.224213	25.153270	-0.115684	43.205850
-0.145500	7.960330	-0.224213	25.583090	-0.108528	43.446550
-0.150270	8.390153	-0.223020	26.012910	-0.103758	43.919360
-0.158618	8.819976	-0.223020	26.442740	-0.098988	44.065498
-0.161004	9.249800	-0.223020	26.872560	-0.091832	44.495320
-0.164582	9.679624	-0.223020	27.302380	-0.085869	44.925150
-0.169352	10.109450	-0.220635	27.732210	-0.077520	45.354970
-0.172930	10.539270	-0.219442	28.162030	-0.071557	45.784790
-0.178893	10.969090	-0.218250	28.591860	-0.064402	46.214620
-0.182471	11.398920	-0.218250	29.021680	-0.057246	46.644440
-0.184856	11.828740	-0.217057	29.451500	-0.045320	47.074260
-0.187241	12.258560	-0.215864	29.881330	-0.036971	47.504080
-0.189627	12.688390	-0.214672	30.311150	-0.023852	47.933910
-0.190819	13.118210	-0.213479	30.740970	-0.014311	48.363730
-0.194397	13.548030	-0.212286	31.170790	0.000000	48.793550
-0.197975	13.977860	-0.211094	31.600620	0.009541	49.223380
-0.200360	14.407680	-0.209901	32.030440	0.021467	49.653198
-0.203938	14.837500	-0.207516	32.460260	0.035779	50.083030
-0.206323	15.267330	-0.205131	32.890090	0.041742	50.332320
-0.208709	15.697150	-0.203938	33.319910		Bottom
-0.211094	16.126970	-0.201553	33.749730		

* Charge was at a slight angle to the camera axis which allowed the measurement of detonation velocity along side as well as breakout.

TABLE A-25. TIME VS. BREAKOUT POSITION DATA, SHOT E693, READING A FOR
50.87 mm DIA. CAST COMP B WITH 12.68 mm THICK STEEL COLLAR
AT END

Time (μ s)	X (mm)	Time (μ s)	X (mm)	Time (μ s)	X (mm)
	Top	-0.179484	-14.201220	-0.040683	-44.759570
0.000000	0.000000	-0.193843	-18.284380	-0.019145	-46.049850
-0.005983	-0.318487	-0.203415	-22.367540	0.002393	-46.866480
-0.017948	-1.135117	-0.201022	-25.225740	0.021538	-47.683110
-0.025128	-1.543431	-0.195039	-25.552401	0.045469	-48.499740
-0.059828	-2.768378	-0.195039	-26.450690	0.063418	-49.316370
-0.102904	-5.218274	-0.185467	-30.533850	0.068204	-49.724690
-0.108887	-5.969575	-0.153160	-34.617010	0.070597	-50.084010
-0.117263	-6.361558	-0.126835	-38.700170	0.076580	-50.133010
-0.131622	-6.851536	-0.076580	-42.783320		Bottom
-0.149570	-10.118060	-0.051452	-44.163430		

TABLE A-26. TIME VS. BREAKOUT POSITION DATA, SHOT E693, READING 2 FOR
50.87 mm DIA. CAST COMP B WITH 12.66 mm THICK STEEL COLLAR
AT END

Time (μs)	X (mm)	Time (μs)	X (mm)	Time (μs)	X (mm)
Top		-0.238848	17.055940	-0.241237	34.609920
0.000000	0.000000	-0.241237	17.464170	-0.238848	35.018150
-0.002388	0.318421	-0.241237	17.872400	-0.236460	35.426390
-0.010748	0.726653	-0.246014	18.280640	-0.236460	35.834620
-0.020302	1.134885	-0.250791	18.688870	-0.234071	36.242850
-0.026273	1.543117	-0.255568	19.097099	-0.231683	36.651080
-0.039410	1.951350	-0.250791	19.505330	-0.229294	37.059320
-0.048964	2.359582	-0.255568	19.913570	-0.224518	37.467550
-0.060906	2.767814	-0.256762	20.321800	-0.222129	37.875780
-0.068072	3.176046	-0.257956	20.730030	-0.219741	38.284010
-0.078820	3.584278	-0.257956	21.138260	-0.219741	38.692240
-0.088374	3.992510	-0.256762	21.546490	-0.216158	39.100470
-0.096734	4.400743	-0.256762	21.954730	-0.212575	39.508710
-0.102705	4.808975	-0.261539	22.362960	-0.207798	39.916940
-0.109870	5.217207	-0.261539	22.771190	-0.204215	40.325170
-0.119424	5.625439	-0.261539	23.179420	-0.199438	40.733398
-0.123007	5.829555	-0.260345	23.587660	-0.195856	41.141640
-0.131367	6.262281	-0.260345	23.987660	-0.192273	41.549870
-0.131367	6.441903	-0.261539	24.404120	-0.188690	41.958099
-0.138532	6.850135	-0.265122	24.812350	-0.182719	42.366330
-0.143309	7.258367	-0.267510	25.040960	-0.179136	42.774570
-0.151669	7.666600	-0.266316	25.351220	-0.171971	43.182800
-0.157640	8.074832	-0.267510	25.626820	-0.169582	43.591030
-0.166000	8.483064	-0.266316	26.037050	-0.163611	43.999260
-0.168388	8.891296	-0.263927	26.445280	-0.162417	44.227870
-0.176748	9.299529	-0.262733	26.853510	-0.157640	44.578950
-0.177942	9.707760	-0.261539	27.261740	-0.154057	44.815730
-0.181525	10.115990	-0.260345	27.669970	-0.148086	45.223960
-0.188690	10.524220	-0.260345	28.078210	-0.142115	45.632190
-0.193467	10.932460	-0.259151	28.486440	-0.136144	46.040420
-0.195856	11.340690	-0.257956	28.894670	-0.131367	46.448650
-0.198244	11.748920	-0.255568	29.302900	-0.123007	46.856880
-0.203021	12.157150	-0.256762	29.711140	-0.113453	47.265120
-0.206604	12.565390	-0.255568	30.119370	-0.106287	47.673350
-0.210187	12.973620	-0.255568	30.527599	-0.094345	48.081580
-0.216158	13.381850	-0.253179	30.935830	-0.088374	48.489820
-0.218546	13.790080	-0.251055	31.344060	-0.076431	48.898050
-0.219741	14.198310	-0.249996	31.752300	-0.066878	49.306280
-0.220935	14.606550	-0.249596	32.160530	-0.054935	49.714510
-0.223323	15.014780	-0.248402	32.568760	-0.047770	50.122740
-0.228100	15.423010	-0.248402	32.976990	-0.035827	50.530980
-0.230489	15.831240	-0.247208	33.385220	Bottom	
-0.230489	16.239480	-0.244820	33.793460		
-0.234071	16.647710	-0.243625	34.201690		

Figures A-1 to A-5 are single record readings of the (Z,X) data from each experiment. The Z positions were obtained by multiplying $(t-t_0)$ data by the detonation velocity (see Equation 2) for that charge diameter.

APPENDIX B

ERROR ANALYSIS

This appendix outlines the error analysis used for this work. A general treatment of errors is given in the first section. Specific examples of errors in trace angle, detonation wave angles at the edge of the charge, times of arrival of detonation wave at the curved surface, and the placement of marks at specific angles on the curved surface are treated in the following sections.

GENERAL TREATMENT OF ERRORS

The error in a quantity is the uncertainty in its measurement. The value of a quantity may depend on several parameters. Each of these parameters is uncertain to some degree. To estimate the total uncertainty in the quantity requires a prescription for calculating the error which includes the propagation of errors. The present error analysis gives such a prescription which depends on obtaining analytical expressions of the error in terms of known parameters. The analysis is based on a book by Yardley Beers.^{B-1}

To avoid confusion some definitions are in order. The two main types of errors normally encountered are systematic and experimental (random). Systematic errors are usually caused by errors in calibration of equipment, experimental variation of external conditions such as room temperature, personal errors and imperfect techniques. Experimental errors are caused by judgement or ability to read an instrument the same for a number of readings, fluctuating conditions such as line voltage, etc.

These random errors are distributed around a "most probable" value which is to be the average deviation rather than the standard deviation in this report. The standard deviation is 1.25 times the value of the average deviation.^{B-1}

The errors are reported in the shorthand form " $f \pm \epsilon$ " where ϵ is the average deviation of f . The probability that f is between $f \pm \epsilon$ is 57 percent; $f \pm 2\epsilon$ is 89 percent; and $f \pm 3\epsilon$ is 98 percent.

For independent error, there is a possibility of compensation among the various contributions. It is expected that the total error will be algebraically less than the sum of the separate contributions. Combining the separate contributions is done by taking the square root of the sum of their squares (hereafter called SRSS) which has the correct compensating property. The rule for combining random (experimental) errors is

$$\epsilon_i = \left[\left(\frac{\partial f}{\partial x} \right)^2 \epsilon_x^2 + \left(\frac{\partial f}{\partial y} \right)^2 \epsilon_y^2 \right]^{1/2} \quad (B-1)$$

where $f = F(x, y)$, x and y are the independent measured parameters. The function f can depend on any number of parameters. The choice of only two parameters for Equation (B-1) is made only for illustrative purposes.

Nonindependent errors combine algebraically because compensation among the various contributions is not likely. Therefore,

$$\epsilon_{ni} = \frac{\partial f}{\partial x} \epsilon_x + \frac{\partial f}{\partial y} \epsilon_y \quad (B-2)$$

When both independent and nonindependent errors, ϵ_i and ϵ_{ni} respectively, are encountered the total error is found by taking the SRSS of both separate contributions to give a total estimate of error for that particular parameter.

$$\epsilon^2 = \sqrt{\epsilon_i^2 + \epsilon_{ni}^2} \quad (B-3)$$

From a set of measurements of a parameter, the best value available is the average value. The error associated with this average value is not the average of the deviations from this average value but is the average of these deviations divided by the square root of the number of measurements. In other words, the precision improves in proportion to the square root of the reciprocal of the number of measurements in the sample set.

Fitting data to a straight line is encountered frequently. It is useful to review how to evaluate errors for such fits. A straight line is given by

$$y = a + b x \quad (B-4)$$

where a is the intercept, b is the slope and x, y are the rectilinear coordinates. Y. Beers^{B-1} gives the formulas for calculating the best least squares fit for a and b assuming all the error is in y .

In practice, the streak record is read a number of times and the average value from these various least squares fits is used for determining the magnitude of b . The average deviation from the least squares fit for slope b is given by^{B-1}

$$\epsilon_b^2 = \frac{\sum (\delta y_n)^2 k}{(1.25)^2 (k-2) [k \sum x_n^2 - (\sum x_n)^2]} \quad (B-5)$$

and

$$\epsilon_a = \epsilon_b \sqrt{\frac{\sum x_n^2}{k}}$$

where $\delta y_n = y_n - (a + b x_n)$, Σ means to sum over all n , and k is the total number of x, y pairs. This statistical random error in a and b can be obtained from the least squares fitting routine.

To determine the total random error in b , the average deviation from the average is calculated and combined, using the SRSS rule, with the average deviations of the least squares fitted parameter (i.e., Equation (B-5)).

ERROR IN THE TRACE ANGLE

The trace angle error on a streak camera film is the largest contributor to the total error in determining the angle that the detonation wave makes with the edge of the charge. A detailed discussion on the systematic error in trace angle Γ (see Figure B-1) is given here.^{B-2} Estimates of the systematic errors in determining trace angles on the camera records are similar to those of Dubovik.^{B-3} There are four separate contributions to this error: (1) the film alignment in the reader instrument, (2) the fuzziness of the trace, (3) the reader instrument accuracy, and (4) the spatial resolution. Each is treated as independent

of the other, which is not strictly true. However, this is a reasonable assumption to make since the sole purpose is to obtain a reasonable estimate of the error.

The first contribution to the systematic error in Γ is due to the alignment of the film parallel to the time axis for reading. This error ϵ_A is ≤ 0.001 radian based on an accuracy of ± 0.1 mm per 100 mm which can be realized in practice. This error is very small and will be ignored.

The second and largest contribution to the systematic error in Γ is due to the fading and fuzziness of the trace, which depends on the camera slit width and response of the film to different exposure times. The recording of the motion of an opaque plane moving at a constant speed parallel to the slit plane (along the length of the slit) results in a cut-off of the light to the camera. The cut-off is not recorded as a sharp loss of light because of the finite width of the slit and diffraction. Rather, it is a line of some width made up of many thin lines each at different optical densities and at an angle Γ to the space axis (y) of the film. The optical density of the broad line varies from high to low density in the direction of the camera sweep (i.e., increasing time). The geometry of the envelope of lines is shown in Figure B-1.

An analytical expression for the systematic error in Γ due to trace fuzziness can easily be derived from the geometry, resulting in

$$\epsilon_\Gamma = SW \sin \Gamma / (S - SW \cos \Gamma) \quad (B-6)$$

where SW is the camera slit width, Γ is the angle of the trace, and S is the trace length. Note that since ϵ_Γ is a small number,

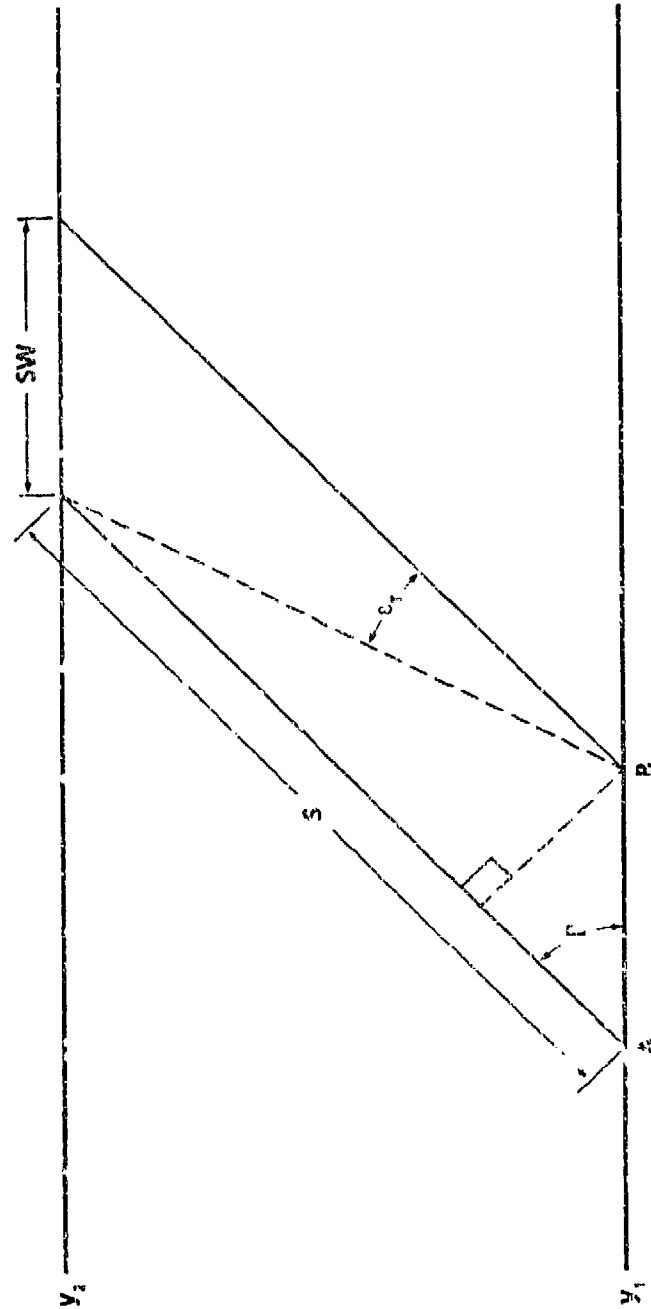


FIGURE B-1. ENVELOPE OF PARALLEL LINES THAT MAKE UP STREAK CAMERA FILM TRACE

the approximation of $\tan \epsilon_T \approx \epsilon_T$ was used in deriving Equation (B-6).

It should be emphasized that the above analysis for the error in Γ is a pessimistic one. The analysis was limited to the error between two data points while the actual measurement of the angle typically results from several data points which are least-squares fitted to a straight line. The least-squares fitting of the data reduces the measuring error. In addition, placing the film reader's hairlines on film coordinates of about the same optical density reduces the trace width to less than the slit width. To compensate for these factors, personal judgment must be used. A reduction of one-third of the error given by Equation (B-6) is used as a reasonable estimate. Therefore, the error due to trace fuzziness is $\epsilon_f = \epsilon_T/3$.

The third contribution to the systematic error is due to the accuracy of the Vanguard analyzer in determining Γ . By assuming this error (ϵ_v) can be assigned to one reader variable, then Equation (B-6) is applicable. The slit width SW in Equation (B-6) is replaced by the smallest distance measurable by the Vanguard analyzer (0.005 mm). A typical error ϵ_v is 0.001 radian for $\Gamma = 0.998$ rad and $S = 3$ mm.

The fourth contribution to the systematic error is due to the spatial resolution. The smallest distinguishable spatial distance on the film was about 0.03 mm for the camera in a simulated experimental setup. Treating this uncertainty as independent of the others, an expression for this error becomes

$$\epsilon_{SR} = \left(\frac{0.03 \text{ mm}}{S} \right) \cdot \cos \Gamma \quad . \quad (B-7)$$

The typical contribution for this systematic error is 0.005 radian when $S = 3$ mm and $\Gamma = 0.998$ radian.

The various contributing errors in determining the angle Γ for a straight line on the film are given in Table B-1. The values used here are for evaluating the error in α discussed in the next section. It is obvious by comparing the typical contributions given for each factor that the largest systematic error is due to the fuzziness of the trace ϵ_f . Note that the total error ϵ_r in Γ is the SRSS of the independent systematic and experimental (random) errors.

ERROR IN THE DETONATION WAVE ANGLE AT THE EDGE OF THE CHARGE

The detonation wave angle α at the edge of the charge for steady waves is depicted in Figure B-2, where α is related to the angle Γ on the film by

$$\tan \alpha = \tan \Gamma u_c / (M_f D) \quad (B-8)$$

and D is the detonation velocity, Γ is the corresponding angle on the film, M_f is the image to object magnification on the film,

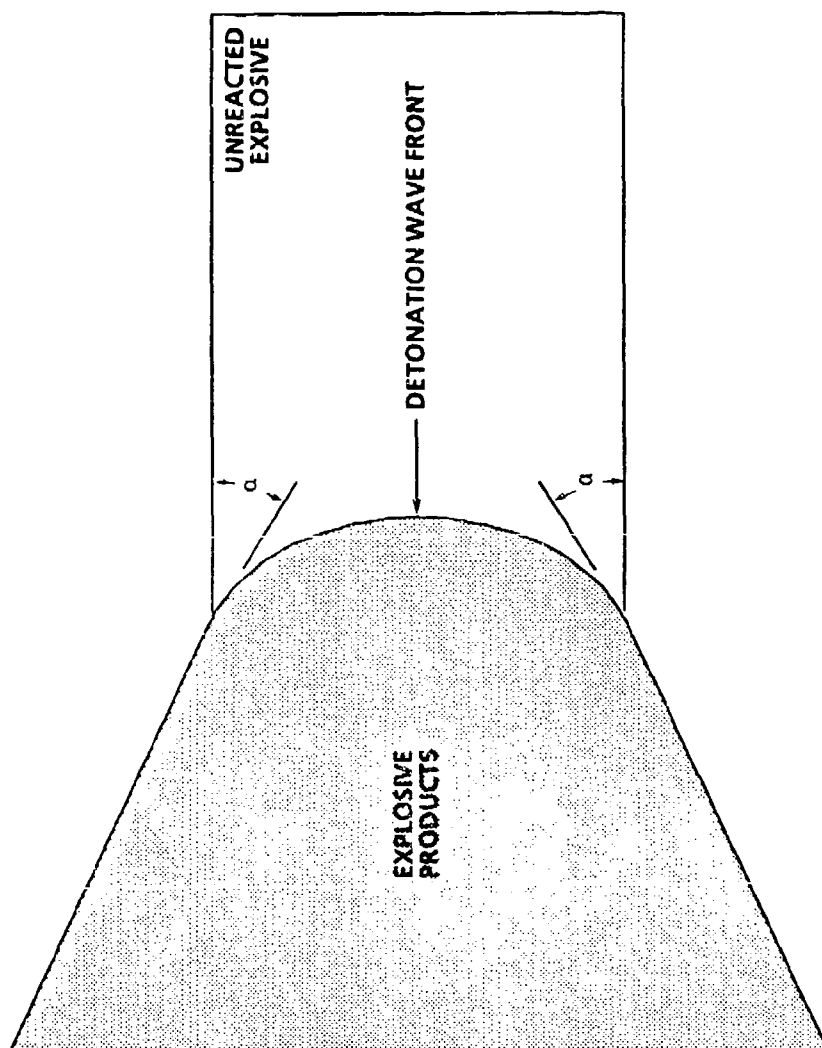


FIGURE B-2. ANGLE THAT THE CURVED DETONATION WAVE FRONT MAKES WITH THE EDGE OF THE CHARGE

TABLE B-1. ERROR IN ANGLE Γ ON FILM*

LSQ fit** ϵ_r (rad)	Random** ϵ_r (rad)	ϵ_v (rad)	ϵ_{sr} (rad)	ϵ_f (rad)	Total ϵ_r (rad)
0.0044	0.0062	0.001	0.005	0.020	0.022

*For $\Gamma = 57.1^\circ$, $S = 3.0$ mm and $SW = 0.2$ mm

$$**\epsilon_r = \cos^2(\Gamma) \epsilon_{\tan(\Gamma)} = \frac{D M_f}{u_c} \cos^2(\Gamma) \epsilon_{\tan(\alpha)}$$

and u_c is the camera speed. Taking the differential with respect to the variables on both sides of Equation (B-8) and following the general treatment for errors of Equation (B-1) results in the following expression for total error in angle α

$$\epsilon_\alpha^2 = \frac{\sin^2(2\alpha)}{4} \left[\left(\frac{2 \epsilon_r}{\sin(2\Gamma)} \right)^2 + \left(\frac{\epsilon_{u_c}}{u_c} \right)^2 + \left(\frac{\epsilon_{M_f}}{M_f} \right)^2 + \left(\frac{\epsilon_D}{D} \right)^2 \right] \quad (B-9)$$

Determination of the error in ϵ_r was given in Section B-2. Table B-2 gives the values for the various parameters required to evaluate ϵ_α . To illustrate the magnitude of ϵ_α , the parameters for the wave curvature experiment (see Table 1 in main text) with the 48.12 mm diameter PBXN-111 charge were used. Table B-2 clearly shows that the major contributor of error in α is in determining the trace angle Γ .

Note that there is a practical limit to the length of the trace (S) which can be least squares fitted to a straight line since the trace on the film is curved. The data are fitted to a straight line equation (first order polynomial) and a second order polynomial. It was found that a S of 3 mm can be fitted by straight lines before the curvature significantly affects the result.

TABLE B-2. ERROR IN DETONATION WAVE ANGLE α AT EDGE OF CHARGE

$\frac{2 \epsilon_r^{**}}{\sin(2\Gamma)}$ (rad)	$\frac{\epsilon_D}{D}$	$\frac{\epsilon_{u_c}}{u_c}$	$\frac{\epsilon_{M_f}}{M_f}$	ϵ_α (rad)
0.048	0.01	0.006	0.005	0.020

* $\alpha = 61.93^\circ$ **Total ϵ_r from Table B-1

ERROR IN TIME BETWEEN TWO POINTS ON A CURVED LINE ON FILM

A line on the film is exposed to light for a time equal to the slit width divided by the camera speed. The sharpness of the line's edge is a function of the amount of light reaching the film, diffraction, and film response. The discussion on how the line is put on the film was presented earlier. It is still reasonable that the measuring instrument can be placed at the same line density for both points which reduces this contributing error by one-third. Therefore, the systematic error due to fuzziness of the trace in reading a point x on the film is given by

$$\epsilon_{x_v}^2 = M_v^2 \left(\frac{SW}{3} \right)^2 + (\epsilon_v)^2 \quad (B-10)$$

where ϵ_v is the error (0.05 mm) of placing the crosshairs of the Vanguard reader on a point on the film. Note, that in principle, the total error ϵ_{x_v} would be the SRSS of Equation (B-10) and the experimental error. However, the experimental error is negligible in this case.

The time difference between two points along a curved line on a streak camera record is defined by the following expression.

$$dt = t_1 - t_0 = (x_{1f} - x_{0f}) / u_c = (x_{1v} - x_{0v}) / (u_c M_v) \quad (B-11)$$

where x_{1f} is a location on the film and x_{1v} is the corresponding location on the film in record analyzers coordinates. The error in dt can be determined by taking the differential of

Equation (B-11) with respect to the variables and using Equation (B-1) which results in the following expression

$$\epsilon_{dt}^2 = [2(\frac{\epsilon_{x_v}}{u_c M_v})^2 + dt^2(\frac{\epsilon_{u_c}}{u_c})^2 + dt^2(\frac{\epsilon_{M_v}}{M_v})^2] \quad (B-12)$$

Recall that the errors in ϵ_{x_1} and ϵ_{x_0} have the same magnitude which results in the factor of 2 in Equation (B-12) for the ϵ_{x_v} term. Table B-3 gives the representative values for the corner turning experiment D of Table 2. It is clear that the dominant error is in the ϵ_{x_v} term.

The error in dt for a wave arriving at the curved surface in a corner turning experimental is calculated by taking the SRSS of ϵ_{dt} from Equation (B-12) and ϵ_R/U_s , where U_s is the wave speed.

ERROR IN ANGLE ON CURVED SOLID BOWL SURFACE ON CORNER TURNING EXPERIMENTS

Figure B-3 shows a schematic of the solid bowl with the angle θ marked. A line perpendicular to the camera's slit plane was drawn with a black ink pen on the reflecting Teflon tape attached to the solid bowls curved surface. This line does not allow much light to reflect back to the camera resulting in a distinct line on the streak film. These lines are placed at specific angles on the curved surface. The relation between the angle θ , the height from the top of the bowl h , and the radius of curvature of the surface R is

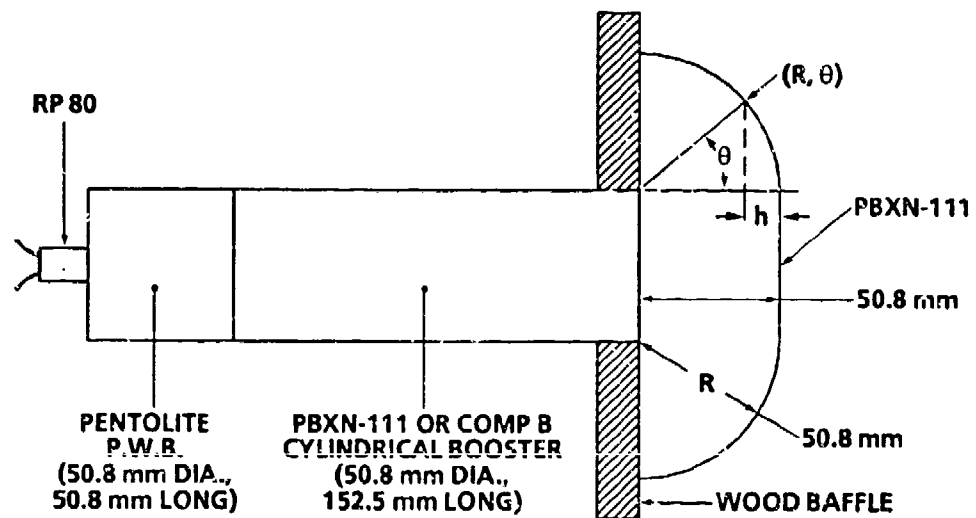


FIGURE B-3. DETONATION WAVE CORNER TURNING EXPERIMENTAL ARRANGEMENT

TABLE B-3. ERROR IN DIFFERENCE OF TIME dt BETWEEN TWO POINTS ON THE FILM*

$\frac{SW M}{3}$ (mm)	ϵ_v (mm)	ϵ_{x_v} (mm)	$\frac{\epsilon_{u_c}}{u_c}$	$\frac{\epsilon_{M_v}}{M_v}$	ϵ_{dt} (μs)
0.236	0.05	0.241	0.006	0.005	0.019

* For $dt = 0.2 \mu s$, $u_c = 5 \text{ mm}/\mu s$, $SW = 0.2 \text{ mm}$, and $M_v = 3.54$

$$\cos \theta = 1 - \frac{h}{R} \quad (B-13)$$

The error in θ is found by taking the differential of Equation (B-13) with respect to all the variables and using Equation (B-1) results in the expression for the error of

$$\epsilon_{\theta}^2 = \frac{1}{\sin^2 \theta} \left[\left(\frac{\epsilon_h}{R} \right)^2 + \left(\frac{\epsilon_R}{R} \right)^2 \sin^2 \theta \right] \quad (B-14)$$

A typical error in θ is given in Table B-4 along with the parameters required to evaluate the error. The systematic error in h is from two sources. The first is the accuracy of the height gauge which is ± 0.009 mm (i.e., one-third the smallest division) while the second is the uncertainty in h due to the line width marked on the charge. This error is less than one-third of the lines width times $\sin \theta$. Therefore, the error in h is given by

$$\epsilon_h^2 = (0.009)^2 + (0.133 \sin \theta)^2 \quad (B-15)$$

where ϵ_h is in mm. The error in the radius R is found by measuring the curvature with a circle gauge and by fitting the marker line's height and spacing on the curved surface to the best R . The error in R on these charges was less than 0.10 mm.

TABLE B-4. ERROR IN ANGLE θ OF CORNER TURNING EXPERIMENTS*

$\frac{\epsilon_h}{R}$	$\frac{\epsilon_R}{R}$	ϵ_θ (rad)
0.003	0.002	0.003

* For angle $\theta = 45^\circ$, and $R = 50.4$ mm

REFERENCES

- B-1. Beers, Yardley, Theory of Error, Addison-Wesley Publishing Company, Inc., June 1962.
- B-2. Forbes, J. W., Experimental Investigation of the Kinetics of the Shock Induced Alpha to Epsilon Phase Transformation in Armco Iron, NSWC TR 77-137, 1977.
- B-3. Dubovik, A. S., Photographic Recording of High Speed Process, NASA Technical Translation No. NASA TTF-377, 1965.

DISTRIBUTION

COPIES

ATTN F MENZ	1	ATTN TECHNICAL LIBRARY	1
USD (A) DDRE (R AT ET)		DIRECTOR	
STAFF SPECIALIST FOR WEAPONS		DEFENSE RESEARCH AND ENGINEERING	
TECHNOLOGY		WASHINGTON DC 20305	
THE PENTAGON			
WASHINGTON DC 20301		ATTN TECHNICAL LIBRARY (FRIES)	1
		INSTITUTE FOR DEFENSE ANALYSES	
ATTN R SIEWART	1	1801 N BEAUREGARD ST	
OUSDRE R&AT MST		ALEXANDRIA VA 22311	
THE PENTAGON			
WASHINGTON DC 20301		ATTN LIBRARY	1
		DIRECTOR	
ATTN G KOPCSAK (OM)	1	DEFENSE ADVANCED RESEARCH	
D ANDERSON (NW&M)	1	PROJECTS OFFICE	
OUSDRE TWP		1400 WILSON BOULEVARD	
THE PENTAGON		ARLINGTON VA 22209	
WASHINGTON DC 20301			
		ATTN TECHNICAL LIBRARY	1
ATTN SURFACE WARFARE	1	SPSP (P CASTLEBERRY)	1
AIR WARFARE	1	SPSP (J CONNELL)	1
SUBS ASW	1	SPSD (J DEPLITCH)	1
OASN RE&S		SPSD (K GOERING)	1
THE PENTAGON		SPSD (K STEIN)	1
WASHINGTON DC 20301		SPSP (M FRANKEL)	1
		SPSP (T FREDRICKSON)	1
ATTN I BLATSTEIN (TD)	1	SP (C MCFARLAND)	1
NAVAL SURFACE WARFARE CENTER		DIRECTOR	
WASHINGTON DC 20362		DEFENSE NUCLEAR AGENCY	
		WASHINGTON DC 20305	
ATTN TECHNICAL LIBRARY	12		
DEFENSE TECHNICAL		ATTN DDESB KT	1
INFORMATION CENTER		DDESB KT1 (J WARD)	1
CAMERON STATION		DEPARTMENT OF DEFENSE EXPLOSIVE	
ALEXANDRIA VA 22304-6145		SAFETY BOARD	
		HOFFMAN BUILDING 1	
ATTN TECHNICAL LIBRARY	1	2461 EISENHOWER AVENUE	
COMMANDER		ALEXANDRIA VA 22331-0600	
CENTER FOR NAVAL ANALYSIS			
200 N BEAUREGARD ST		ATTN TECHNICAL LIBRARY	1
ALEXANDRIA VA 22311		A WILLIAMS	1
		COMMANDING OFFICER	
		NAVAL RESEARCH LABORATORY	
		WASHINGTON DC 20350-5000	

NSWCDD/TR-92/164

ATTN ONR(S) 1132P (R MILLER)	1	COMMANDER	
ONR(T) (P QUINN)	1	NAVAL SURFACE WARFARE CENTER	
ONR(T) (E ZIMET)	1	CARDEROCK DIVISION	
ONR(T) 213 (D SIEGEL)	1	BETHESDA MD 20084	
ONR(T) 23 (A FAULSTICH)	1		
ONR(T) 232 (D HOUSER)	1	ATTN TECHNICAL LIBRARY	1
OFFICE OF THE CHIEF OF NAVAL		COMMANDING OFFICER	
RESEARCH		NAVAL SURFACE WARFARE CENTER	
800 N QUINCY ST BCT1		NAVAL COASTAL SYSTEMS STATION	
ARLINGTON VA 22217-5000		PANAMA CITY FL 32407-5000	
ATTN OP 005	1	ATTN SEA 05R	1
OP 02	1	SEA 06APR (MUIR)	1
OP 03	1	SEA 06B	1
OP 035	1	SEA 06R	1
OP 0354	1	SEA 06U	1
OP 07	1	SEA 62	1
OP 987B	1	SEA 62Z31E (SCHONER)	1
CHIEF OF NAVAL OPERATIONS		SEA 662	1
WASHINGTON DC 20350		SEA 6622	1
		SEA 665	1
ATTN AIR 540	1	SEA 6652	1
AIR 540TF	1	SEA 99612	1
AIR 5404	1	PMS 422 16 (LUBIN)	1
AIR 54051	1	PMS 422G	1
AIR 54043	1	CHENG T1 (RITTER)	1
TECHNICAL LIBRARY	1	COMMANDER	
COMMANDER		NAVAL SEA SYSTEMS COMMAND	
NAVAL AIR SYSTEMS COMMAND		WASHINGTON DC 20362-5105	
WASHINGTON DC 20361			
ATTN SPAWAR 05	1	ATTN TECHNICAL LIBRARY	1
COMMANDER		COMMANDING OFFICER	
SPACE AND NAVAL WARFARE		NAVAL EXPLOSIVES ORDNANCE	
SYSTEMS COMMAND		DISPOSAL TECHNOLOGY CENTER	
WASHINGTON DC 20363-5100		INDIAN HEAD MD 20640	
ATTN CODE 177	1	ATTN TECHNICAL LIBRARY	1
TECHNICAL LIBRARY	1	CODE 363 (R NADOLINK)	1
COMMANDER		COMMANDER	
DAVID TAYLOR RESEARCH CENTER		NAVAL UNDERWATER WARFARE	
UERG		CENTER DIVISION	
PORTSMOUTH VA 23709		NEWPORT RI 02841-5047	
ATTN TECHNICAL LIBRARY	1	COMMANDING OFFICER	1
R GARRISON	1	NAVAL INTELLIGENCE SUPPORT CENTER	
S WANG	1	4302 SUITLAND ROAD	
JW SYKES	1	WASHINGTON DC 20390-5140	
W CONLEY	1	ATTN CODE 2730D	1
F FISCH	1	TECHNICAL LIBRARY	1
CODE 17	1	J CHANG	1
CODE 172	1		

NSWCDD/TR-92/164

P DENDOR	1	CODE 3894 (M WAGENHALS)	1
S MITCHELL	1	CODE 3894 (A LINDFORS)	1
L NEWMAN	1	CODE 39	1
COMMANDING OFFICER		CODE 3917	1
NAVAL SURFACE WARFARE CENTER		TECHNICAL LIBRARY	1
INDIAN HEAD DIVISION		COMMANDER	
INDIAN HEAD MD 20640		NAVAL AIR WARFARE WEAPONS DIVISION	
		CHINA LAKE CA 93555-6001	
ATTN LIBRARY	1	ATTN LIBRARY	1
CODE 470A	1	COMMANDING GENERAL	
CODE 35	1	MARINE CORPS DEVELOPMENT AND	
M KRAM	1	EDUCATION COMMAND	
L LEONARD	1	MARINE CORPS LANDING FORCE	
J ZEHMER	1	DEVELOPMENT CENTER	
J ROUDABUSH	1	QUANTICO VA 22134	
COMMANDING OFFICER		ATTN LIBRARY	1
NAVAL ORDNANCE STATION DETACHMENT		CODE 3031 (E NEAL)	1
NAVAL WEAPONS STATION		CODE 50D (A NORRIS)	1
YORKTOWN VA 23691-5000		CODE 505 (J SHORT)	1
		CODE 90 (A WHITNER)	1
ATTN CODE 32	1	COMMANDING OFFICER	
CODE 3205 (F MARKARIAN)	1	NAVAL SURFACE WARFARE CENTER	
CODE 3205 (S DEMAY)	1	CRANE DIVISION	
CODE 3208	1	CRANE IN 47522	
CODE 321	1	ATTN TECHNICAL LIBRARY	1
CODE 32103	1	COMMANDER	
CODE 3211	1	NAVAL COMMAND AND CONTROL OCEAN	
CODE 3212	1	SURVEILLANCE CENTER	
CODE 3212 (E LUNDSTROM)	1	SAN DIEGO CA 92152-5000	
CODE 3213	1	ATTN CODE 2145	1
CODE 3213 (T MOORE)	1	COMMANDER	
CODE 3213 (H JOHN)	1	PACIFIC MISSILE TEST CENTER	
CODE 3214	1	POINT MUGU CA 93042	
CODE 326 (MCCUBBIN)	1	COMMANDING OFFICER	1
CODE 326B (L JOSEPHSON)	1	NAVAL SURFACE WARFARE CENTER	
CODE 3261 (WEEKS/FASIS)	2	PORT HUENEME DIVISION	
BUCKLEY)	1	PORT HUENEME CA 93043	
CODE 3263	1	COMMANDING OFFICER	1
CODE 3264	1	NAVAL UNDERSEA WARFARE DIVISION	
CODE 3266	1	KEWPORT WA 98345-0580	
CODE 327	1	COMMANDER	1
CODE 32904 (STEPHENS)	1	NAVAL WEAPONS EVALUATION FACILITY	
CODE 3293 (COPE/MAURER)	2	KIRTLAND AIR FORCE BASE	
CODE 381	1	ALBUQUERQUE NM 87117	
CODE 385	1		
CODE 3850	1		
CODE 3853	1		
CODE 3853	1		
CODE 389 (T BOGGS)	1		
CODE 38906 (PEARSON)	1		
CODE 3891 (M CHAN)	1		
CODE 3984 (ALEXANDER)	1		

NSWCDD/TR-92/164

ATTN LIBRARY	1	ABERDEEN PROVING GROUND MD	21005
SUPERINTENDENT			
NAVAL POSTGRADUATE SCHOOL		ATTN LIBRARY	1
MONTEREY CA 93940		DELHD DE OM (K WARNER)	1
		COMMANDING OFFICER	
ATTN TECHNICAL LIBRARY	1	HARRY DIAMOND LABORATORIES	
PRESIDENT		2800 POWDER MILL ROAD	
NAVAL WAR COLLEGE		ADELPHI MD 20783	
NEWPORT RI 02841			
		ATTN AMSLC TD (R VITALI)	1
COMMANDING OFFICER	1	COMMANDER	
SEAL TEAM 2		US ARMY LABORATORY COMMAND	
FPO AE 09510-4633		2800 POWDER MILL ROAD	
		ADELPHI MD 20783-1145	
ATTN AMSMI RD ST WF (D LOVELACE)	1		
COMMANDER		ATTN DRSMC TD	1
US ARMY MISSILE COMMAND		DDRSMC LCE	2
REDSTONE ARSENAL AL 35898-5247		DRDSMC LCE (E BAKER)	1
		DRSMC LCE C	1
ATTN DRXSY D	1	DRSMC LCE D	2
DRXSY J (J MCCARTHY)	1	DRSMC LCM	2
DIRECTOR		DRSMC LCM SA (R WESTERDAHL)	1
ARMY MATERIALS SYSTEMS		DRSMC LCU	2
ANALYSIS AGENCY		DRSMC LCU E	1
ABERDEEN PROVING GROUND MD	21005	COMMANDER	
		US ARMY ARMAMENT RESEARCH	
ATTN SMCCR DDP	1	DEVELOPMENT AND ENGINEERING	
COMMANDER		CENTER	
US ARMY CHEMICAL RESERACH		DOVER NJ 07806-5000	
DEVELOPMENT AND ENGINEERING			
CENTER		ATTN G R HUSK	1
ABERDEEN PROVING GROUND MD	21010-	COMMANDER	
5423		US ARMY RESEARCH OFFICE	
		PO BOX 12211	
ATTN DRDAR BLP	1	RESEARCH TRIANGLE PARK NC	27709-
SLCRB TB E	1	2211	
SLCRB IB I (P KASTE)	1		
V BOYLE	2	ATTN T MATUSKO	1
R FREY	1	COMMANDER	
J FRASIER	1	AIR FORCE OFFICE OF SCIENTIFIC	
F GRACE	1	RESEARCH	
W HILLSTROM	1	BOLLING AIR FORCE BASE	
R JAMIESON	1	WASHINGTON DC 20332	
J STARKENBERG	1		
H REEVES	1	ATTN AFIS INTAW (MAJ R ESAW)	1
L VANDEKIEFT	1	COMMANDER	
W WALTERS	1	AIR FORCE INTELLIGENCE SERVICE	
J WATSON	1	BOLLING AIR FORCE BASE	
TECHNICAL LIBRARY	1	WASHINGTON DC 20332-5000	
STINFO OFFICE	1	ATTN C MERRILL	1
COMMANDING OFFICER		F ROBERTO	1
ARMY BALLISTIC RESEARCH LAB		COMMANDER	

NSWCDD/TR-92/164

AIR FORCE ASTRONAUTICS LABORATORY
ATATL MKPL
EDWARDS AFB CA 93521

ATTN WL MNF (R BOULET 1
R ERHART) 1
WL MNW (E POSTON) 1
WL MNE (S AUBERT 1
J CORLEY/ G GLENN 2
R MCKENNEY JR 1
I G PARSONS) 1
MSD SES (F WEST) 1
MSD XRS (J JENNS JR) 1

COMMANDER
AFATL MN
EGLIN AFB FL 32542-5434

ATTN H JEAN HIGHBY (L53) 1
K BAHL 1
P CRAWFORD 1
L GREEN 1
J HUMPHREY 1
J KURY 1
E LEE 1
K SCRIBNER 1
R SIMPSON 1
W TAO 1
C TARVER 1
P URTIEW 1
R WEINGART 1

UNIVERSITY OF CALIFORNIA
LAWRENCE LIVERMORE NATIONAL
LABORATORY
PO BOX 808
LIVERMORE CA 94550

ATTN E AUSTIN TECH LIBRARY
REPORTS RECEIVING CLERK 1
SANDIA NATIONAL LABORATORY
PO BOX 5800
ALBUQUERQUE NM 87185

ATTN DARLENE M LOLL FOR
TECHNICAL LIBRARY 1

SANDIA NATIONAL LABORATORY
PO BOX 969
LIVERMORE CA 94550-0096

ATTN LIBRARIAN 1
E LISZKA 1

APPLIED RESEARCH LABORATORY
PENNSYLVANIA STATE UNIVERSITY
PO BOX 30 UNIVERSITY PARK
STATE COLLEGE PA 16804

ATTN M 8 1
MST DO MS G 756 1
I ASAY 1
J BDZIL 1
A BOWMAN 1
G BUNTAIN 1
L CHAPMAN 1
M COBURN 1
J DAVIS 1
J DICK 1
B DOBRATZ 1
C FOREST 1
J GOFORTH 1
J HOPSON 1
P HOWE 1
J N JOHNSON 1
J KENNEDY 1
T LARSON 1
W MAUTZ 1
S PETERSON 1
R RABIE 1
J REPA 1
S SHEFFIELD 1
L STRETZ 1
P TANG 1
M URIZAR 1
J WACKERLE 1

LOS ALAMOS NATIONAL LABORATORY
PO BOX 1663
LOS ALAMOS NM 87545

NSWCDD/TR-92/164

ATTN R WATSON DEPARTMENT OF THE INTERIOR BUREAU OF MINES PITTSBURGH RESEARCH CENTER COCHRANS MILL ROAD PITTSBURGH PA 15236-00700	1	ATTN JOSEPHINE HUGGINGS BATELLE MEMORIAL LABORATORY TACTICAL TECHNOLOGY CENTER 505 KING AVENUE COLUMBUS OH 43201	1
ATTN T W CHRISTIAN THE JOHNS HOPKINS UNIVERSITY APPLIED PHYSICS LABORATORY CHEMICAL PROPULSION INFORMATION AGENCY JOHNS HOPKINS ROAD LAUREL MD 20707-6099	1	ATTN E WILHELM R HELZER BOEING AEROSPACE COMPANY PO BOX 3707 SEATTLE WA 98124	1 1
ATTN DEANNA JONES FOR TECHNICAL LIBRARY JOHNS HOPKINS UNIVERSITY APPLIED PHYSICS LABORATORY JOHNS HOPKINS ROAD LAUREL MD 20707-6099	1	ATTN R SEWELL COMARCO INC WEAPON SUPPORT DIVISION RIDGECREST CA	1
ATTN SECURITY ADMINISTRATOR (ELIZABETH A TILL) CODE TERA (M KEMPTON) CODE CETR (T JOYNER P PERSSON) NEW MEXICO INSTITUTE OF MINING TECHNOLOGY CAMPUS STATION SOCORRO NM 87801	1 1 1 2	ATTN J MOSCHEL C STROSBERG J MEIER M BRAMMER CHAMBERLAIN MFG CORP 550 ESTHER STREET WATERLOO IA 50704-2524	1 1 1 1
ATTN G CHIN AEROJET ORDNANCE AND MANUFACTURING COMPANY 9236 EAST HALL ROAD DOWNEY CA 90241	1	ATTN R WEST P CHOU DYNA EAST CORPORATION 320 ARCH STREET PHILADELPHIA PA 19104-2588	1 1
ATTN KENNETH GRAHAM ATLANTIC RESEARCH CORPORATION 5945 WELLINGTON ROAD GAINESVILLE VA 22055-1699	1	ATTN SAM MIGUEL FORD AEROSPACE AND COMMUNICATIONS CORPORATION AERONAUTRONIC DIVISION FORD ROAD JAMBOREE NEWPORT BEACH CA 92658-9983	1
ATTN F LASCHER E MOULIC AVCO TECHTRON SYSTEMS INC 201 LOWELL STREET WILMINGTON MA 01887	1 1	ATTN G WILLIAMS HERCULES INCORPORATED ROCKET CENTER PO BOX 210 ROCKET CENTER WV 26726	1
		ATTN M KLAKKEN M BERGER G BUTCHER L LOSEE T SPEED HERCULES BACCHUS WORKS MAGNA UT 84044	1 1 1 1 1

NSWCDD/TR-92/164

ATTN L WFBER	1	S CUBED	
HUGHES AIRCRAFT INC		A DIVISION OF MAXWELL LABS INC	
MISSILE SYSTEMS GROUP		PO BOX 1620	
8433 FALLBROOK AVENUE		LAJOLLA CA 92038	
CANOGA PARK CA 91304-9976			
ATTN TIMOTHY PENDERGRASS	1	ATTN D GARFINKLE	1
KAMAN SCIENCES CORP		SCIENCE APPLICATIONS INTERNATIONAL	
600 BLVD SOUTH SUITE 208		26679 W AGOURA ROAD	
HUNTSVILLE AL 35802		CALABASAS CA 91307	
D R KENNEDY ASSOCIATES	1	ATTN K L CHRISTIANSON	1
PO BOX 4003		J L HOULTON	1
MOUNTAIN VIEW CA 94040		G JOHNSON	1
RADKOWSKI ASSOCIATES	1	ALLIANT TECHSYSTEMS INC	
P O BOX 5474		7225 NORTHLAND DRIVE	
RIVERSIDE CA 92517		BROOKLYN PARK MN 55428	
KORNHAUSER CONSULTING SERVICES 1		ATTN C ANDERSON	1
620 ARGYLE AVENUE		H GRYTING	1
WYNNEWOOD PA 19096		A WENTZEL	1
ATTN R HODGES	1	SOUTHWEST RESEARCH INSTITUTE	
J SMITH	1	PO DRAWER 28510	
LOCKHEED MISSILES & SPACE CO		SAN ANTONIO TX 78284	
PO BOX 504		ATTN D SHERWOOD	1
SUNNYVALE CA 94086		M COWPERTHAWAITE	1
ATTN J FLOWERS	1	SRI INTERNATIONAL	
LTV AEROSPACE & DEFENSE CO		333 RAVENSWOOD AVENUE	
LTV AEROSPACE PRODUCTS GROUP		MENLO PARK CA 94025	
PO BOX 655907		ATTN L WEBER	1
DALLAS TX 95265-5907		J NEWQUIST	1
ATTN H FUEHRER	1	TELEDYNE BROWN ENGINEERING	
MARTIN MARIETTA CORPORATION		PO BOX 070007	
ORLANDO AEROSPACE MISSILE SYSTEMS		HUNTSVILLE AL 35807	
PO BOX 555837		ATTN R CHURCH	1
ORLANDO FL 32855		TRW	
ATTN T KITCHEN	1	SAN BERNADINO CA 92401	
ORLANDO TECHNOLOGY INC		ATTN G WEEDING	1
PO BOX 855		UNIVERSITY OF DENVER	
SHALIMAR FL 32579		COLORADO SEMINARY	
ATTN W ZARR	1	PO BOX 10758	
RAYTHEON COMPANY		DENVER CO 80210	
HARTWELL ROAD		ATTN A MELLOR	1
BEDFORD MA 01730		VANDERBILT UNIVERSITY	
ATTN R SEDGWICK	1	NASHVILLE TN 37235	
		ATTN L ZERNOW	1
		ZERNOW TECHNICAL SERVICES INC	

NSWCDD/TR-92/164

PO BOX 54
SAN DIMAS CA 91773

ATTN H ADOLPH 1
S JACOBS 1
J W WATT 1

ADVANCED TECHNOLOGY AND
RESEARCH INC
LAUREL TECHNOLOGY CENTER
14900 SWEITZER LANE
LAUREL MD 20707

ATTN W SMITH 1
ADVANCED TECHNOLOGY INC
2121 CRYSTAL DRIVE
ARLINGTON VA 22202

ATTN R DICK 1
UNIVERSITY OF MARYLAND
DEPARTMENT OF MECHANICAL ENG
COLLEGE PARK MD 20742

ATTN P J DIBONA 1
FMC CORPORATION
NAVAL SYSTEMS DIVISION M170
4800 EAST RIVER ROAD
MINNEAPOLIS MINNESOTA 55421

ATTN J ENIG 1
ENIG ASSOCIATES INC
SUITE 500
11120 NEW HAMPSHIRE AVENUE
SILVER SPRING MD 20904-2633

ATTN D DAVISON 1
SHOCK TRANSIENTS INC
PO BOX 5357
HOPKINS MN 55343

ATTN S EIDELMAN 1
SCIENCE APPLICATIONS
INTERNATIONAL CORP
1710 GOODRIDGE DRIVE
MCLEAN VIRGINIA 22102

ATTN LIBRARY 1
M D COOK ET1 BLDG X3 1
A CUMMINGS ET BLDG X59 1
B HAMMANT 1
P HASKINS ET1 BLDG X51 1
G HOOPER 1
D MULLENGER ET1 BLDG X50 1

DEFENSE RESEARCH AGENCY
FORT HALSTEAD SEVENOAKS
KENT TN14 7BP
UNITED KINGDOM

ATTN LIBRARY 1
H P JAMES 1
ATOMIC WEAPONS ESTABLISHMENT
FOULNESS ISLAND
ESSEX SS3 9XE
UNITED KINGDOM

ATTN J JENKINS 1
B D LAMBOURN 1
D C SWIFT 1
MOD(PE)
ATOMIC WEAPONS ESTABLISHMENT AWE(A)
ALDERMASTON
READING BERKSHIRE RG7 4PR
UNITED KINGDOM

ATTN W LEEMING 1
NEC
ARDEER SITE
STEVENSTON AYRESHIRE KA20 3LN
SCOTLAND

ATTN P JONES 1
THE BRITISH EMBASSY BRITISH DEFENCE
STAFF
3100 MAS\SACHUSETTS AVENUE NW
WASHINGTON DC 20008

ATTN M CHICK 1
D D RICHARDSON 1
D A JONES 1
M PODLESAK 1

MATERIAL RESEARCH LABORATORY
PO BOX 50
ASCOT VALE VICTORIA 3032
AUSTRALIA

ATTN D L KENNEDY 1
ICI EXPLOSIVES
GATE 1
BALLARAT ROAD
DEER PARK VICTORIA 3023
AUSTRALIA

ATTN R STENSON (S DIV) 1
ORDNANCE BOARD

NSWCDD/TR-92/164

EMPRESS STATE BUILDING
LILLIE ROAD LONDON SW6 1TR
UNITED KINGDOM

ATTN J COOPER 1
G A LEIPER 1

I J KIRBY 1
ICI EXPLOSIVES
STEVENSTON KA20 3LN
UNITED KINGDOM

ATTN M GUNGER 1
ORLANDO TECHNOLOGY INC
PO BOX 855
SHALIMAR FL 32579

ATTN J N OECONOMOS 1
F CHAISSE 1

CEA
CENTRE D'ETUDES
DE VAUJOURS-MORONVILLIERS
B P N° 7 77181 COUNTRY
FRANCE

ATTN: M. HELD 1
MESSERSCHMITT-BOLKOW-BLOHM GMBH
RESEARCH DEPARTMENT
8898 SCHROBENHAUSEN
GERMANY

ATTN: CONRAD BELANGER 1
ROCCO FARINACCIO 1
IRENE HOOTON 1
GRANT MCINTOSH 1

DEFENSE RESEARCH ESTABLISHMENT
VALCARTIER
PO BOX 8800
COURCELETTE QUEBEC
CANADA
GOA 1R0

ATTN: J. D. RENICK 1
DEFENCE NUCLEAR AGENCY
FIELD COMMAND
KIRTLAND AFB NEW MEXICO 87115-
5000

ATTN: P. E. WILLIAMS 1
NEW MEXICO INSTITUTE OF MINING AND
TECHNOLOGY
ENERGETIC MATERIALS RESEARCH AND

TESTING CENTER
SOCORRO NM 37801

ATTN J CZECHANSKI
INTERFEROMETRICS INC
8150 LETSBURG PIKE
VIENNA VA 22182-2799

INTERNAL DISTRIBUTION:

C72W	1
E231	2
E23	3
G10	1
G13 (D L DICKINSON)	1
G13 (T WASMOND)	1
G20	1
G22	1
G22 (C GARNETT)	1
G22 (W HOLT)	1
G22 (W MOCK)	1
G22 (T SMITH)	1
G22 (T SWIERK)	1
G22 (S WAGGENER)	1
G22 (L WILSON)	1
R	1
R01	1
R04	1
R06	1
R101	1
R102	1
R10	1
R10B	1
R11	1
R11 (E ANDERSON)	1
R11 (D CICHRA)	1
R11 (S COLLIGON)	1
R11 (R DOHEREY)	1
R11 (F GALLANT)	1
R11 (J GOLDWASSER)	1
R11 (C GOTZMER)	1
R11 (N JOHNSON)	1
R11 (J LEAHY)	1
R11 (L NOCK)	1
R11 (Y TRAN)	1
R12	1
R12 (B GLANCY)	1
R12 (J LAIB)	1
R12 (P SPAHN)	1
R13	1
R13 (R BAKER)	1

NSWCDD/TR-92/164

R13 (R BERNECKER)	1	G92 (R GODZUK)	1
R13 (R BARDO)	1	G92 (W HINCKLEY)	1
R13 (C COFFEY)	1	G92 (A KOENIGSBERG)	1
R13 (J DAVIS)	1	G92 (K MCDONALD)	1
R13 (D DEMSKE)	1	G92 (R MCKEOWN)	1
R13 (J FORBES)	10	G92 (J MENTGES)	1
R13 (R GUIRGUIS)	1	G92 (T MOORE)	1
R13 (P GUSTAVSON)	1	G92 (C NIGGINS)	1
R13 (H JONES)	1	G92 (B PARK)	1
R13 (RICHARD LEE)	1	G92 (C SMITH)	1
R13 (WOODROW LEE)	1	G92 (D TAM)	1
R13 (E LEMAR)	3	G92 (L TAYLOR)	1
R13 (T LIDDIARD)	1	G92 (W WALKER)	1
R13 (P MILLER)	1		
R13 (C RICHMOND)	1		
R13 (H SANDUSKY)	1		
R13 (C STANTON)	1		
R13 (G SUTHERLAND)	3		
R13 (D TASKER)	1		
R13 (W WILSON)	1		
R13 (D WOODY)	1		
R13 (C WONG)	1		
R13 (F ZERILLI)	1		
R14	1		
R14 (R BARASH)	1		
R14 (T FARLEY)	1		
R14 (J GASPIN)	1		
R14 (J KOENIG)	1		
R14 (D LEHTO)	1		
R14 (H MAIR)	1		
R14 (P MONTANARO)	1		
R14 (J POWELL)	1		
R14 (M SWISDAK)	1		
R15	1		
R16 (B BAUDLER)	1		
R16 (L HUDSON)	1		
R16 (L MENSI)	1		
R16 (L MONTESI)	1		
R16 (T SPIVAK)	1		
R16 (P WALTER)	1		
R44	1		
R44 (W SZYMCZAK)	1		
G822 (O PARRENT)	1		
G91	1		
G91 (W FURR)	1		
G91 (R PLENGE)	1		
G91 (D HINELY)	1		
G91 (J JEROSKI)	1		
G92 (D BETANCOURE)	1		
G92 (J BURNS)	1		
G92 (H CHEN)	1		
G92 (A DARE)	1		

REPORT DOCUMENTATION PAGE

Form Approved
OMB No. 0704-0188

Public reporting burden for this collection of information is estimated to average 1 hour per response, including the time for reviewing instructions, searching existing data sources, gathering and maintaining the data needed, and completing and reviewing the collection of information. Send comments regarding this burden estimate or any other aspect of this collection of information, including suggestions for reducing this burden, to Washington Headquarters Services, Directorate for Information Operations and Reports, 1215 Jefferson Davis Highway, Suite 1204, Arlington, VA 22202-4302, and to the Office of Management and Budget, Paperwork Reduction Project (0704-0188), Washington, DC 20503.

1. AGENCY USE ONLY (Leave blank)		2. REPORT DATE 19 March 1992	3. REPORT TYPE AND DATES COVERED	
4. TITLE AND SUBTITLE Detonation Wave Curvature, Corner Turning, and Unreacted Hugoniot of PBXN-111			5. FUNDING NUMBERS	
6. AUTHOR(S) J. W. Forbes, E. R. Lemar, G. T. Sutherland, and R. N. Baker				
7. PERFORMING ORGANIZATION NAME(S) AND ADDRESS(ES) Naval Surface Warfare Center Dahlgren Division, White Oak Detachment 10901 New Hampshire Avenue Silver Spring, MD 20903-5640			8. PERFORMING ORGANIZATION REPORT NUMBER NSWCDD/TR-92/164	
9. SPONSORING/MONITORING AGENCY NAME(S) AND ADDRESS(ES)			10. SPONSORING/MONITORING AGENCY REPORT NUMBER	
11. SUPPLEMENTARY NOTES				
12a. DISTRIBUTION/AVAILABILITY STATEMENT Approved for public release; distribution is unlimited.			12b. DISTRIBUTION CODE	
13. ABSTRACT (Maximum 200 words) This study was undertaken to develop a data base on the detonation properties of PBXN-111 (formerly PBXW-115) and to improve our understanding of its divergent flow properties. This data base can be used to test curved wave front detonation theories and two-dimensional hydrodynamic flow detonation models which take into account the initiation and the growth of reactions and multiple energy release rates. A high-speed streak camera was used to measure the wave front curvature and the corner turning ability of PBXN-111. The unreacted Hugoniot was measured using quartz and multiple <i>in situ</i> manganin stress gauges. These Hugoniot samples were dynamically loaded by the impact of projectiles from a light gas gun.				
14. SUBJECT TERMS PBXCN-111 PBXW-115 Detonation properties			15. NUMBER OF PAGES 117	
			16. PRICE CODE	
17. SECURITY CLASSIFICATION OF REPORT UNCLASSIFIED	18. SECURITY CLASSIFICATION OF THIS PAGE UNCLASSIFIED	19. SECURITY CLASSIFICATION OF ABSTRACT UNCLASSIFIED	20. LIMITATION OF ABSTRACT SARF	

NSN 7540-01-280-5500

Standard Form 298 (Rev. 2-89)
Prescribed by ANSI Std. Z39-18
298-102